UCRL 9714

UNIVERSITY OF CALIFORNIA

Ernest O. Lawrence

Radiation Laboratory

TWO-NUCLEON TRANSFER REACTIONS IN THE LIGHT ELEMENTS

DISCLAIMER

UCRL-9714
UC-34 Physics
TID-4500 (16th Ed.)

UNIVERSITY OF CALIFORNIA
Lawrence Radiation Laboratory
Berkeley, California

Contract No. W-7405-eng-48

TWO-NUCLEON TRANSFER REACTIONS IN THE LIGHT ELEMENTS

Joseph Cerny III

(Ph. D. Thesis)

May 23, 1961

Printed in USA. Price $2.25. Available from the
Office of Technical Services
U. S. Department of Commerce
Washington 25, D.C.

TWO-NUCLEON TRANSFER REACTIONS IN THE LIGHT ELEMENTS

Contents

TWO-NUCLEON TRANSFER REACTIONS IN THE LIGHT ELEMENTS

Joseph Cerny III

(Ph. D. Thesis)

Lawrence Radiation Laboratory
University of California
Berkeley, California

May 23, 1961

ABSTRACT

α,d reactions in the light elements have been investigated in an attempt to determine their usefulness as spectroscopic probes. Deuteron energy spectra from the $Li^6(\alpha,d)Be^8$, $Li^7(\alpha,d)Be^9$, $C^{12}(\alpha,d)N^{14}$, $N^{14}(\alpha,d)O^{16}$, and $N^{15}(\alpha,d)O^{17}$ reactions were measured and angular distributions are given for deuteron groups arising from the formation of resolvable final states.

Selection rules for two-nucleon transfer reactions are discussed. Direct-reaction α,d or d,α transitions between 0+, T=0 and 0+, T=1 states are shown to involve difficulties with angular momentum and parity conservation in addition to requiring nonconservation of isotopic spin. The unobserved $C^{12}(\alpha,d)N^{14*}$ (2.31-Mev) transition is interpreted from this point of view.

Marked variation in the relative cross sections of final states was observed in most of the deuteron spectra. Some evidence was obtained that the captured nucleons prefer to enter equivalent shell-model levels and, lacking that, adjacent levels. No final states definitely known to involve more than two excited nucleons were observably populated; however, very few states of this nature have been theoretically established.

Glendenning's two-nucleon stripping theory was applied to the deuteron angular distributions, and several excellent fits were obtained. The fits, in general, showed little dependence on the nature of the final nuclear configuration when several were reasonable, so that no spectroscopic identification of final states appears to be possible at these high-momentum transfers. Angular distribution fits using Butler theory are shown for comparison.

I. INTRODUCTION

The successful interpretation of simple direct nuclear reactions involving the transfer of a single nucleon has been followed by an increasing interest in two-nucleon transfer reactions. The mechanisms involved in these latter reactions, and especially their utility as spectroscopic probes, are of considerable importance; many He^3,p reactions, primarily at low beam energies ($\approx$5 Mev), and a few t,p and He^3,n reactions have been investigated.[1,2,3] By contrast, few α,d reactions have been reported,[4,5,6] and in these little attention has been devoted to the spectroscopic nature of the final states formed or to the use of this reaction to determine isotopic spin impurities.[7] Of the inverse reactions, primarily the d,α and p,t have been reported(e.g., Refs. 8,9).

The α,d reaction in the light elements with 48-Mev helium ions leading to fairly low-lying states of the final nucleus might be expected to proceed predominantly by a direct-reaction mechanism, since the previous α,d studies[4,6] at 43 and 48 Mev (also the $C^{12}(\alpha,p)N^{15}$ reaction[10,11] at helium ion energies of 31 to 40 Mev, and various α,t reactions[12] at 48 Mev) show strong direct-reaction effects. With the recent appearance of fairly detailed two-nucleon transfer theories---such as Glendenning's plane-wave, finite-size incident particle, two-nucleon stripping theory[13]---the possibility of spectroscopic identification of states through fitting the deuteron angular distribution from an α,d reaction can be studied; of course, a plane-wave approximation theory applied to α,d reactions may not be very successful, since interactions strong enough to break up an incident helium ion are expected to cause considerable distortion of the outgoing deuteron wave.[14]

If, in the α,d reaction, the helium ion can be considered to transfer a deuteron directly to the target nucleus in a single interaction, the captured particles will be in a relative $^3S_1$ state unless the interaction potential causes a spin flip of only one of the transferred nucleons. The final states which are strongly populated might arise from the preference of the captured pair to enter equivalent shell-model states rather

than inequivalent ones; e.g., higher cross sections for stripping both particles into the same shell rather than into different shells might be observed. Also, transitions to final states whose description involves three or more excited nucleons, should not be appreciably observed, assuming that core (target nucleus) excitation is improbable in these transfer reactions.

If nuclear forces are charge-independent, α,d reactions can produce only those final states which have the same isotopic spin as the target nucleus; dependent upon the detector resolution available, it may be possible to determine the isotopic spin quantum numbers of those final states whose configurations involve two-nucleon excitation, or less, by their presence or absence from the deuteron spectra. Many $0+,\ T=0 \rightarrow 0+,\ T=1$ d,α transitions--which obey the same selection rules as the α,d reactions--have been studied from this point of view.[7,15] Such transitions produced by a compound-nucleus mechanism are inhibited by angular momentum and parity conservation in addition to conservation of isotopic spin.[16] It will be shown that for α,d stripping reactions (and d,α pickup reactions) the angular momentum and parity selection rules strongly inhibit these particular transitions, and that very similar difficulties arise in α,α' inelastic scattering reactions in which $1+,\ T=0 \rightarrow 0+,\ T=1$ transitions are used to measure isotopic spin impurities.

In order to investigate the above potentialities of the α,d direct reaction in the light nuclei, experiments were undertaken on one even-even target nucleus (C^{12}), two odd-odd target nuclei (Li^6 and N^{14}), and two odd-even target nuclei (Li^7 and N^{15}).

II. SELECTION RULES AND EVALUATION OF ISOTOPIC SPIN IMPURITIES

It is the purpose of this section to develop the selection rules arising from angular momentum and parity conservation which are applicable to two-nucleon transfer reactions and to indicate their approximate validity. In addition, certain of these transfer reactions give information on the isotopic spin impurities of various nuclear states through observed failure of isotopic spin conservation; the nature of these breakdowns is discussed and two of the usual transitions investigated to measure them are analyzed.

A. Total Angular Momentum and Parity Conservation in Direct Reactions

The conservation of total angular momentum between the initial and final states of a system produces selection rules on the values of the total orbital angular momentum L that may be transferred in a given stripping reaction, and it is L that characterizes the angular distribution of the outgoing particle. In general, the conservation of parity then further restricts these values of L. Consider an α, d reaction on a target nucleus J_i, π_i producing final states J_f, π_f. The conservation laws require

$$\overline{J}_f = \overline{J}_i + \overline{L} + \overline{S}, \quad \text{where} \quad \overline{L} = \overline{\ell}_n + \overline{\ell}_p, \quad \overline{S} = \overline{s}_n + \overline{s}_p \tag{II-1}$$

(ℓ_n, ℓ_p are the orbital angular momentum quantum numbers of the states about the target nucleus "core" into which the neutron and proton are captured, and s_n, s_p, are their intrinsic angular momenta),

and $$\pi_f = \pi_i (-)^{\ell_n + \ell_p} \tag{II-2}$$

(which assumes that the reaction does not change the parity of the core).

This parity selection rule would not additionally restrict the values of L obtainable from Eq. (II-1) and the definition $\overline{L} = \overline{\ell}_n + \overline{\ell}_p$, and so would, in general, permit contributions from both even and odd L in a given transition. However, recent two-nucleon stripping theories[13, 17]

show

$$\pi_f = \pi_i(-)^{\ell_n+\ell_p} = \pi_i(-)^L , \qquad \text{(II-3)}$$

which relates the total orbital angular momentum transfer to the parity change of the reaction. The reason for this, as given by Glendenning,[13] is the following. One may resolve L into a center-of-mass angular momentum Λ and a relative angular momentum λ of the pair of nucleons to be captured from the incident (plane-wave) helium ion. Then $\overline{L} = \overline{\Lambda} + \overline{\lambda}$ is the angular momentum of the captured pair and $(-)^{\Lambda+\lambda}$ is their parity. Since in the incident nuclide the nucleons are predominantly in their lowest states, i.e., in s states, one obtains $\lambda = 0$ as an excellent approximation by neglecting any minor contributions from higher relative angular momenta the captured pair might possess.[18] From this, the parity selection rule (II-3) readily follows.

Selection rules on the total spin S of the captured particles for several two-nucleon stripping reactions are listed below[13,17]--the foregoing discussion is applicable to all of them:

$$\begin{aligned} &\alpha, d \rightarrow S=1, \\ &He^3, p \rightarrow S=0, 1, \\ &t, p \text{ and } He^3, n \rightarrow S=0. \end{aligned} \qquad \text{(II-4)}$$

A simple development of these rules is given in the following section, and they are valid unless a spin flip of only one of the captured particles can occur.

B. Isotopic Spin Conservation

1. General Discussion--Direct Reactions

If, as experiment continues to validate, one may assume the charge independence of specifically nuclear forces--i.e., that p-p, n-n, and n-p forces are equivalent after correction for Coulomb effects--it is possible to treat low-Z nuclei as assemblies of identical particles. This can be done by introducing a general particle called the nucleon with two isotopic-spin projections: $+1/2$ for a neutron and $-1/2$ for a proton. These are then defined to be eigenvalues of t_3, the z component of a new quantum number (and constant of the the motion for the nuclear Hamiltonian, which omits Coulomb forces) called the isotopic spin T; t_3 may be defined in general for an arbitrary nucleus as $t_3 = \frac{1}{2}(N-Z)$. This concept has been developed in detail,[7, 19-22] and we are concerned with its results in terms of the classification of nuclear states using the J^π, T quantum numbers and the application of isotopic spin selection rules to nuclear reactions.[23] Since He^4 and H^2 are both $t_3=0, T=0$ nuclei, $\overline{T}_{initial} = \overline{T}_{final}$ requires that an α, d or a d, α direct reaction can lead only to final nuclear states possessing the same isotopic spin as the target nucleus provided that the isotopic spin is a good quantum number; hence, for example, α, d reactions on $C^{12}(T=0)$ can not produce $T=1$ states in N^{14}. Similarly, the fact that He^3 and H^1 are both $t_3=\pm 1/2, T=1/2$ nuclei permits He^3, p or p, He^3 transitions to final nuclear states that differ by zero or one unit of isotopic spin from the target nucleus.

We can obtain the selection rules on $\overline{S}$ by considering which relative S states are available for the two particles being captured, as governed by isotopic spin conservation and the Pauli principle and subject to the earlier assumptions. The Pauli principle restricts this system of identical particles to antisymmetric wave functions; these wave functions can be taken to be simple, antisymmetrical products of separate space, spin, and isotopic spin functions.[7]

a. a,d reaction

Here $\overline{T}_{\text{incoming helium ion}} - \overline{T}_{\text{outgoing deuteron}} = \overline{T}_{\text{transferred pair}} = \overline{T}_a - \overline{T}_d = \overline{0} - \overline{0} = 0.$

This restricts the n-p system of relative orbital S motion to its T=0 state. (i.e., space symmetric, isotopic-spin antisymmetric), so that S=1 is required. Hence the two nucleons enter in a $^{13}S_1$ state; the notation is $^{(2T+1)(2S+1)}\chi_{\overline{\lambda}+\overline{S}}$, which for this discussion is $^{(2T+1)(2S+1)}S_S$.

b. He^3,p reaction

Here $\overline{T}_{He^3} - \overline{T}_p = \overline{1/2} - \overline{1/2} = 0,1.$

An over-all antisymmetric wave function requires S=1, 0, respectively, hence the two nucleons can be captured in relative $^{13}S_1$ and $^{31}S_0$ states.

c. t,p or He^3,n reaction.

Here $\overline{T}_t - \overline{T}_p = \overline{1/2} - \overline{1/2} = 0,1$ (this also holds for He^3,n). However, the n-n (or p-p) system possesses only T=1 states, so that S=0 is required and the only allowed state of entry of the two nucleons is $^{31}S_0$.

2. Isotopic Spin Impurity

The isotopic spin operator does not commute with the nuclear Coulomb force operator, and the resulting mixing of different eigenstates of the isotopic spin is often calculated by treating the Coulomb force as a first-order perturbation of the system, thereby mixing states of isotopic spin T', $\psi^{J^\pi}(T')$, into states of initially pure isotopic spin T, $\psi^{J^\pi}(T)$. The amplitude of this mixing, $a_T(T')$, is given by $a_T(T') = H^C_{TT'}/(E_T{}^{J^\pi} - E_{T'}{}^{J^\pi})$, where H^C represents the Coulomb force operator.[7] One would expect $H^C_{TT'}$ to be much larger for heavier nuclei than for light, which decreases the usefulness of isotopic spin for heavy nuclei; the neutron excess in intermediate and heavy nuclei also limits the application of isotopic spin, since the theory usually treats a given nucleus as a system of particles in equivalent states about a

single closed shell. The existence of isotopic spin impurities in the nuclear states means that the isotopic spin selection rule is not strictly obeyed, but can be weakly violated through the impurities.

The effect of the isotopic spin impurity depends upon the mechanism of the nuclear reaction. For direct reactions, an isotopic spin forbidden transition can occur only through the isotopic spin impurities of the initial and final states, which for ground and low-lying states in general are small. Macdonald has calculated the total isotopic spin impurity of the ground states of various light nuclei, and the values range from 1×10^{-5} in He^4 to 4×10^{-3} in O^{16} to 2×10^{-2} in Cl^{34}.[21,24,25]

For compound-nucleus reactions leading to excited intermediate states, however, greater isotopic spin impurities may be present owing to the closer proximity of levels of the same J^π and different T. For this case, Lane and Thomas[15] and Wilkinson[26] have shown that two energy ranges of the compound system exist within which the isotopic spin selection rules should be obeyed.

(a) At low excitation of a compound nucleus, the Coulomb force matrix element may be much less than the average spacing between levels of the same J^π – that is $\langle H^C \rangle \ll D^{J^\pi}$ – so that the Coulomb force will be too weak to mix effectively states of different isotopic spins. Thus the intermediate states will possess fairly pure isotopic spins and the conservation law will be obeyed.

(b) The formation of a highly excited compound nucleus in a region of large level widths $\langle \Gamma^{J^\pi} \rangle$ (lifetimes $\approx \hbar / \langle \Gamma^{J^\pi} \rangle$) initially produces a "total" state which approximates as closely as possible the isotopic spin of the initial system. This total state arises from many simultaneously excited overlapping levels, each of which is no longer expected to have a well-defined isotopic spin; it is characterized by a time-dependent picture involving the changing phase relationships of these levels, and a suitable choice of their phase relationships can be used to approximate the initial system isotopic spin. Then, if the total state breaks up before the Coulomb forces--which act in a characteristic time[27] $\approx \hbar / \langle H^C \rangle$ -- produce appreciable isotopic spin mixing, i.e., for $\langle H^C \rangle \ll \langle \Gamma^{J^\pi} \rangle$,

the conservation rules should be obeyed. In between these regions where neither of the above inequalities is satisfied, strong isotopic spin nonconservation may be observed. For light 4n-type nuclei ($A \leq 20$) Wilkinson estimates the intermediate region to begin at 14 to 22 Mev and to end at 22 to 30 Mev.[26]

Although we are mainly concerned with transfer reactions, some consideration of the isotopic spin impuritiy of compound-nucleus intermediate states is required in the following section.

(C.) Measurements of Isotopic Spin Impurity in Nuclear Reactions

Many d,α isotopic spin "forbidden" transitions, primarily at compound-nucleus energies, have been investigated. (Reference 15 gives a summary of these and other similar investigations through ca 1956.) Many of the specific transition studied, however, have been 0+, T=0 → 0+, T=1 d,α reactions (and 1+, T=0 → 0+, T=1 α,α' reactions), and these involve difficulties with angular momentum and parity conservation in addition to requiring nonconservation of isotopic spin. The 0+, T=0 → 0+, T=1 α,d transition, which is involved in one of the experiments to be discussed, presents the same problem as the d,α above. These transitions are discussed in the following pages.

1. 0+, T=0 → 0+, T=1 α,d and d,α Reactions

For concreteness, let us consider the transition $C^{12}[0+, T=0]\,(\alpha, d)N^{14*}[2.31\ \text{Mev}, 0+, T=1]$ with 48-Mev helium ions--an expected direct reaction, and one of the reactions investigated in this thesis. It is apparent that this transition is isotopic-spin forbidden (Section II-B1), and might be used to determine isotopic spin impurities. However, Eq. (II-1) as recast (angular momentum conservation),

$$J_f + J_i + S \geq L \geq |\bar{J}_f + \bar{J}_i + \bar{S}|_{min}, \qquad \text{(II-5)}$$

readily shows that the production of a J=0 final state from a J=0 target through capturing a pair of nucleons coupled to S=1 requires L=1; conversely, the parity-selection rule (II-3) restricts this transition to even values of L. Hence, to the extent that the assumptions made in obtaining

Eq. (II-3) and (II-4) are valid, the reaction under consideration is also forbidden by angular momentum and parity conservation. Since, in general, low-lying 0+ levels in light odd-odd nuclei formed from the odd neutron and proton in equivalent states about an undisturbed even-even core are T=1, many 0+ → 0+ α,d and d,α transfer reactions will be strongly inhibited by both angular momentum and parity conservation and isotopic spin conservation. Transitions to highly excited 0+ states of other than the previous origin, for which Coulomb interactions might have produced great isotopic spin mixing, would still be inhibited by the angular momentum and parity selection rules.

Hashimoto and Alford show that 0+ → 0+ d, α (or, α, d) transitions are not strongly inhibited by angular momentum and parity conservation when the reactions proceed through formation of a compound nucleus[16] -- the only requirement is that the angular momentum of the incident and emitted particles be equal. (The angular distribution of the outgoing particles from this transition will be symmetric about 90 deg.) This requirement deters the reaction as follows: a d,α reaction on a 0+ target produces intermediate states with spin $j = \ell_d$, $\ell_d \pm 1$ and parity $(-)^{\ell_d}$, and only one-third of these (the states of spin ℓ_d) can possibly decay by alpha emission to a 0+ final state. These compound-nucleus reactions from 0+, T=0 → 0+, T=1 states are then further inhibited by isotopic spin conservation dependent upon the isotopic spin impurities of the particular compound nucleus involved and of the initial and final states.

In principle, then, α,d or d,α transitions in which compound-nucleus processes dominate should more readily measure isotopic spin mixing. Since estimates of isotopic-spin breakdown usually arise through comparison of the "forbidden" transition with an allowed transition to an adjacent level, it is necessary to (a) estimate the relative cross section if both reactions were isotopic-spin-allowed, and (b) be certain that the reference transition contains little direct-reaction component. If the latter condition is not met, the amount of isotopic spin impurity may be underestimated,[28] because "forbidden" transitions arising from direct-reaction effects should be very small under these conditions.

Under expected α,d direct-reaction conditions--as for the particular $C^{12}(\alpha,d)N^{14*}$ transition cited--any "forbidden" deuterons that might be observed would probably result from one of the following:

a. from the stripping part of this α,d reaction, through

(i) a breakdown of the parity selection rule (II-3) from contributions of other than S states of relative angular momentum in the projectile, operating in conjunction with the isotopic spin impurities of the initial and final states, and (or)

(ii) a spin flip of only one of the incoming nucleons, coupled with the isotopic spin impurities of the initial and final states; or

b. from a possible compound-nucleus part which would then be limited by a low compound-nucleus probability for deuteron emission and the restrictions on these 0+ → 0+ transitions, and then allowed through the various isotopic spin impurities (the 43-Mev excitation of the compound nucleus places it well in the high-energy region where the isotopic spin selection rule is expected to be fairly well obeyed).

If this transition proceeds according to these mechanisms, the origin of any "forbidden" deuterons will not be clearly defined. An experimental comparison of the cross section for $C^{12}(\alpha,d)N^{14*}$ (2.31-Mev) 0+, T=1 with the cross section for $C^{12}(\alpha,d)N^{14}$ (g.s.) 1+, T=0 will at least indicate the extent of the various "breakdowns" listed under (a) and (b) above. As will be presented later, the cross-section ratio $\frac{d\sigma_{2.31}}{d\Omega} / \frac{d\sigma_{g.s.}}{d\Omega}$ at 15 deg was < 0.95%.

These circumstances indicate that measurements of isotopic spin impurities in α,d and d,α transfer reactions should be made for other than 0+, T=0 → 0+, T=1 transitions.

2. 1+, T=0 → 0+, T=1 α,α' Reactions

The difficulties in obtaining meaningful information on isotopic spin impurities in these reactions are very similar to those for the above case.

For direct-interaction inelastic scattering involving single-nucleon excitations, the angular momentum restrictions on L arise

from Eq. (II-5), with $\overline{S} = \overline{S}_{\substack{\text{incoming} \\ \text{particle}}} - \overline{S}_{\substack{\text{outgoing} \\ \text{particle}}} = \overline{0} - \overline{0} = 0$; and the parity selection rule is $\pi_f = \pi_i (-)^L$.[14] Evaluating these selection rules for $1+$, $T=0 \rightarrow 0+$, $T=1$ α, α' transitions again shows that angular momentum conservation requires $L=1$, whereas parity conservation requires L even. Since these selection rules are expected to be rigorous, this transition through a direct-interaction mechanism should not be allowed, independently of the extent of conservation of isotopic spin. The same would of course be true for $0+$, $T=0 \rightarrow J(-)^{J+1}$, $T=1$ α, α' single-particle excitations.

Compound-nucleus inelastic scattering between these states follows an identical analysis to the above compound-nucleus d, α reactions. Care should also be taken here in evaluating isotopic spin impurities to be certain that the reference transition used contains only a negligible surface-interaction component.

III. EXPERIMENTAL METHOD

A. General Procedure

Deuteron spectra and angular distributions were obtained from 48-Mev helium-ion bombardments of Li^6, Li^7, C^{12}, N^{14}, and N^{15}, using the deflected external beam of the Crocker Laboratory 60-inch cyclotron. As shown in Fig. 1, the beam was brought through a quadrupole focusing magnet, a small steering magnet, and a 3/16-inch-diameter graphite collimator into a 36-inch-diameter scattering chamber.

The deuterons were distinguished from other charged particles in the following manner: First, the particles passed through a transmission counter (CsI crystal or silicon detector) which measured an energy loss ΔE proportional to their rate of energy loss $\frac{dE}{dx}$, and then they were stopped in a NaI crystal which measured their remaining energy, E. Second, these pulses were fed into an electronic particle identifier,[29,30] the output of which is proportional to the product of the mass of the particle times the square of its charge. Third, pulses from the particle identifier that corresponded to deuterons were used to trigger a Penco 100-channel pulse-height analyzer, which then recorded the energy spectrum of the deuterons. A more detailed description of the equipment and its operation is given below.

B. Scattering-Chamber Area Equipment

The primary equipment in the experimental area is shown in H through L, Fig. 1. The detectors were mounted on a remotely controlled rotating table which comprised the bottom of the 36-inch-diameter scattering chamber.[31,32,33] Although the detectors could be rotated to any desired angle within the scattering chamber, measurements at less than 10 deg or greater than 167 deg (laboratory system) were not possible because the edge of the detector mount intercepted part of the helium ion beam. A remotely controlled target holder was mounted in the lid of the chamber. The scattering chamber was evacuated by a local pumping system, which consisted of a refrigerated 6-inch diffusion pump backed by a Kinney mechanical pump.

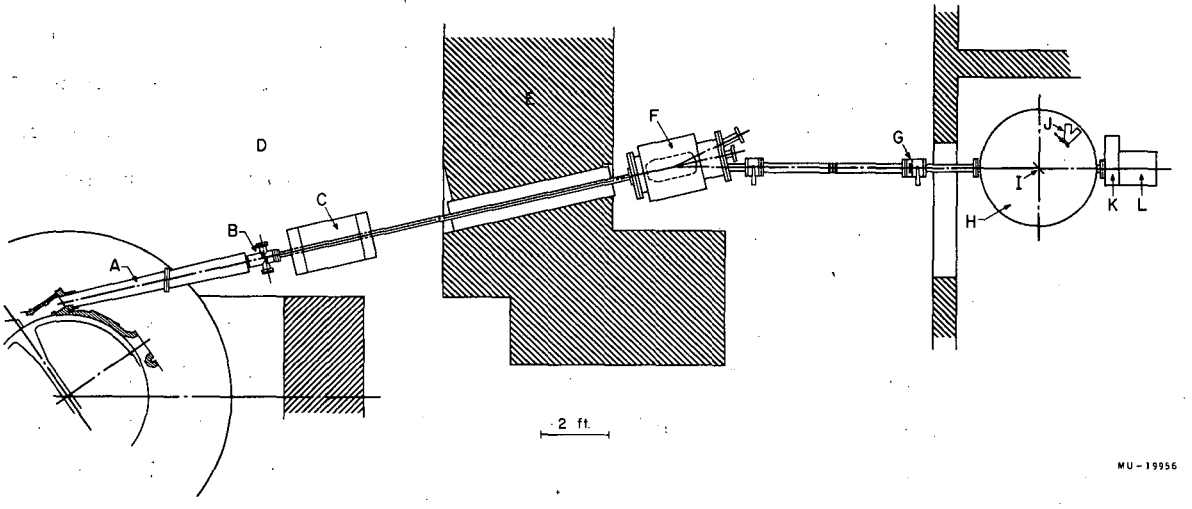

Fig. 1. Experimental arrangement. A, Iron pipe; B, adjustable slit; C, quadrupole focusing magnet; D, cyclotron vault; E, shielding wall; F, steering magnet; G, 3/16-in.-diameter collimator; H, 36-in. scattering chamber; I, target; J, counter and foil wheel; K, foil wheel for measuring beam energy; and 1, Faraday cup.

A foil wheel with various amounts of aluminum absorber, which could be operated by remote control, was placed in front of the counter telescope. This permitted variation in the energy of the particles incident on the detectors, which was useful in establishing energy scales. It was also used in adjusting the particle identifier, as described later.

The beam intensity was measured with a Faraday cup connected to an integrating electrometer; the former was placed at the back of the scattering chamber. Two remotely controlled twelve-position foil wheels, located between the scattering chamber and the Faraday cup, contained varying amounts of aluminum absorber and were used to determine the beam energy. This was done by interposing sufficient aluminum to measure the beam range; these ranges in aluminum were converted into energies by means of helium ion range-energy tables[34] based on experimental proton range-energy data.[35]

Target thickness was continuously monitored by measuring the helium ions elastically scattered from the target at a fixed angle (approx 20 deg). The monitor was a CsI(Tl) crystal mounted outside the scattering chamber and separated from it by a thin aluminum window.

C. Detectors and Electronics

1. ΔE Detectors

During the course of the experimental work, two different ΔE detectors were employed, and both detector systems are represented schematically in Fig. 2. The detector first used for measuring the ΔE proportional to the rate of energy loss of the particles was a CsI crystal, 135 mg/cm^2 thick and 5/16 inch in diameter. This crystal was viewed at an angle of 45 deg and a distance of 4 cm by a Dumont 6292 photomultiplier tube, which was operated at approx 1100 volts. The CsI resolution -- full-width at half maximum -- for incident deuterons of 20.5 Mev (elastically scattered deuterons degraded from approx 24 Mev to permit greater energy loss in the crystal) was 14.2% for a 3.1-Mev energy drop.

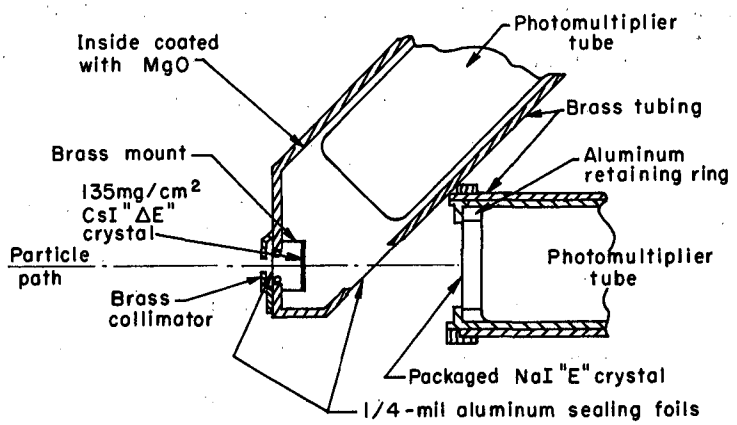

CsI - NaI counter telescope

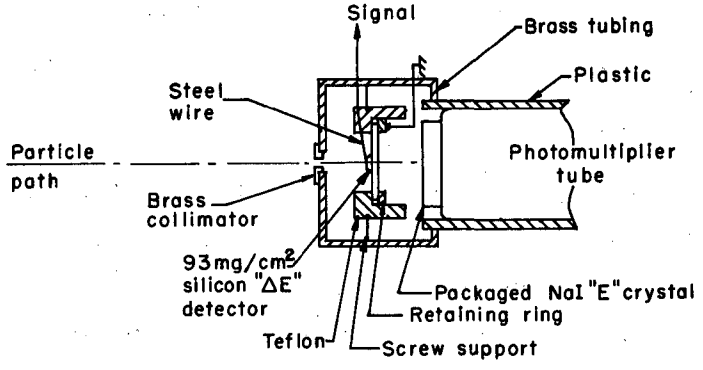

Si - NaI counter telescope

MU-23766

Fig. 2. The ΔE-E counter-telescope systems used.

Development of semiconductor radiation detectors at the Lawrence Radiation Laboratory led to the investigation of diffused-junction p-n detectors in the hope of obtaining better resolution than was possible with the CsI crystal. A very satisfactory detector was developed[36] which consisted of a 15.5-mil-thick silicon wafer with phosphorus diffused on the side that faced the beam, and a eutectic formed on the opposite side with evaporated aluminum. As shown in Fig. 2, the silicon detector was mounted in a Teflon holder and the signal was taken from the n side; the output pulses were then fed into a low-noise preamplifier[37] and sent to the counting area. Its resolution for 20.5-Mev incident deuterons was 10.9% for only a 2.1-Mev energy drop in the 62-mg/cm^2 depletion layer produced by a reverse bias of 180 volts. This greatly improved resolution led to the incorporation of the silicon detector as the standard ΔE counter. An example of the improvement in the particle-identifier spectra taken with the silicon detector as compared with the CsI crystal will be shown below.

2. E Detector

A NaI(Tl) crystal, 1/4 inch thick and 1 inch in diameter, was used to measure the particle energy that remained after passing through the ΔE counter. The crystal was packaged in an airtight aluminum container which was 0.00025 inch thick in the region where the particles entered it; a Dumont 6292 photomultiplier tube, operated at about 850 volts, was placed in contact with a transparent window on the crystal. Analysis of the various deuteron energy spectra showed that this system gave 3 to 4% resolution.

The counter system was usually placed so that the brass collimator, which preceded the ΔE detector and defined the solid angle, was from about 8 to 10.5 inches from the target.

3. Electronic Particle Identifier

The theory and operation of this electronic system have been discussed at length elsewhere,[29] so that only a brief discussion is given here.

The principle of operation of this particle identifier arises from an approximate relationship obtained from the nonrelativistic equation for the rate of energy loss of charged particles in their passage through matter. This equation can be stated[38]

$$\frac{dE}{dx} = \frac{C_1 MZ^2}{E} \ln C_2 \frac{E}{M} ,$$

where M, Z, and E are the mass, charge, and energy of the particle, respectively, and C_1, C_2 are products of constants. It has been shown[30] that the addition of a properly selected constant E_0 to the total energy of a particle will partially compensate for the log factor in the above equation, so that over a wide range of energies the product of $(E+E_0)$ and dE/dx will be closely proportional to the mass times the square of the charge of the particle. Since the measurement of dE/dx in practice requires a finite energy loss, ΔE, it is also necessary to add to the measured energy from the stopping counter a certain amount of this ΔE as $K\Delta E$, in order that E and ΔE may correspond to the same particle energy (in first approximation K would be 1/2). A final expression for MZ^2 would then be

$$MZ^2 \sim (E + E_0 + K\Delta E)\Delta E.$$

The multiplication of the E and ΔE pulses that are fed into the particle identifier is accomplished electronically by utilizing the relation

$$(A+B)^2 - (A-B)^2 = 4AB,$$

where $A = E + E_0 + K\Delta E$ and $B = \Delta E$. The squaring necessary is performed by two Raytheon QK-329 square-law tubes.

In the actual operation of this pulse multiplier, K and E_0 are left as adjustable parameters to permit optimization of the particle separation. Since E_0 is introduced as a dc bias on the deflectors of the square-law tubes, it is possible to have spurious output pulses arising from the product of E_0 and ΔE in those cases in which particles stop in the ΔE detector without striking the E detector. These

spurious pulses are eliminated in the particle identifier output spectra--to be called multiplier spectra -- by requiring a coincidence between an E pulse and this output pulse. In this manner, multiplier pulses are obtained which, if only charge-1 particles are considered, have an amplitude nearly proportional to the mass of the particle observed, over a wide range of energies.

4. Pulse-Height Analyzer

A Penco 100-channel pulse-height analyzer was used to analyze the pulses from the crystals and the multiplier. The Penco has a coincidence circuit, so that signal pulses can be required to possess a corresponding trigger pulse. A minor modification of the Penco permitted "single-channel" analysis of the trigger pulses through the use of variable upper and lower discriminators.

5. Over-All Circuitry

A block diagram of the counting equipment as set up with the silicon ΔE detector is shown in Fig. 3. When the CsI ΔE detector was used, the circuit was essentially the same except that the photomultiplier output was sent to a cathode follower rather than to the preamplifier.

The multiplier circuitry required positive pulse input, so the Franklin 1-μsec DD-2 amplifiers on the E and ΔE lines to the multiplier were followed by pulse shapers that eliminated the negative half of the DD-2 output. The rest of the electronic equipment performed its standard function.

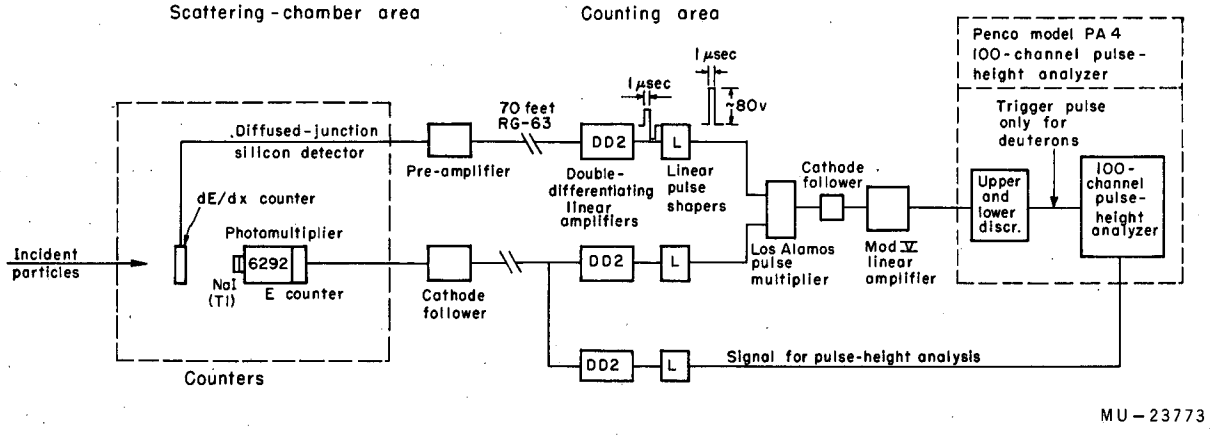

Fig 3. Block diagram of counting equipment for recording deuteron energy spectra.

D. Method of Operation

1. Multiplier Spectra

The initial tuning of the multiplier was achieved by the procedure of Briscoe.[29] Then, 24-Mev deuterons were elastically scattered from a target foil (often gold) at 15 deg (lab), and the multiplier output, which should be primarily a single peak arising from the deuterons, was displayed on the pulse-height analyzer. The energy of the deuterons incident on the counter telescope was varied down to approx 10 Mev by means of appropriate absorbers, and E_0 and K were adjusted to obtain a multiplier pulse height that was as nearly as possible independent of the deuteron energy. Final adjustment of the multiplier was made during helium ion bombardment of the target to be investigated. (At small angles an absorber thick enough to stop the intense beam of elastically scattered helium ions, which would otherwise have saturated the electronics, was placed before the counter telescope; the amount of absorber was progressively decreased with increasing angle, usually reaching zero at 45 deg.) The multiplier output in coincidence with an E trigger was again displayed on the Penco, and three peaks corresponding to protons, deuterons, and tritons were observed. Small changes in E_0 and K were made to optimize the separation of the groups. A typical multiplier spectrum from $C^{12}+He^4$, using the CsI ΔE detector, is shown in Fig. 4; little separation of the small triton group could be obtained. Figure 5 shows a multiplier spectrum, again from $C^{12}+He^4$, but with the silicon ΔE detector; this particular spectrum was adjusted for maximum deuteron-triton separation for purposes of comparison with the CsI results. All multiplier spectra presented subsequently were taken with the silicon ΔE detector.

2. Energy Spectra

The energy spectra of deuterons from various bombardments were obtained by counting with the Penco all E pulse signals in coincidence with a multiplier pulse trigger that corresponded to deuterons. This trigger was established by using the multiplier output as both

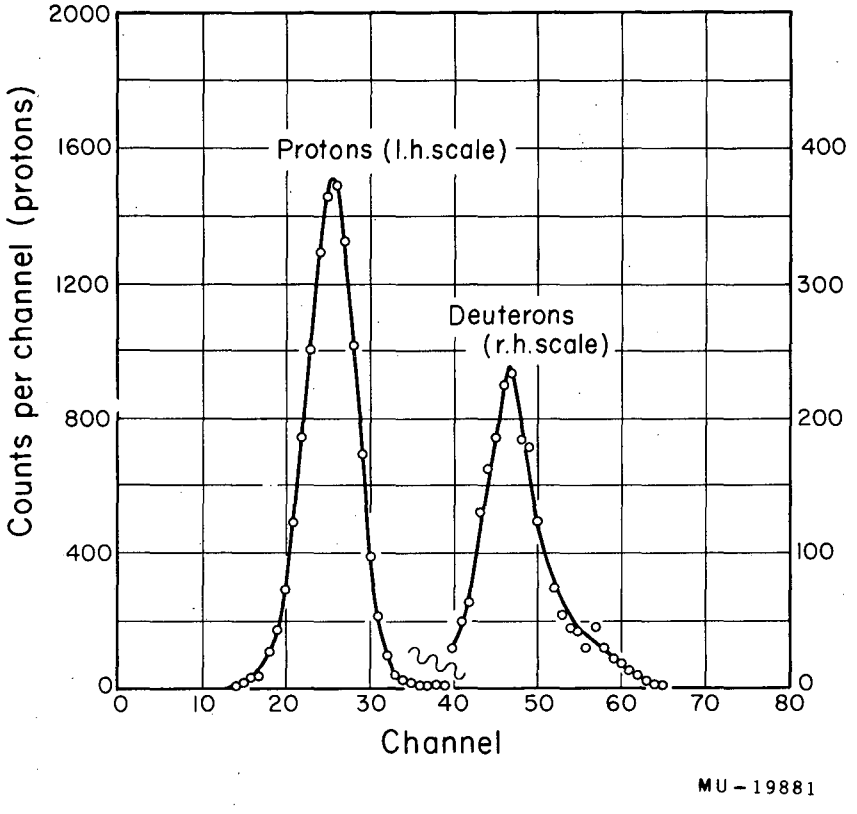

Fig. 4. Multiplier spectrum from C^{12}+He^{4} obtained with the CsI "ΔE" detector.

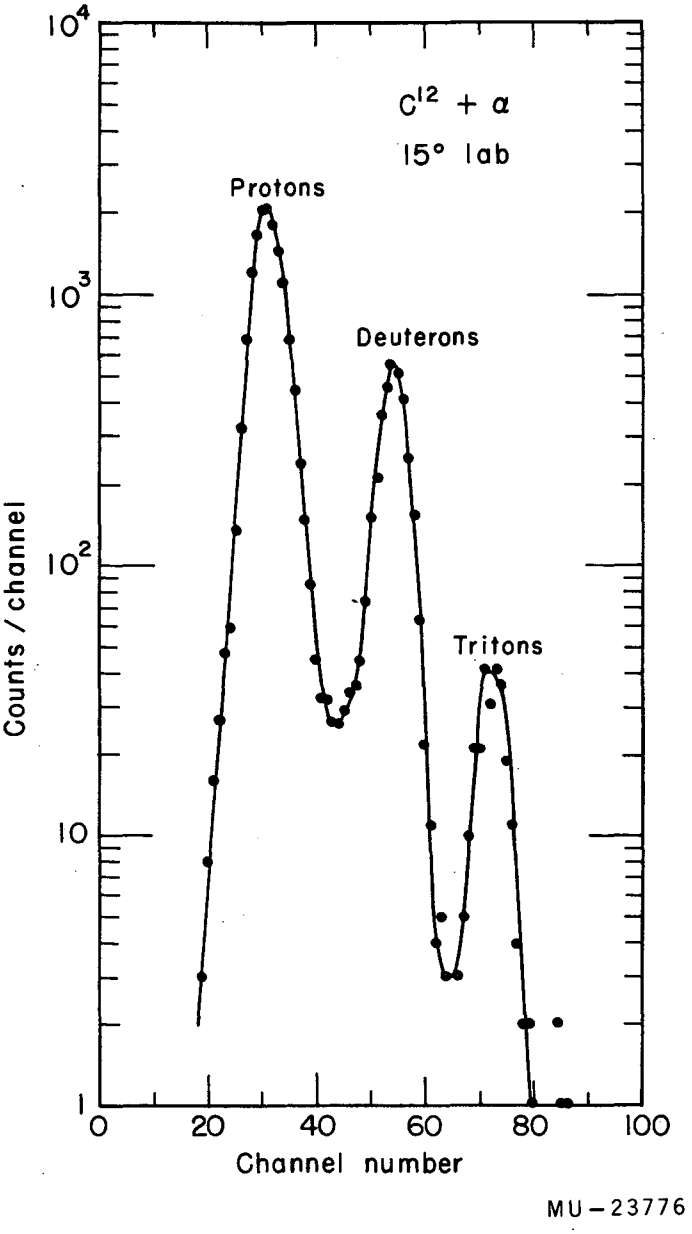

Fig. 5. Multiplier spectrum from C^{12}+He^4 obtained with the silicon "ΔE" detector.

signal and trigger to the Penco and then by adjusting the lower discriminator on the gate to correspond to the center of the proton-deuteron valley and the upper discriminator to correspond to the center of the deuteron-triton valley, so that only the deuteron peak was observed on the Penco. When this was set, the trigger pulse was left unchanged and the E pulse was introduced as the signal to the Penco.

Frequent checks were made which established that the number of deuterons counted as signal pulses corresponded to the number of deuteron triggers that should arise from correctly set discriminators. This was done by recording the total multiplier spectrum with an E trigger for a given amount of beam and determining the number of pulses that arose from deuterons. The trigger discriminators were then set for deuterons and an energy spectrum was obtained for the same amount of beam. The total number of deuterons counted was compared with the number expected from the multiplier spectrum; these numbers agreed within 2%.

Deuteron spectra from various targets were obtained at laboratory angles between 10 deg and 90 to 120 deg. The low differential cross sections observed in the region of the latter angles did not seem to make it worth while, in terms of counting time, to go to larger angles. In order to be certain that only deuterons were recorded in the energy spectra, multiplier spectra were observed and the discriminator settings on the deuteron peak re-set at about 10-deg intervals.

E. Targets

1. Solid Targets

The Li^6 and Li^7 targets were unsupported foils rolled from 99.3% enriched Li^6 metal (obtained from Oak Ridge National Laboratory) and from natural lithium, respectively. Target thicknesses of both were determined by measuring the beam range with the target both in and out and then converting[34,39] this differential range in Al to the range in Li^6 or natural lithium. The Li^6 was approx 9.8 mg/cm^2 thick, and the Li^7, approx 3.8 mg/cm^2; comparisons of absolute α,d cross

sections calculated from independent runs showed the thickness determined above to be accurate to only ±30% because of the nonuniformities in these targets.

The carbon targets were prepared by carbonizing circles of Whatman filter paper clamped between two graphite blocks. These targets were fairly uniform and quite easy to handle. In a preliminary run on the $C^{12}(\alpha,d)N^{14}$ reaction, a deuteron peak arising from the $O^{16}(\alpha,d)F^{18*}$ transition (approx 1.0 Mev) was observed. The oxygen impurity was almost completely removed by heating the targets to 1400 °C in a vacuum for several hours and then allowing them to cool to below 200 °C before exposure to air. However, a residual trace of this deuteron group remained which was not removed by a second vacuum-furnace treatment of the targets. The thickness of the foils was measured by weighing a known area; two foils that were bombarded together gave a total thickness of 3.57 mg/cm^2.

In order to avoid errors in relative cross-section measurements introduced by possible nonuniformities in all the above foils, the targets were positioned at a constant angle to the beam, usually 45 deg, for the entire series of measurements.

2. Gas Targets

Gases were bombarded in a 3-inch-diameter, 2.5-inch-high gas holder placed on the target mount inside the scattering chamber. The gas holder had two approx 120 deg, 0.001-inch Dural, 3/4-inch-high windows, and could be rotated to permit measurements at any laboratory-system angle. This system was connected to an external manometer and to a pumping unit so that the gas pressure could be read and the gas changed if desired. An additional 1/8-inch-diameter slit was placed about 5.5 to 7 inches ahead of the counter collimator to define the solid angle for gas target bombardments.

Both natural nitrogen and 94.6% N^{15} obtained from the Isomet Corporation were investigated. The effective helium ion energy was about 46.5 Mev when the gas holder contained nitrogen at 76 cm Hg and 20 °C.

F. Data Reduction

1. Energy-Level Analysis

In order to determine the energies of the various final states populated, it was necessary to establish a correspondence between the channel number of a deuteron group on the pulse-height analyzer and its energy. After the E signal to the Penco was adjusted to utilize as much of the Penco range as possible, cyclotron-accelerated deuterons were used to establish an energy scale on the NaI crystal from approx 20 Mev down to about 10 Mev by using appropriate absorbers. Then, this scale was extrapolated and used to identify well-known isolated deuteron groups at higher energies, which arose from the particular α, d reaction being investigated. The points from these identified groups and from the accelerated deuterons established an energy-vs-channel calibration of the Penco which covered the entire region of interest. Spectra were taken at various angles and the energies of other groups in the α, d reaction spectrum were obtained. The difference in energy between these groups and the ground-state transition was determined; these differences were converted to energy separations between the particular excited states and the ground state of the product nucleus. After it had been verified that each energy separation determined was relatively constant over a wide angular region -- which indicated that the reaction was following the kinematics of the particular $A(\alpha, d)B^*$ transition investigated and not one from a known or unknown impurity -- the values of this quantity were averaged to establish the excitation of the final state populated.

2. Differential and Total Cross Sections

The conversion of the number of counts observed in a given deuteron peak per μcoulomb of beam to a differential cross section for either solid or gas targets was done by standard methods (e.g., Ref. 40). Total cross sections were obtained by integration of the differential cross sections according to the equation

$$\sigma = 2\pi \int_0^{\pi} \frac{d\sigma}{d\Omega} \sin\theta \, d\theta = 2\pi \int_{-1}^{1} \frac{d\sigma}{d\Omega} \, d(\cos\theta).$$

In practice, the second expression was evaluated by plotting $\frac{d\sigma}{d\Omega}$ vs $\cos\theta$ and obtaining the area under this curve with a planimeter.

The major error in the total cross sections for those cases in which the target thickness could be accurately measured was the statistical error in the determinations of the differential cross sections. The errors due to counting statistics varied from about 2 to 3 % at small angles to about 6 to 9 % at the largest angles investigated. For this reason, the error in the total cross sections is expected to amount to ± 10 % after additional minor errors arising from uncertainties in target thickness, beam measurement, and solid-angle evaluation are incorporated. In some cases the subtraction of a fairly high background was required, and this introduced appreciable error. Whenever target thickness or background subtraction uncertainties produced an absolute error greater than ± 10 %, the nature of the contributing error and the absolute accuracy to be expected are discussed in the appropriate results section.

IV. NUCLEAR STRIPPING THEORIES APPLIED

In order to determine the possibility of spectroscopically identifying final states in an α, d reaction through fitting the angular distributions of the outgoing particle by use of a fairly detailed theory, the two-nucleon stripping theory of Glendenning[13] has been utilized. In addition, the nature of the fits should indicate the extent to which the approximations of this theory are satisfactory, thereby indicating the degree to which distorted wave calculations, for example, might be required to represent these data. Comparisons with the results of Butler theory are made, since this theory has been fairly successful in interpreting single-nucleon transfer reactions and has been applied in some cases[4,5,6] to two-nucleon transfer reactions. The use of Butler theory would be most appropriate for transitions to final states which possessed a strong cluster parentage of the target plus a deuteron. The results of both these theories have been programmed for the University of California IBM 704 computer.

A. Butler Stripping and Knockout Theory

The primary mechanism considered in the analysis of these α, d reactions is that of stripping two nucleons from the incident helium ion. However, two of the target nuclei investigated, Li^6 and N^{14}, can be visualized as an even-even core plus a deuteron, and for their α, d mechanism the possibility that the incident helium ion "knocks out" this deuteron and is then captured is investigated. For this latter case, a high parentage of both "core" + d for the target and "core" + α for the final state should be required. The conditions favoring stripping or knockout processes in general are discussed by Banerjee.[41]

The general Butler expression[14] used is

$$\frac{d\sigma}{d\Omega} \propto \left| \frac{1}{q^2 + \kappa^2} \; W\left[j_L(qR_0),\; h_L(\kappa R_0) \right] \right|^2,$$

with the following definitions holding for both mechanisms:

$$k_i = 2.187 \times 10^{12} \left[\frac{m_a m_T}{m_a + m_T} E_a \right]^{1/2} \text{ (in cm}^{-1}\text{)} ,$$

$$k_f = 2.187 \times 10^{12} \left[\frac{m_d m_F}{m_d + m_F} (Q + E_a) \right]^{1/2} \text{ (in cm}^{-1}\text{)} ,$$

where M_T and M_F are the masses of the target and final nuclei (in amu) and E_a is the incident helium ion energy (in Mev) in the center-of-mass system.

For stripping reactions,

$$\vec{q} = \vec{k}_i - \frac{M_T}{M_F} \vec{k}_f$$

and $$\kappa = [4.783 m_c B + 6.887 m_c Z_1 Z_2 / R_0]^{1/2} \times 10^{12} \text{ (in cm}^{-1}\text{)},$$

where m_c is the reduced mass (in amu) of the captured particle in the residual nucleus, B is the binding energy of the captured particle in the residual nucleus (in Mev), and Z_1 and Z_2 are the atomic numbers of the captured particle and the target nucleus.

For knockout reactions,

$$\vec{q} = \left(\frac{M_T - M_d}{M_T} \right) \vec{k}_i - \left(\frac{M_F - M_a}{M_F} \right) \vec{k}_f$$

and

$$\kappa = \left\{ \left[4.783 m_1 \zeta_1 + 6.887 \left(\frac{m_1 Z z_1}{R_0} \right) \right]^{1/2} \right.$$

$$\left. + \left[4.783 m_2 \zeta_2 + 6.887 \left(\frac{m_2 Z z_2}{R_0} \right) \right]^{1/2} \right\} \times 10^{12} \text{ (in cm}^{-1}\text{)} ,$$

where m_1, ζ_1, and z_1 (or m_2, ζ_2, z_2) are the ejected (or incident) particle's reduced mass (in amu) in the initial nucleus (or final nucleus), binding energy (in Mev) in the initial nucleus (or final nucleus), and charge, respectively; and Z is the charge of the core.

B. Glendenning Two-Nucleon Stripping Theory

The two-nucleon stripping reaction was first considered by El Nadi[42,43] and later by Glendenning[13] and Newns.[17] Glendenning's treatment leads to an expression for the angular distribution which has angular momentum and parity conservation built into it, whereas El Nadi's does not; Newns's treatment is similar to Glendenning's except that the latter considers explicit nuclear structure factors (in the j-j coupling limit) whereas the former leaves them in a general undefined form.

Glendenning's primary assumptions are:

(a) plane waves are used to describe the center-of-mass motion of the incident and outgoing particles;

(b) the target nucleus, unexcited by the reaction, forms the core of the final nucleus with the captured neutron and proton in spin-orbit states about it;

(c) a Gaussian form is chosen to represent the spatial distribution of the internal wave function of the incident particle;

(d) no internal wave function for a deuteron as the outgoing particle is introduced (Newns[17] states that when the alpha-particle wave function is Gaussian, the shape of the resulting angular distribution will be independent of the form of an S-state deuteron spatial wave function); and

(e) the capture of the particles takes place when both are at the nuclear surface.

The general differential cross section is given by

$$\frac{d\sigma}{d\Omega} \propto e^{-\kappa^2/8\gamma^2} \sum_L \frac{C_L}{2L+1} \left| B\left(\ell_n \ell_p L\,; Q\right) \right|^2 , \qquad \text{(IV-1)}$$

where $B(\ell_n\ \ell_p\ L.\,;Q)$ contains the angular dependence of the reaction [except for the damping factor $\exp(-\kappa^2/8\gamma^2)$] and the C_L are nuclear structure factors arising from the extreme j-j coupling scheme used.

[When conservation of angular momentum and parity permits a single-nucleon stripping reaction to occur with more than one value of

the total orbital angular momentum of the transferred nucleon, the angular distribution of the outgoing particle is generally characterized by the lowest of these L values. In some cases, however, the shell-model configuration of the final state requires the captured particle to possess a value of L greater than the lowest value allowed by the conservation laws, and one of the successes of the shell model is that this greater L is usually observed strongly in the angular distribution (see Ref. 44). The detailed two-nucleon stripping theories, however, result in angular distributions involving sums over most of the L values allowed by the conservation laws, so that the nuclear structure factors represent the shell-model-dependent relative weightings of the transferred angular momenta.].

A different C_L is required for each of the three types of target nuclei: even-even, odd-odd, and odd-even (or even-odd). The definitions of the symbols in this equation are

$\vec{\kappa} = \vec{k}_d - \frac{\vec{k}_a}{2}$, the momentum transferred to the outgoing deuteron,

$\vec{Q} = \vec{k}_a - \frac{M_T}{M_F}\vec{k}_d$, the momentum carried into the nucleus by the stripped pair,

$$B(\ell_n \ell_p L;Q) = \sum_{n=0}^{\infty} (-1)^n (2n+1)\, I_{n+1/2}(4\gamma^2 R_0^2) \sum_{\lambda_n=|\ell_n-n|}^{\ell_n+n,\,2}$$

$$\times \sum_{\lambda_p=\max(|\ell_p-n|,\,|L-\lambda_n|)}^{\min(\ell_p+n,\,L+\lambda_n),\,2} j_{\lambda_n}(QR_0/2)\, j_{\lambda_p}(QR_0/2) \sqrt{(2\lambda_n+1)(2\lambda_p+1)}$$

$$\times i^{\lambda_n+\lambda_p} W(\ell_n \ell_p \lambda_n \lambda_p; Ln)\, C^{\lambda_n \lambda_p L}_{0\,0\,0}\, C^{\ell_n\, n\, \lambda_n}_{0\,0\,0}\, C^{\ell_p\, n\, \lambda_p}_{0\,0\,0},$$

where R_0 is the interaction radius chosen,

and $I_{n+1/2}(\rho) = i^{n+1/2} J_{n+1/2}(-i\rho)$.

The constant, γ, in the α-particle internal wave function $\exp(-\gamma^2 \Sigma r_{ij}^2)$ was established as follows: various values of γ were used in attempts to fit the $Li^6(\alpha,d)Be^8$(g.s.), $Li^6(\alpha,d)Be^{8*}$(2.90-Mev), $C^{12}(\alpha,d)N^{14}$(g.s.), and $N^{14}(\alpha,d)O^{16}$ (g.s.) angular distributions, since these experimental results (as will be shown below) possess well-defined structure. The theoretical angular distributions were found to be fairly insensitive to changes in γ, except for the large-angle damping to be discussed in Section G-2, and good sets of fits to these data can be obtained by using γ's corresponding to α-particle radii from 1.30 to 1.45 f. Over this range of radii, the positions of the maxima and minima of these fits vary 1 to 2 deg, and the individual interaction radii vary about 0.1 f. Values of γ corresponding to appreciably different α-particle radii, such as the measured rms radius of the α-particle charge density (1.68 f,[45] or $\gamma = 0.223\times10^{13}$ cm^{-1}), do not produce sets of fits which are as satisfactory as those to be presented, which use an α-particle radius of 1.34 f (or $\gamma=0.280\times10^{13}$ cm^{-1}). That this analysis points to a smaller radius than the electron scattering results may be attributable to approximations in the theory. However, it is also consistent with our expectations based on the following. The wave function used to describe the internal motion of the nucleons in the helium ion does not contain any correlations, although such are certainly there because of the hard core in the internucleon force. Therefore the momentum distribution of the nucleons in the real α-particle will contain higher components than the distribution belonging to our wave function. To get these higher components the radius of the uncorrelated wave function has to be made smaller.

$$\text{Further, } C_L(e\text{-}e) = \{a_{LIJ_f}(j_n j_p)\}^2 , \qquad \text{(IV-2)}$$

where a_{LSJ} is the transformation coefficient from LS to jj coupling, j_n, j_p are the captured particles' total angular momenta, and the final coupling arises from $\overline{J}_f = \overline{J}_i + \overline{J}$, $\overline{J} = \overline{j}_n + \overline{j}_p$.

$$\text{Also, } C_L(o\text{-}o) = \sum_{I=|L-1|}^{L+1} (2I+1)[W(J_i J_f j_n j_p'; I j_p) \times a_{LII}(j_n j_p')]^2 \qquad \text{(IV-3)}$$

For this case an additional restriction is placed on the coupling scheme--the target nucleus is considered to consist of the odd neutron and proton about a spin zero core ($\vec{j}_n + \vec{j}_p = \vec{J}_i$), and one of the captured particles (j_n in the above) is required to enter the same shell-model state as one of the original pair and couple with it to zero total angular momentum; the other captured particle (j_p') couples with j_p to form J_f. Finally,

$$C_L(o\text{-}e) = \sum_{I=|L-1|}^{L+1} (2I+1)[W(Ij_p' j_n J; J_f j_p) \times a_{L1I}(j_n j_p)]^2, \qquad \text{(IV-4)}$$

where $\vec{J}_{core} + \vec{j}_p' = \vec{J}_i$ and $\vec{J}_{core} = \vec{0}$ is assumed,

j_n, j_p are the captured particles' total angular momenta, and the final coupling arises from $\vec{j}_p' + \vec{j}_p = \vec{J}$, $\vec{J} + \vec{j}_n = \vec{J}_f$.

Two simplifications of the above treatment are also investigated to determine their effect on the calculated angular distribution. One involves approximating $B(\ell_n \ell_p L; Q)$ in Eq. (IV-1) by

$$B(\ell_n \ell_p L; Q) = C \begin{pmatrix} \ell_n & \ell_p & L \\ 0 & 0 & 0 \end{pmatrix} j_L(QR_0). \qquad \text{(IV-5)}$$

The other involves treating the α-particle as a point cluster of nucleons, rather than as possessing a finite size. For this, $B(\ell_n \ell_p L; Q)$ is given by Eq. (IV-5), and $\gamma \to \infty$, eliminating the damping factor.

The detailed equation and the two approximate equations were coded by using FORTRAN for the IBM 704 computer. A copy of the FORTRAN listing is in the Appendix. Comparisons between the detailed and the approximate expressions for $B(\ell_n \ell_p L; Q)$ were made to determine the latter's validity; the point α-particle approximation was used in attempts to produce better fits to the large-angle data. These results are discussed subsequently.

V. RESULTS AND CONCLUSIONS

A. General Discussion

The various α,d reactions investigated are treated separately in the following, and the analysis of the results follows the general lines stated in the introduction. The energy levels of the product nuclei observed in these reactions are correlated where possible with their expected configurations in an effort to determine the nature of any preferential population of final states that might arise.

Primary attention in the analysis of the angular-distribution data has been directed toward determining the closeness of fits obtainable from the detailed Glendenning theory[13] (the approximations mentioned in Section IV B are used only when so stated) and the possibility of acquiring spectroscopic information from these fits about the product levels observed. As noted earlier, the nuclear-structure factors of this theory are based on explicit coupling schemes in the j-j coupling limit. However, many features of the level structure of the 1 p -shell nuclei (all but one of the reactions studied take place entirely within this shell) have been described by coupling intermediate between L-S and j-j: Li^6 is near the L-S limit, with the relative strength of the spin-orbit forces increasing as the shell fills, resulting in considerable j-j coupling near the shell closure.[46,47,48] From this, it might be expected that the theory would be more successful in describing the $N^{14}(\alpha,d)O^{16}$ reaction than the $Li^6(\alpha,d)Be^8$ reaction. In all calculations using this theory, only the simple shell-model configuration of the target nucleus is employed.

B. $Li^6(\alpha,d)Be^8$

Figures 6 and 7 show a typical multiplier spectrum and a typical deuteron energy spectrum (27.5 deg), respectively, for Li^6 + helium ions. Smooth curves have been drawn through the experimental results for all the energy spectra to be presented, but without indicating the statistical certainties of various peaks. Table I shows the energy levels of Be^8 observed and their statistically weighted cross sections: in addition, the reduced α-particle width in terms of the Wigner limit (θ_α^2) of each level

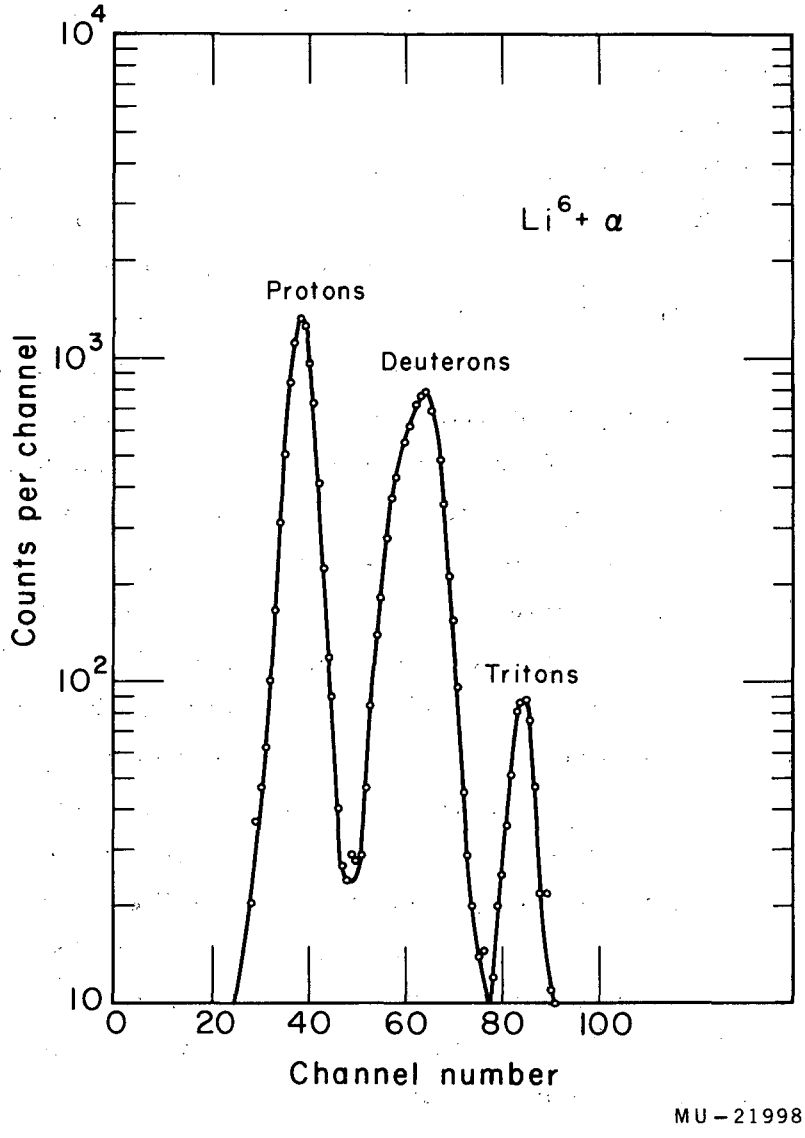

Fig. 6. Multiplier spectrum from the bombardment of Li^6 with 48-Mev helium ions.

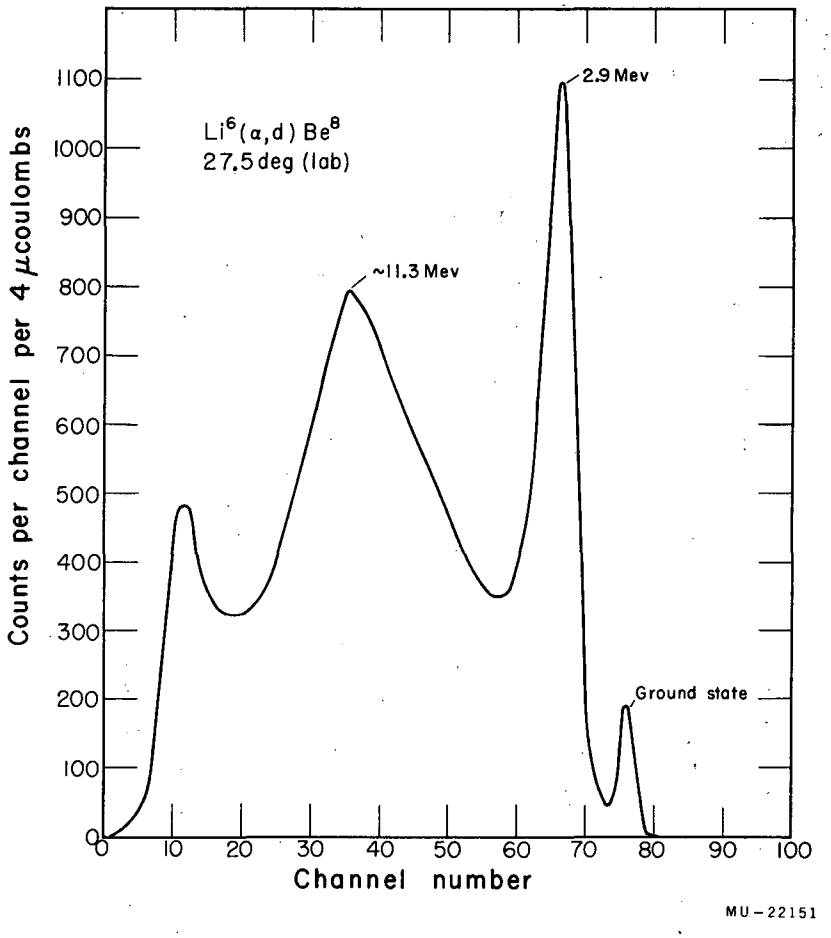

Fig. 7. Deuteron energy spectrum from the reaction $Li^6(\alpha, d)Be^8$; Q values for the various peaks are shown.

Table I. Correlation of Be^8 levels observed in this experiment with those previously reported.

Levels identified	Previously reported levels[a]				$\frac{\langle\sigma_f\rangle^c}{2J_f+1}$	Angular interval over which $\langle\sigma_f\rangle$ was calculated.
(Mev)	Energy (Mev) ;	J^π, T ;	Decay ;	θ_a^2	(mb)	(deg, c.m.)
0[b]	0	0+, 0	α	0.15	1.0_2	12.8 - 104.5
2.9[b]	2.90	2+, 0	α	0.7	1.4_2	13.0 - 88.8
11.3 ± 0.4	11.4	4+, 0	α	0.95	$2.67^{+0.37}_{-0.22}$	12.5 - 85.6

a. References 49, 50, 51.

b. These levels were identified by means of a deuteron energy scale constructed by the use of cyclotron-accelerated deuterons. After satisfactory identification, deuterons corresponding to these levels were used to extend the scale to higher energies.

c. The absolute value of these cross sections is not known to better than ± 30%, owing to uncertainties in the Li^6 target thickness.

is given. The estimated error to be expected in this and subsequent determinations of well-defined levels is about ± 0.2 Mev; for broad levels, ± 0.4 Mev. Ground-state Q values were taken from Ashby and Catron[52] in all cases. The first three levels of Be^8 have been described as $\alpha+\alpha$ clusters, and some indication of the validity of this description can be obtained by correlating with each state the appropriate θ_α^2 as obtained from the scattering of helium ions on helium -- large reduced widths should belong to states which are well represented by $\alpha+\alpha$ clusters.[51] The cross sections for transitions to these three levels recorded in Table I are seen to increase as do their reduced widths; this result would be difficult to interpret if the reaction mechanism involved were stripping onto a Li^6 "core," since all three levels on a simple shell-model picture arise from capturing two nucleons into $p_{3/2}$ states and might be expected to possess comparable α,d reaction cross sections. The Li^6 ground state, however, may possess considerable $d+\alpha$ cluster parentage,[51,53] and a reaction mechanism involving

(a) stripping a deuteron from the incident helium ion which couples to an α particle with the deuteron cluster present in the Li^6 configuration, or

(b) knocking out this deuteron cluster

might be expected to result in reaction cross sections with the observed behavior.

The angular distributions of deuterons corresponding to the ground state and the 2.90-Mev state of Be^8 are shown in Figs. 8 and 9, respectively. The errors shown (size of the point or extension bars on it) in these and subsequent graphs represent counting statistics only; the angular accuracy in all cases is about ± 1 deg.

The angular distributions of both states are very similar to those obtained by Zeidman and Yntema[4] in their investigation of this reaction with 43-Mev helium ions: (a) the positions of the maxima and minima and the shape of the ground-state angular distribution and (b) the slope of the 2.90-Mev state differential cross sections are about the same at both energies. The angular distribution of protons from the $C^{12}(\alpha,p)N^{15}$ reaction is equally insensitive to the helium ion energy in the range 33.6 to 38.6 Mev (the highest studied).[10]

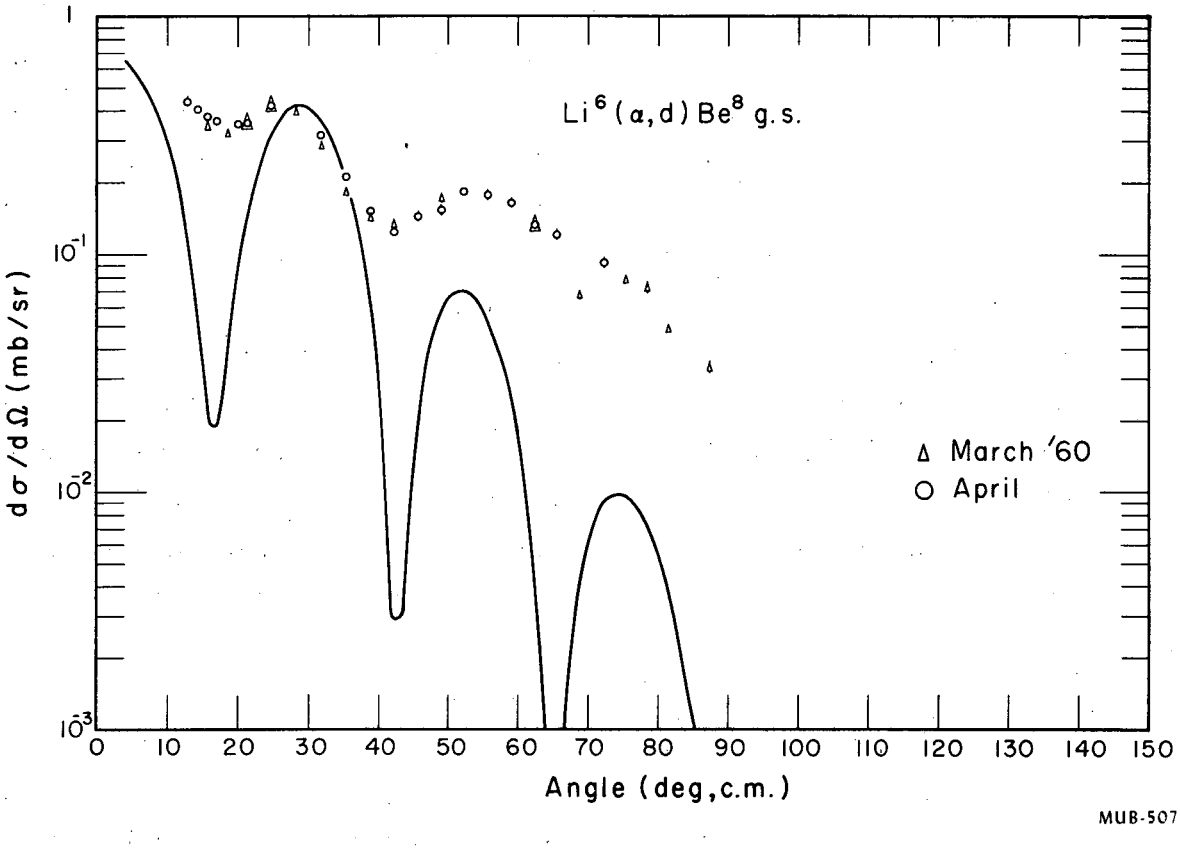

Fig. 8. Angular distribution of deuterons from formation of the ground state of Be^8. The solid line was calculated from the Glendenning equation by using $j_n = j_p = 3/2$, $R_0 = 7.6$ fermis.

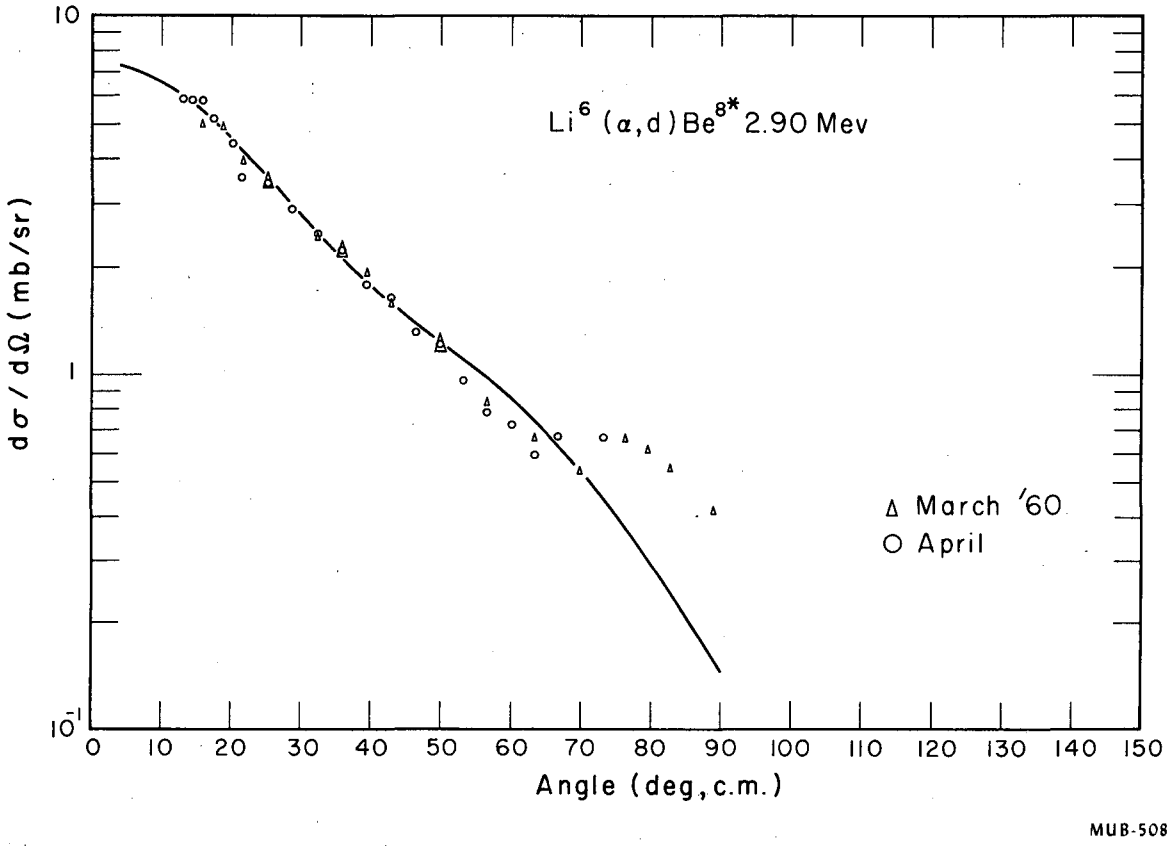

Fig. 9. Angular distribution of deuterons from formation of the 2.90-Mev level of Be^8. The solid line was calculated from the Glendenning equation by using $j_n = j_p = 3/2$, $R_0 = 2.1$ fermis.

In applying Glendenning's theory to these results, the nuclear structure factors which are used are those of Eq. (IV-3), $C_L(o\text{-}o)$. As noted earlier, the restrictions placed on these C_L require that at least one of the captured particles enter the same shell-model state as one of the original pair (the target nucleus is considered to consist of a pair of nucleons about a spin zero core). For the $Li^6(\alpha,d)Be^8$ (g.s.) results, the restrictions define only a single set of reasonable individual-particle total angular momentum states in the final nucleus, therefore only the interaction radius (R_0) can be varied to fit the data; for the $Li^6(\alpha,d)Be^{8*}$ (2.90-Mev) data, the $[(p_{3/2})^3(p_{1/2})]_{2+}$ final-state configuration was compared with the expected[47] $[(p_{3/2})^4]_{2+}$ configuration.

The reactions, shell-model states of the captured particles, final nuclear configurations, radii that gave fits, and figure numbers corresponding to the plotted results of the better fits for these transitions and the reactions involving the other odd-odd target nucleus N^{14} (which are discussed in that section) are given in Table II. In addition, the ratio of

$$\frac{C_{L'\,max}}{C_{L'\,min}} = \frac{C_{L\,max}/(2L_{max}+1)}{C_{L\,min}/(2L_{min}+1)} ,$$

i.e., the relative weighting of the total orbital angular momentum transfers involved in the reaction, is tabulated. The allowed values of L are given by Eqs. (II-1) and (II-3). For the $Li^6(\alpha,d)Be^8$ (g.s.) transition, $1+ \rightarrow 0+$, the angular momentum conservation equation (II-5) requires $L = 0, 1, 2$, and the parity selection rule restricts this to $L = 0,2$. The additional restriction $\overline{L} = \overline{\ell}_n + \overline{\ell}_p$ has no effect in this case, since the two particles are captured into the p shell. However, for the $Li^6(\alpha,d)Be^{8*}$ (2.90-Mev) transition, $1+ \rightarrow 2+$, Eq. (II-5) and parity conservation leave $L = 0, 2, 4$; the capture of the pair into the p shell then restricts this to $L = 0, 2$.

The fit to the $Li^6(\alpha,d)Be^8$ (g.s.) results is fairly unsuccessful. Since Li^6, as noted above, may be visualized as an even-even core plus a deuteron, it is interesting to compare both Butler stripping fits and

Table II. Results of the application of Glendenning's theory to the $Li^6(a,d)Be^8$ and $N^{14}(a,d)O^{16}$ reactions.

Reaction	Captured j_n	Captured j_p	Final nuclear configuration	Radius for best fit (f)	Figure number of graph	$\frac{C_{L'max}}{C_{L'min}}$
$Li^6(a,d)Be^8$(g. s.)	3/2	3/2	$\left[(p_{3/2})^4\right]_{0+}$	7.6	8	$\frac{C_{2'}}{C_{0'}} = 0.0400$
$Li^6(a,d)Be^{8*}$(2.90-Mev)	3/2	3/2	$\left[(p_{3/2})^4\right]_{2+}$	2.1	9	$\frac{C_{2'}}{C_{0'}} = 0.513$
" "	3/2	1/2	$\left[(p_{3/2})^3(p_{1/2})^1\right]_{2+}$	No fit as acceptable	-	$\frac{C_{2'}}{C_{0'}} = 3.10$
$N^{14}(a,d)O^{16}$(g. s.)	1/2	1/2	$\left[(p_{1/2})^4\right]_{0+}$	5.35	22	$\frac{C_{2'}}{C_{0'}} = 4.00$
$N^{14}(a,d)O^{16*}$(6.14-Mev)	1/2	5/2	$\left[(p_{1/2})^{-1}(d_{5/2})^1\right]_{3-}$	6.20	23	$\frac{C_{3'}}{C_{1'}} = 0.345$
$N^{14}(a,d)O^{16*}$(8.88-Mev)	1/2	5/2	$\left[(p_{1/2})^{-1}(d_{5/2})^1\right]_{2-}$	5.48	24	$\frac{C_{3'}}{C_{1'}} = 1.42$
" "	1/2	3/2	$\left[(p_{1/2})^{-1}(d_{3/2})^1\right]_{2-}$	5.46	Equally acceptable but not graphed	$\frac{C_{3'}}{C_{1'}} = 1.71$

knockout fits to the Glendenning result. It should be noted that the similarity of the stripping and knockout kinematics makes it very difficult in most cases to determine the reaction mechanism through differences in the respective Butler fits if fairly wide variations in the interaction radii are permitted. Figure 10 shows the best fit obtained by using Butler stripping theory --- $L = 0$, $R_0 = 6.9$ f --- which is somewhat worse than the Glendenning fit, and there is no equivalent knockout fit for $L = 0$, $R_0 \leq 8$ f. Approximately the same results were obtained by Zeidman and Yntema,[4] who also tried simple Butler theory and both stripping and knockout parameters. In all cases the interaction radii are too large to be meaningful.

The extremely successful fit to the $Li^6(\alpha, d)Be^{8*}$ (2.90-Mev) results (no Butler stripping or knockout fit) occurs at a very small interaction radius --- one which would correspond to interaction within the nuclear volume. This small radius, the absence of an acceptable ground-state fit, and the uncertainty in applying a stripping theory based on j-j coupling to low-lying Be^8 levels, however, prevents a conclusion that the $Li^6(\alpha, d)Be^{8*}$ (2.90-Mev) reaction follows a stripping mechanism. It should also be noted that no fit for a $[(p_{3/2})^3 (p_{1/2})]_{2+}$ final state was obtained, so that in this case the use of the theory would aid in configuration assignments.

C. $Li^7(\alpha, d)Be^9$

Figures 11 and 12 show a typical multiplier spectrum and a typical deuteron energy spectrum (10 deg, lab), respectively, for Li + helium ions. Since a natural lithium target was used, two groups due to the $Li^6(\alpha, d)Be^8$ reaction were also detected. Table III compares the Be^9 energy levels observed in this experiment with those previously reported. Little is known experimentally about the Be^9 levels; the combination of high backgrounds and an inability to follow the kinematics of various deuteron groups over a wide angular region restricted our confirmation of some of the excited states previously reported. The theoretical determination of the nature of the Be^9 levels has, of course,

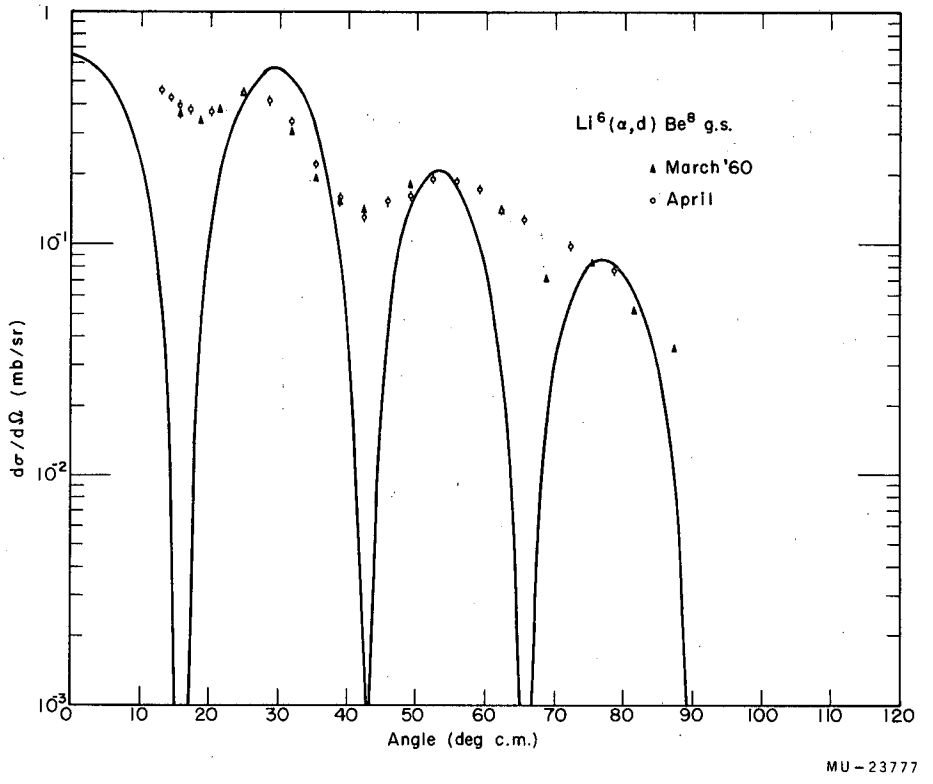

Fig. 10. Angular distribution of deuterons from formation of the ground state of Be^8. The solid line was calculated from the Butler equation by using L=0, R_0=6.9 fermis.

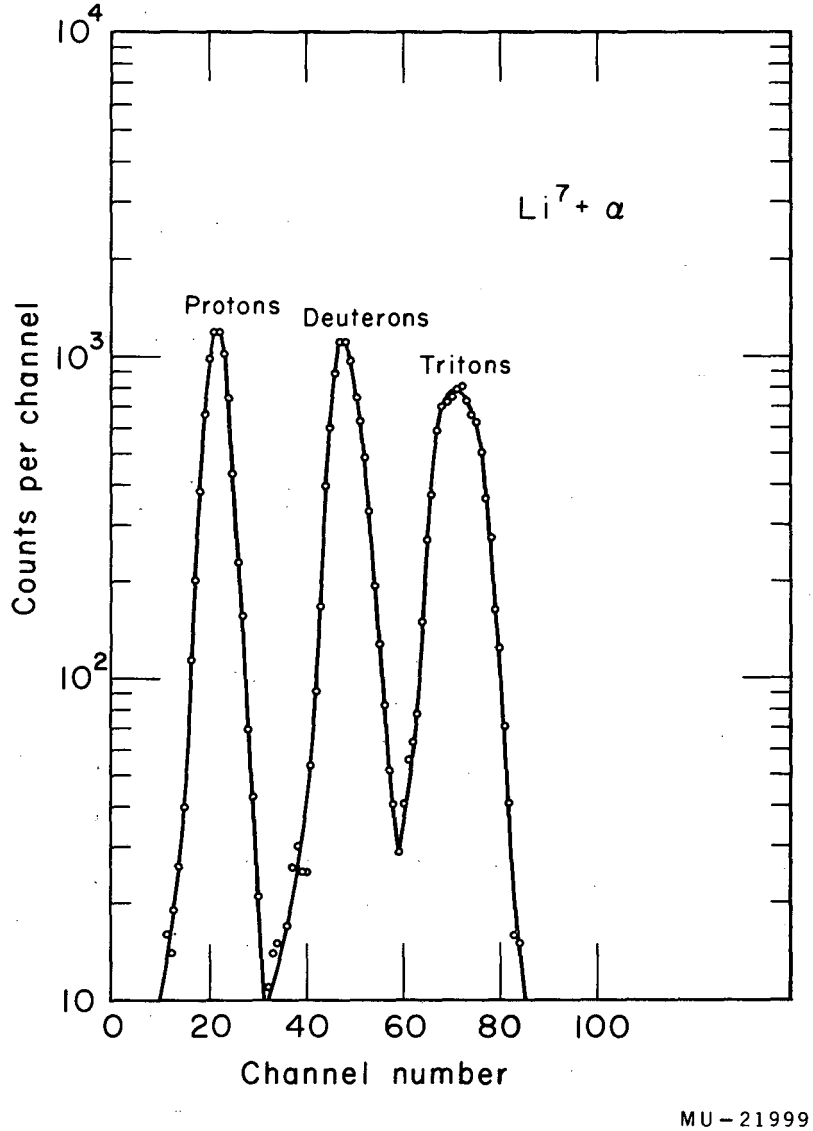

Fig. 11. Multiplier spectrum from the bombardment of natural Li with 48-Mev helium ions.

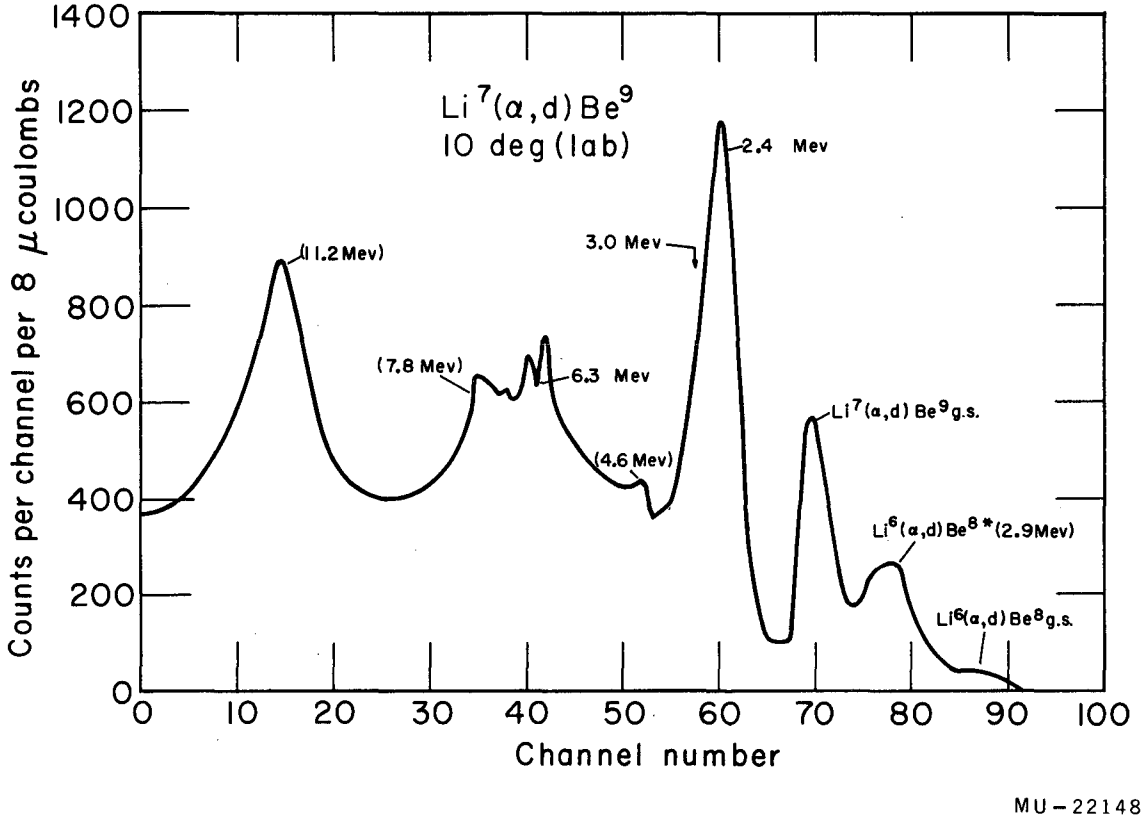

Fig. 12. Deuteron energy spectrum from the reactions Li(α, d)Be. Q values for the various peaks are shown.

Table III. Comparison of Be^9 levels observed in this experiment with those previously reported.[a]

Levels identified (Mev)	Previously reported levels		
	Energy (Mev)	J^π	T
0[b]	0	3/2 -	
	1.75	1/2(+)	
2.4 ± 0.2	2.430	(5/2-)	
3.0 ± 0.2[c]	3.04	(≤3/2)	
(4.6 ± 0.4)[d]	(4.74)		
6.3 ± 0.4	6.76		
(7.8 ± 0.4)[d]	(7.94)		
	(9.1)		
(11.2 ± 0.4)[d]	(11.3)		
	(13.3)		

a. Reference 49

b. See footnote b, Table I.

c. This level was not separately resolved from the 2.4-Mev level; however, the width of the 2.4-Mev level was too great to correspond to that level alone.

d. Although deuterons exciting this level were detected, it is felt that the high background present in the data and the impossibility of following the kinematics over a wide angular interval prevent definite identification.

been severely hampered by the lack of confirmed experimental data. Recent results indicate that the 1.75-Mev state (not observed in this reaction; whether this was due to the background and the presence of a strong 2.4-Mev level is not known) is not a state in the usual sense, but is an aspect of spatial localization produced by a sequence of two-body reactions resulting from the decay of an excited nucleus.[54] In addition, the 2.43-Mev and 3.04-Mev states are interpreted to arise from two-body clusters of $Be^8(2+)+n$ or $Be^8(0+)+n$; the tentative spin and parity assignments for the 3.04-Mev state are 3/2+ or 5/2+. If these parity assignments are correct, the interpretation of the low-lying levels of Be^9 in terms of intermediate coupling in the 1p shell will be in some difficulty, since this analysis explicitly requires negative parity for the 3.04-Mev state.[55, 56]

Figure 13 shows the angular distribution of the deuterons from the ground state of Be^9. The integrated cross section over the angular region covered is 1.1_5 mb; this absolute value is estimated to be accurate to ± 40% because of uncertainties in the Li target thickness and to the necessity of correcting the differential cross section for deuterons from the $Li^6(\alpha,d)Be^{8*}$ (2.9-Mev) reaction, which fell under the ground-state peak at various angles. These corrections were done as follows: (i) the counts at a particular angle due to deuterons from both the $Li^7(\alpha,d)Be^9$(g.s.) and the $Li^6(\alpha,d)Be^{8*}$ (2.9-Mev) reactions were totaled, as were (ii) the counts from the $Li^6(\alpha,d)Be^8$ (g.s.) reaction; then the previously obtained $Li^6(\alpha,d)Be^8$ results were used to establish a ratio, for this angle, of

$$\frac{d\sigma/d\Omega\,(Be^{8*}(2.9\text{-Mev}))}{d\sigma/d\Omega\,(Be^8(\text{g.s.}))},$$

and this ratio was multiplied by the counts (ii) calculated above and subtracted from (i).

In analyzing this angular distribution with the Glendenning equation, two different final-state configurations were investigated to determine whether the theory would prefer one to the other. The transitions assumed were

$$[(\text{core})_0+(p_{3/2})]_{3/2^-} \longrightarrow [(\text{core})_0+(p_{3/2})^2_{J=0}(p_{3/2})]_{3/2^-}$$

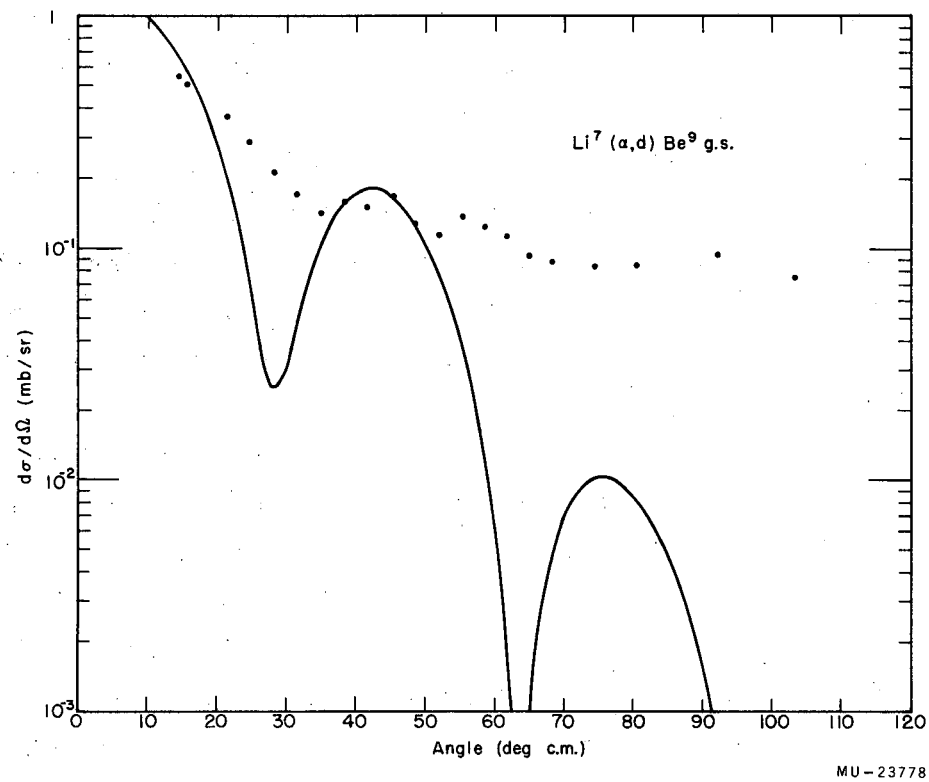

Fig. 13. Angular distribution of deuterons from formation of the ground state of Be^9. The solid line was calculated from the Glendenning equation by using $j_n = j_p = 3/2$, $R_0 = 5.45$ fermis.

(this is the expected j-j coupling shell-model ground state; the ratio of the nuclear structure factors, C_2/C_0, is unchanged for $\vec{J} = \vec{j}_p + \vec{j}_{p'} = 2$ rather than the 0 value chosen here),

and $[(\text{core})_0 + (p_{3/2})]_{3/2^-} \longrightarrow [(\text{core})_0 + (p_{3/2})^2_{J=0} (p_{1/2})]_{1/2^-}$

(the ground-state spin is known to be 3/2-; this final-state configuration is assumed only to test the theory). The nuclear structure factors, C_L(o-e), are given in Eq. (IV-4). Detailed information on the fits similar to that for the odd-odd nuclei discussed earlier is given in Table IV for the $Li^7(\alpha, d)Be^9$ (g. s.) transition [and also for the $N^{15}(\alpha, d)O^{17}$ (g. s.) transition, which is discussed later].

The fits to the fairly structureless experimental angular distribution for both assumed final states are very similar and fairly poor, and the interaction radii differ by only 0.09 f, so that the theory would not indicate a preferred final state. The differences in these two fits, as in the analysis of the $Li^6(\alpha, d)Be^{8*}$ (2.90-Mev) results, arise only from changes in the C_L factors, and not from the $B(\ell_n \ell_p L; Q)$ factors; both factors are varied in the analysis of the $C^{12}(\alpha, d)N^{14}$ and $N^{15}(\alpha, d)O^{17}$ reactions.

The best fit to these data using Butler stripping theory ($L = 2$, $R_0 = 7.2$ f) is shown on Fig. 14, and is somewhat better than the above fits. Additional Butler fits are obtained for $L = 0$, $R = 7.4$ f and for $L = 4$, $R = 6.43$ f; the former is poorer than the plotted fit, whereas the latter is equally acceptable. This multiplicity of fits arises from the high linear momentum transfer present in these experiments and the asymptotic behavior of the spherical Bessel functions. It should also be noted that the interaction radii required by the Glendenning fits are more reasonable than those arising from the Butler fits.

Table IV Results of the application of Glendenning's theory to the $Li^7(a,d)Be^9$ and $N^{15}(a,d)O^{17}$ reactions.

Reaction	Transition			Radius for best fit (f)	Figure number of graph	$\frac{C_{L'max}}{C_{L'min}}$
	initial state	→	final state			
$Li^7(a,d)Be^9$(g.s.)	$[(core)_0+(p_{3/2})]_{3/2^-}$	→	$[(core)_0+(p_{3/2})_0^2(p_{3/2})]_{3/2^-}$	5.45	13	$C_2'/C_0'=1.30$
"	$[(core)_0+(p_{3/2})]_{3/2^-}$	→	$[(core)_0+(p_{3/2})_0^2(p_{1/2})]_{1/2^-}$	5.54	Equally acceptable but not graphed.	$C_2'/C_0'=0.625$
$N^{15}(a,d)O^{17}$(g.s.)	$[(core)_0+(p_{1/2})]_{1/2^-}$	→	$[(core)_0+(p_{1/2})_0^2(d_{5/2})]_{5/2^+}$	6.0_0	28	$C_3'/C_1'=0.583$
"	$[(core)_0+(p_{1/2})]_{1/2^-}$	→	$[(core)_0+(p_{1/2})_0^2(s_{1/2})]_{1/2^+}$	6.3_0	Acceptable but not graphed.	only C_1 allowed

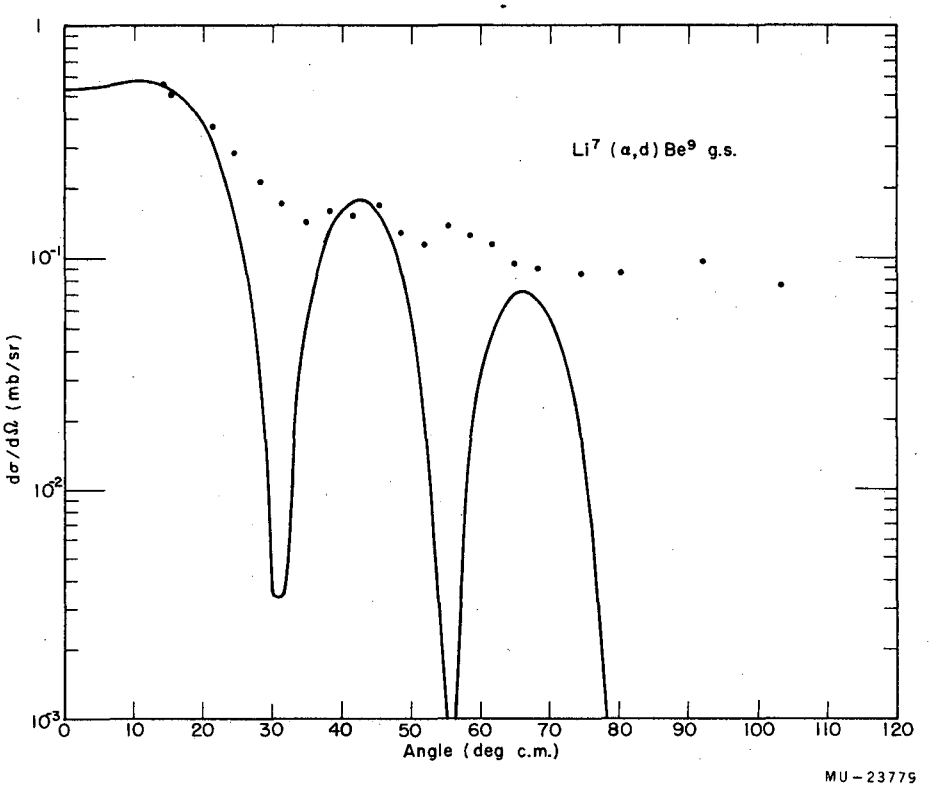

Fig. 14. Angular distribution of deuterons from formation of the ground state of Be^9. The solid line was calculated from the Butler equation using L=2, $R_0 = 7.2$ fermis.

D. $C^{12}(a,d)N^{14}$

Figures 4 and 5 (discussed earlier) show typical multiplier spectra for C^{12} + helium ions; a deuteron energy spectrum at 15 deg (lab) from this reaction is reproduced in Fig. 15. Table V compares the energy levels observed in this experiment with those previously reported; energy-level analyses from two investigations of this reaction are tabulated to indicate the precision obtained in these level determinations. A peak from the $O^{16}(a,d)F^{18*}$ (approx 1.0-Mev) transition from an oxygen impurity in the target is indicated on Fig. 15. To determine the effect of this impurity on possible energy-level and differential cross section analysis, the $O^{16}(a,d)F^{18}$ reaction was briefly investigated. A deuteron group corresponding to a reaction leading to F^{18*} (approx 1.0-Mev) was found to dominate the spectrum at all angles of interest, so that negligible error arises from neglecting this impurity in sections of the $C^{12}(a,d)N^{14}$ spectrum which do not include this group (over most of the angular interval investigated, groups from the $O^{16}(a,d)F^{18*}$ ($\approx$ 1.0-Mev) transition did not interfere with either the $C^{12}(a,d)N^{14}$ (g. s.) or $C^{12}(a,d)N^{14*}$ (3.95-Mev) transition).

At no angle was a deuteron group observed that corresponded to formation of the T=1 first excited state of N^{14}(2.31-Mev). The absence of this group is expected from angular momentum and parity conservation and from isotopic spin conservation, as discussed in Section II for $J_i^{\pi_i} = 0+$, $T_i = 0 \rightarrow J_f^{\pi_f} = 0+$, $T_f = 1$ a, d transitions. The oxygen impurity discussed above obscured at many angles the position on the energy spectrum where deuterons from the T = 1 state might appear. However, an upper limit for the differential cross section at 15 deg for the $C^{12}(a,d)N^{14*}$ (2.31-Mev) transition can be set at $\leq$ 0.95 % of the ground state differential cross section.

An analysis of Table V indicates that the a, d reaction is rather selective in the choice of final states populated, even when no isotopic spin selection rules inhibit the transitions. Only one final state was populated strongly enough to be definitely identified above the background in the energy interval between 7.03 and 9.17 Mev -- see footnote c,

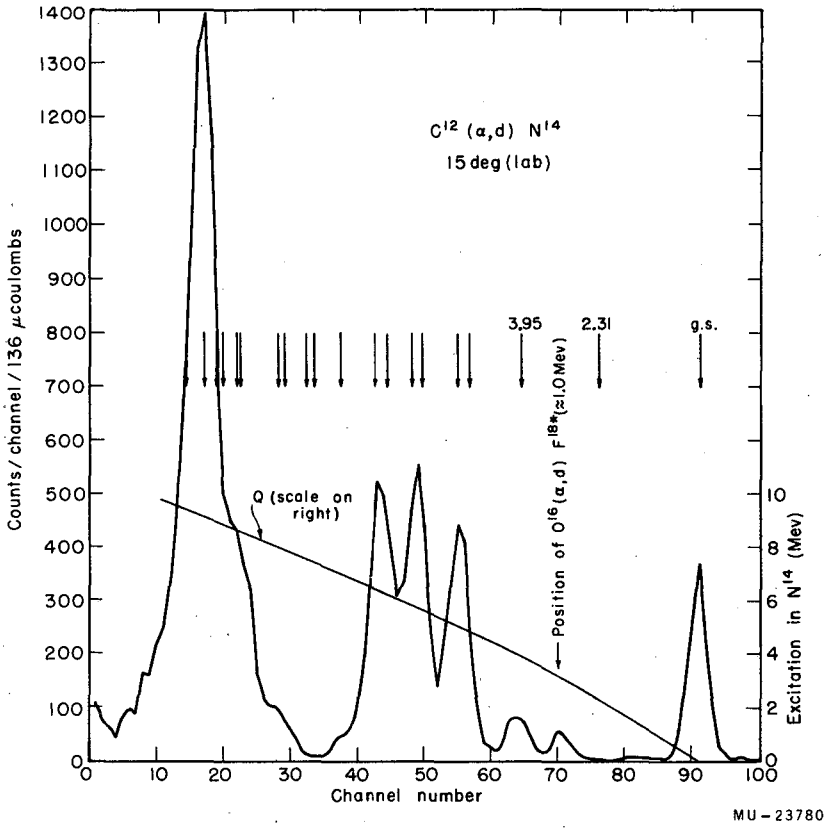

Fig. 15. Deuteron energy spectrum from the reaction $C^{12}(a,d)N^{14}$. Q values for the various peaks are shown.

Table V. Comparison of N^{14} levels observed in this experiment with those previously reported.[a]

N^{14} level energies (Mev)				
Levels Identified		Previously Identified Levels		
November, 1959	December, 1960	Energy	J^{π}	T
0[b]	0[b]	0	1+	0
		2.312	0+	1
3.95[b]	3.95[b]	3.945	1+	0
		4.910	(0-)	0
5.11±0.2	5.16±0.2	5.104	2(-)	0
5.77±0.2		5.685	1(-)	0
	5.86±0.2	5.832	3(-)	?
6.24±0.2		6.23	1(-)	0
	6.46±0.2	6.44	(3)?	0
	c	7.03	(2)?	0
		7.47	? ?	?
		7.60	? ?	?
		7.962	? ?	0
		8.060	1-	1
		8.62	0+	1
		8.71	0-	1
		8.903	3-	(1)
8.84±0.2[d]	9.01±0.2[d]	8.99	(1+)	?
		9.17	(2, 1)(+)	1

a. References 49 and 57.

b. See footnote b, Table I.

c. A weak deuteron group corresponding to an excited state of O^{16} at 7.17±0.2 Mev was observed in these data at several angles.

d. This level is assigned to the known level at 8.99 Mev in both cases, since the neighboring levels are all believed to be T=1. The isotopic spin of the 8.99-Mev level has not been reported; if this assignment is correct, it is a T=0 level.

Table V, however, -- even though three states in this region are known to be T=0 (and the isotopic spins of two of them are not established). However, the energy resolution was not high enough to set low limits for the cross sections to these unobserved, known levels. Except for the 7.03-Mev level (discussed later) no shell-model configuration assignments have been advanced for the non-T=1 levels in this region.[57]

The N^{14} states at 4.91 and 5.69-Mev are expected to arise from $p_{1/2}\, s_{1/2}$ configurations; and the 5.10- and 5.83-Mev states, from $p_{1/2}\, d_{5/2}$ configurations.[57] The formation of these states would involve entry of the captured neutron and proton into different shell-model levels, or else a marked rearrangement of the C^{12} core. At least two of these four states were strongly formed; statistically weighted $(\sigma_f/2J_f+1)$ cross sections for the individual levels would be necessary to determine whether these transitions are as "allowed" as those in which the captured nucleons enter equivalent shell-model levels. The 6.23-Mev state, if present in the peak observed at about this energy, would involve entry of both captured particles into the same shell-model levels, since this state is thought to be an admixture of $(s_{1/2})^2$ and $(d_{5/2})^2$ configurations.[58]

The cross sections were obtained for the $C^{12}(\alpha,d)N^{14}$ (g.s.) transition (1.8 mb integrated from 10 to 133 deg; estimated absolute accuracy ±10%) and the $C^{12}(\alpha,d)N^{14*}$ (3.95-Mev) transition (0.36 mb integrated from 10 to 90 deg; estimated absolute accuracy ±25%).

Since both these cross sections require the same statistical weighting, it appears that the ground state is formed with a cross section 4 to 5 times that of the 3.95-Mev state. Comparing this ratio to that expected from a transfer mechanism for transitions between the shell-model configurations of the various states shows it to be in reasonable agreement: Kurath's intermediate-coupling calculations[48] in the 1 p shell indicate the nucleon configurations in the C^{12} (g.s.) to be $48.7\%\ (p_{3/2})^8 + 40.2\%\ (p_{3/2})^6 (p_{1/2})^2 + 7.2\%\ (p_{3/2})^5 (p_{1/2})^3 + 3.4\%(p_{3/2})^4 (p_{1/2})^4$. Then, if we consider the N^{14} (g.s.) to arise from a $(p_{3/2})^8 (p_{1/2})^2$ configuration and the N^{14*} (3.95 Mev) state from

a $(p_{3/2})^{-1}(p_{1/2})^{-1}$ configuration[57] (although Talmi and Unna[58] state that the ground state has a strong admixture of the $(p_{3/2})^{-1}(p_{1/2})^{-1}$ configuration, and the 3.95-Mev state an admixture of the $(p_{3/2})^{8}(p_{1/2})^{2}$ configuration)[58]; these two transitions should arise thus:

$C^{12}(\alpha,d)N^{14}$(g.s.):

$$(p_{3/2})^{8} \xrightarrow{(p_{1/2})^{2}} (p_{3/2})^{8}(p_{1/2})^{2},$$

$$(p_{3/2})^{6}(p_{1/2})^{2} \xrightarrow{(p_{3/2})^{2}} (p_{3/2})^{8}(p_{1/2})^{2},$$

$C^{12}(\alpha,d)N^{14*}$ (3.95-Mev):

$$(p_{3/2})^{6}(p_{1/2})^{2} \xrightarrow{(p_{3/2}\,p_{1/2})} (p_{3/2})^{7}(p_{1/2})^{3},$$

$$(p_{3/2})^{5}(p_{1/2})^{3} \xrightarrow{(p_{3/2})^{2}} (p_{3/2})^{7}(p_{1/2})^{3}.$$

assuming that no core excitation takes place. It is clear that, even if capture into nonequivalent levels $(p_{1/2}+p_{3/2})$ is as probable as capture into identical levels ($p^{2}_{1/2}$ or $p^{2}_{3/2}$), the ground state transition will be favored, since it can arise from components of the C^{12} wave function which total 88.9%. The components leading to the N^{14} 3.95-Mev state, on the other hand, add up to only 47.4%. The observed ratio is about 4 to 5, however. The theoretical ratio would be about 5 if addition of particles to the $(p_{1/2}+p_{3/2})$ subshells were four times less probable than addition to the same subshells. It is interesting that the 7.03-Mev state is not more strongly populated in this reaction, since it, like the 3.95-Mev state, is expected to arise from a $(p_{3/2}^{-1}\,p_{1/2}^{-1})$ configuration.[57]

The angular distributions of the deuterons from the $C^{12}(\alpha,d)N^{14}$ (g.s.) and $C^{12}(\alpha,d)N^{14*}$ (3.95-Mev) transitions are shown in Fig. 16 and 17, respectively. The low intensity deuteron group corresponding to the latter transition was difficult to separate from deuterons to nearby levels, and the accuracy of the points is probably only ± 20%.

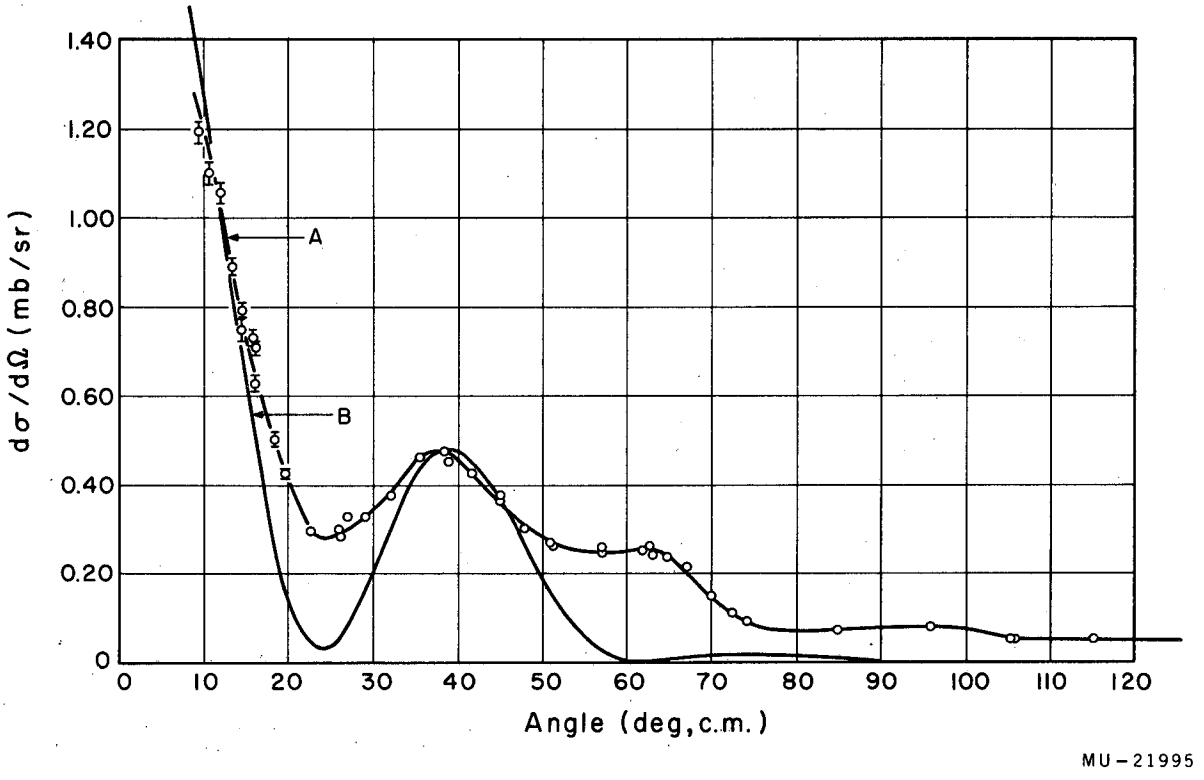

Fig. 16. Angular distribution of deuterons from formation of the ground state of N^{14}. Curve A presents the experimental results; Curve B, calculated results from the Glendenning equation using $j_n=j_p=1/2$, $R_0=4.70$ fermis.

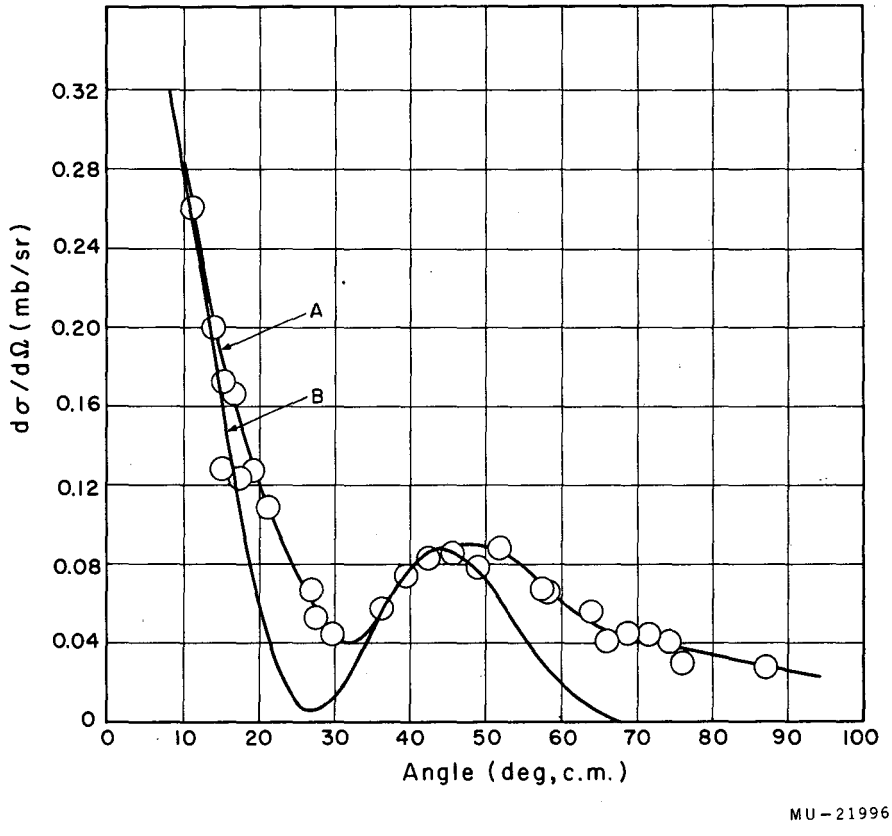

Fig. 17. Angular distribution of deuterons from formation of the 3.95-Mev level of N^{14}. Curve A presents the experimental results; Curve B, calculated results from the Glendenning equation using $j_n = j_p = 1/2$, $R_0 = 4.33$ fermis.

Both these transitions are $0+ \rightarrow 1+$, and angular momentum and parity conservation permit L=0, 2. For angular distribution calculations, the ground-state transition is assumed to involve solely the capture of both nucleons into $p_{1/2}$ levels (i.e., we are using only the predominant part of both the initial- and final-state shell model configurations). If the j-j configuration of this captured $(p_{1/2})^2$ pair about the C^{12} core is expressed on an L-S coupling basis, it becomes[59] $(p_{1/2})^2_{J=1} = 0.861\ {}^3D_1 - 0.192\ {}^3S_1 + 0.471\ {}^1P_1$; the squares of these coefficients for L=0, 2 are the C_L (e-e), Eq. (IV-2), which would arise in using the Glendenning theory to fit the angular distributions. The dominant ${}^3D_1$ term indicates that L=2 capture should be preferred to L=0 capture for the ground-state transition. Since Visscher and Ferrell[60] find that the N^{14} (g.s.) wave function can be represented as

$$\psi = 0.920\ {}^3D_1 + 0.173\ {}^3S_1 + 0.355\ {}^1P_1,$$

and under our assumption that the C^{12} (g.s.) can be treated as a ${}^1S_0$ state, it is seen that the C_L (e-e) for $(p_{1/2})^2$ capture well represent the experimental situation. In order, then, to test whether a fit involving $(p_{1/2})^2$ capture using the Glendenning theory would be unique, $(s_{1/2})^2$ capture (which requires L=0) and $(d_{5/2})^2$ capture (which results in a different C_2'/C_0' ratio) were also investigated. In addition, both L=2 and L=0 were tried with Butler stripping theory to see whether the former L value was preferred using this theory.

Since the $C^{12}(\alpha, d)N^{14*}$ (3.95-Mev) transition cannot be treated with the Glendenning theory using the principal initial-state $(p_{3/2})^8$ and final-state $(p_{3/2}^{-1}\ p_{1/2}^{-1})$ wave functions, the transition is analyzed as if the $(p_{1/2})^2$ configuration admixture in the 3.95-Mev level produced the observed transitions. Visscher and Ferrell, however, find that the L-S wave function of the 3.95-Mev level possesses a dominant ${}^3S_1$ configuration,[60] so that $(s_{1/2})^2$ capture -- which was also tried for this transition and allows only L=0 -- would be expected to fit the data better. (Calculations assuming $(s_{1/2})^2$ capture involve different

C_L (e-e) and different $B(\ell_n \ell_p L;Q)$ than those involved in $(p_{1/2})^2$ capture, for example; however, the variation in the angular distribution due to changes in the $B(\ell_n \ell_p L;Q)$ is expected to be much less than that due to changes in the coupling factors. This is a consequence of Eq. (IV-5), which states that $B(\ell_n \ell_p L;Q)$ can be approximated by $C^{\ell_n \ell_p L}_{0\ 0\ 0}\, j_L(QR_0)$, in which the angular dependence is characterized solely by L. [That this approximation is quite good under these experimental conditions is shown in a subsequent section.] The $C^{\ell_n \ell_p L}_{0\ 0\ 0}$ involved can be grouped with the C_L (e-e) to produce a revised coupling factor. For both these transitions, then, changing the nature of the captured pair - which still must possess positive parity -- can alternatively be viewed as changing the coupling factors to other than j-j coupling for two particles added to a C^{12} core.)

The Butler theory is also applied to the $C^{12}(\alpha,d)N^{14*}$ (3.95-Mev) transition to determine if in this case L=0 capture is preferred to L=2. Detailed information on the resulting fits for both transitions is given in Table VI.

The Glendenning fit to the ground-state angular distribution, Fig. 16, requires a very reasonable r_0 value ($R_0=r_0A^{1/3}+r_\alpha[=1.68f]$) of 1.32 fermi, and approximates fairly well the width of the angular distribution peak at approx 38 deg (c.m.); the Butler fit for L=2, Fig. 18, requires a less reasonable r_0 value of 2.02 fermi, although it adequately fits both experimental peaks at approx 38 and approx 62 deg (c.m.).

Unfortunately, both theories produce equally acceptable fits requiring only minor variations in the interaction radii for both transitions and for all the configurations or L values tried (fits using the Butler theory usually require r_0 values considerably greater than 1.5 fermi). This multiplicity of fits for the ground-state transitions using the Glendenning theory is especially disappointing, since $(p_{1/2})^2$ capture was expected to approximate the experimental situation fairly well.

Table VI. Results of the application of the stripping theories to the $C^{12}(a,d)N^{14}$ reaction.

Reaction	Final nuclear configuration	Radius for best fit (f)	Figure number of graph	$\frac{C_{L'max}}{C_{L'min}}$
Glendenning theory				
$C^{12}(a,d)N^{14}$(g.s.)	$[(p_{1/2})^2]_{1+}$	4.70(r_0=1.32f.)	16	$\frac{C_2'}{C_0'}$ =4.00
$C^{12}(a,d)N^{14}$(g.s.)	$[(s_{1/2})^2]_{1+}$	5.08	a. (see below)	only C_0 allowed
$C^{12}(a,d)N^{14}$(g.s.)	$[(d_{5/2})^2]_{1+}$	4.92	a.	$\frac{C_2'}{C_0'}$ = 0.114
$C^{12}(a,d)N^{14*}$(3.95-Mev)	$[(p_{1/2})^2]_{1+}$	4.33(r_0= 1.16f.)	17	$\frac{C_2'}{C_0'}$ = 4.00
$C^{12}(a,d)N^{14*}$(3.95-Mev)	$[(s_{1/2})^2]_{1+}$	4.67	a.	only C_0 allowed
$C^{12}(a,d)N^{14*}$(3.95-Mev)	$[(d_{5/2})^2]_{1+}$	4.50	a.	$\frac{C_2'}{C_0'}$ = 0.114
Butler theory (stripping)	L			
$C^{12}(a,d)N^{14}$(g.s.)	2	6.3(r_0=2.02)	18	
$C^{12}(a,d)N^{14}$(g.s.)	0	6.4_5	a.	
$C^{12}(a,d)N^{14}$(3.95-Mev)	2	5.5	19	
$C^{12}(a,d)N^{14}$(3.95-Mev)	0	5.7	a.	

a. This fit is acceptable, but is not graphed.

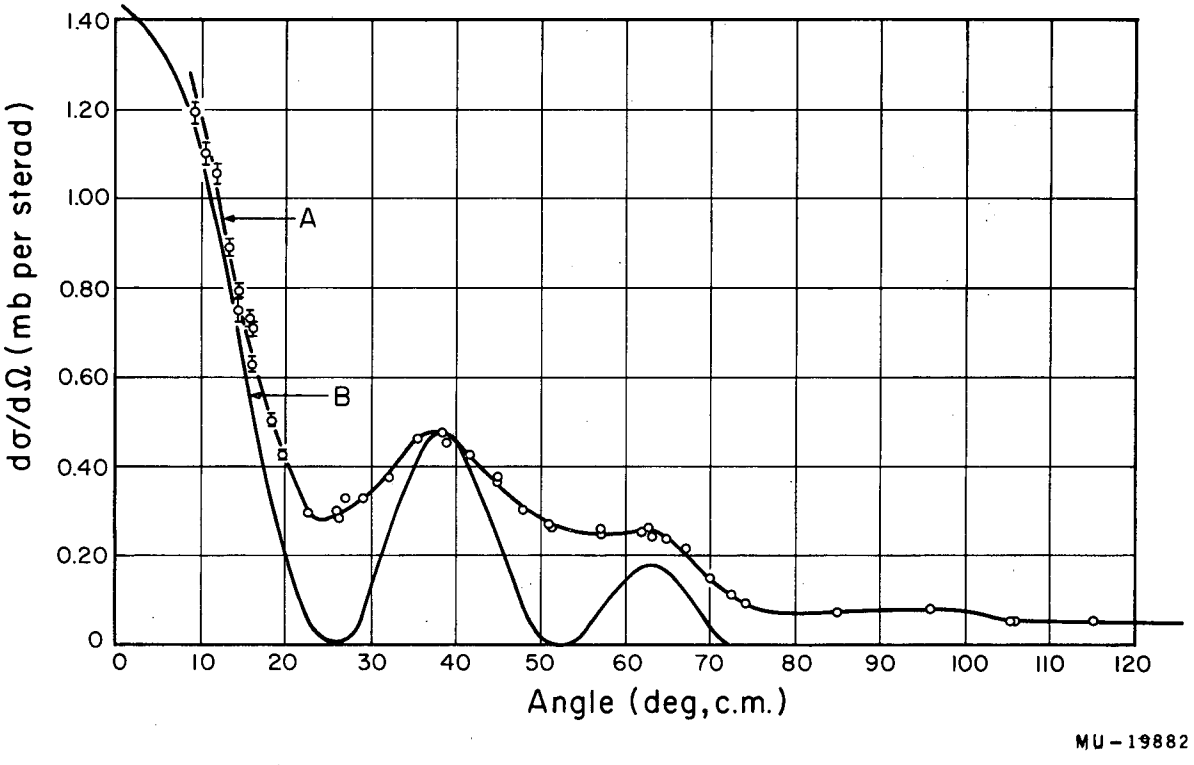

Fig. 18. Angular distribution of deuterons from formation of the ground state of N^{14}. Curve A presents the experimental results; Curve B, calculated results from the Butler equation using L=2, R_0=6.3 fermis.

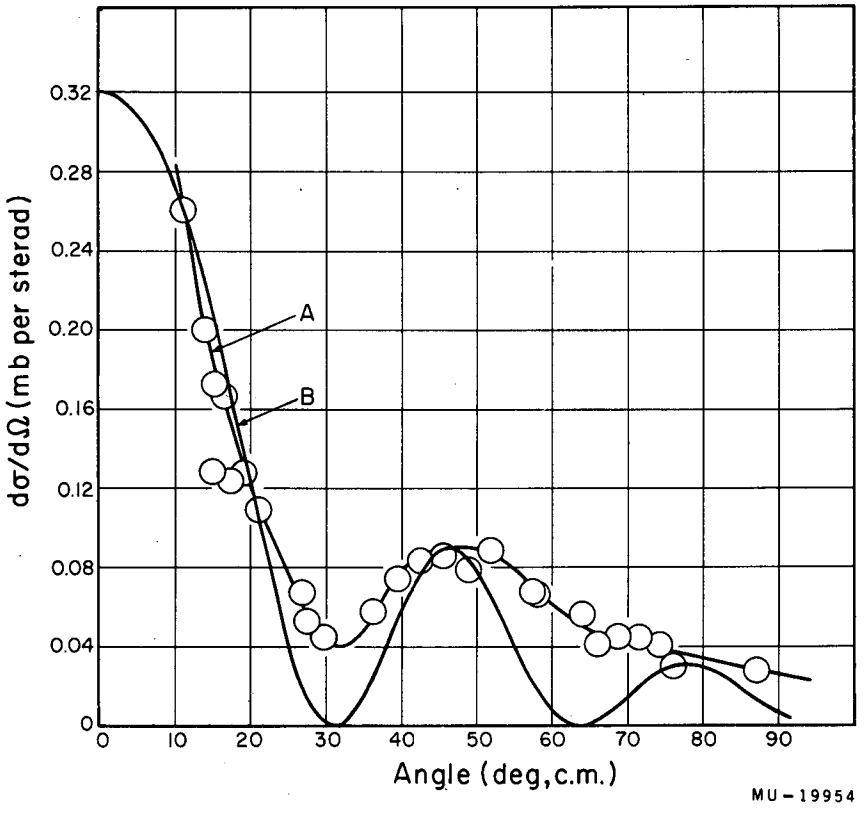

Fig. 19. Angular distribution of deuterons from formation of the 3.95-Mev level of N^{14}. Curve A presents the experimental results; Curve B, calculated results from the Butler equation using L=2, R_0=5.5 fermis.

E. $N^{14}(\alpha, d)O^{16}$

Figures 20 and 21 show a typical multiplier spectrum and a typical deuteron energy spectrum (60 deg, lab), respectively, for $N^{14} + He^4$. A comparison of the levels of O^{16} observed in this reaction with those previously reported by other workers is presented in Table VII; it is again apparent that the (α, d) reaction at these energies does not appreciably populate certain product nuclear states, even when no isotopic spin selection rules are violated. Cross sections were determined for transitions to the ground state (0.65 mb, measured from 11 to 101.4 deg, c.m.; absolute accuracy ±10%), the 6.1-Mev states (2.0$_3$ mb, measured from 11 to 102.7 deg, c.m.; absolute accuracy ± 15%), and the 8.88-Mev state (0.76 mb, measured from 11 to 103.4 deg, c.m.; absolute accuracy ± 15%). Uncertainties in background subtraction and in separation of the 7.0-Mev states from the 6.1-Mev states are major contributors to the greater errors in the cross sections for the excited states.

An analysis of the observed selectivity in the formation of excited states of O^{16} is complicated: first, as noted earlier, the N^{14} ground state is not pure $(p_{1/2})^2$; second, most of the excited states of O^{16} are complex, arising from interactions among many simple shell-model states. However, if the highly populated states in the product nucleus are at most two-particle excitation states -- i.e., again assuming that core (target nucleus) excitation is strongly inhibited -- then at least two levels of O^{16} should not be seen in this reaction. One level is the 9.58-Mev 1- level, which is thought to be a three-particle excitation state.[61] The other is a 0+, T=0 level arising from a $C^{12} + (2s)^4$ configuration calculated[62] to lie at 11.57 Mev -- the nearest established 0+, T=0 level of O^{16} is the state at 11.25 Mev. Table VII indicates that gaps were observed in the energy spectrum which encompass both these levels, although the accuracy of the experimental energy-level determinations is not sufficient to exclude some contribution from the 11.25-Mev level to the observed peak at 11.0 Mev.

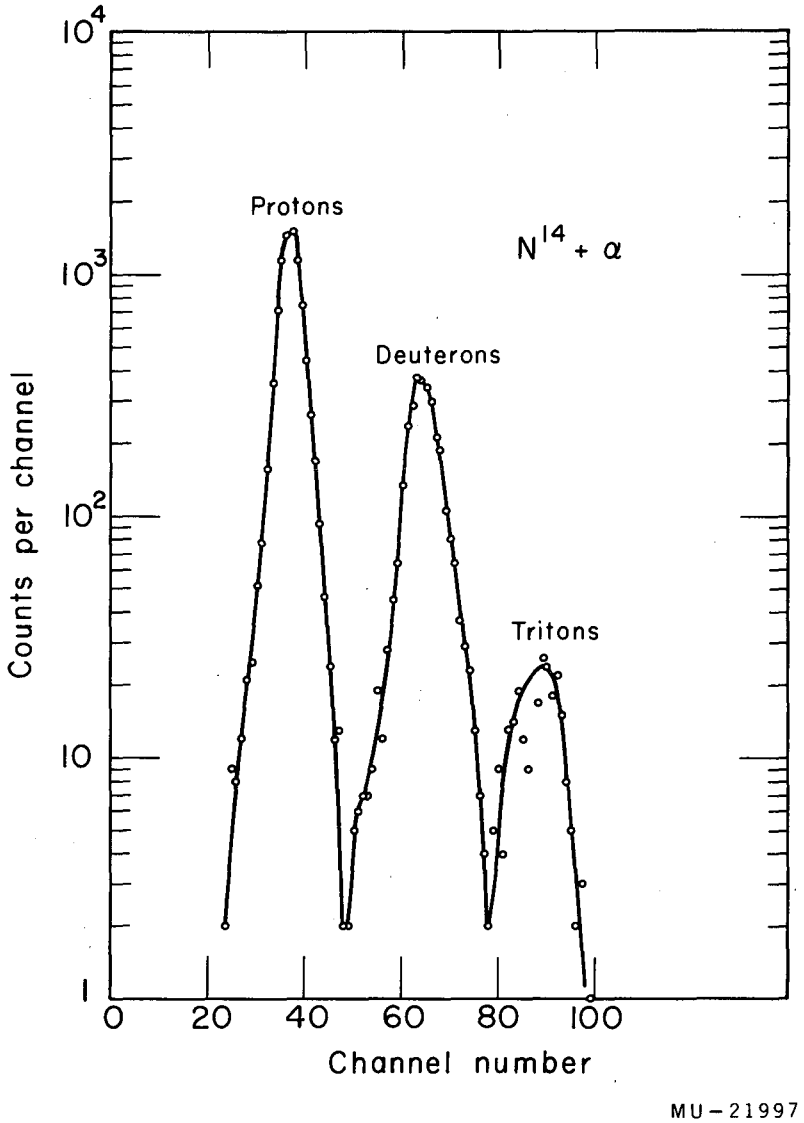

Fig. 20. Multiplier spectrum from bombardment of N^{14} with 46.5-Mev helium ions.

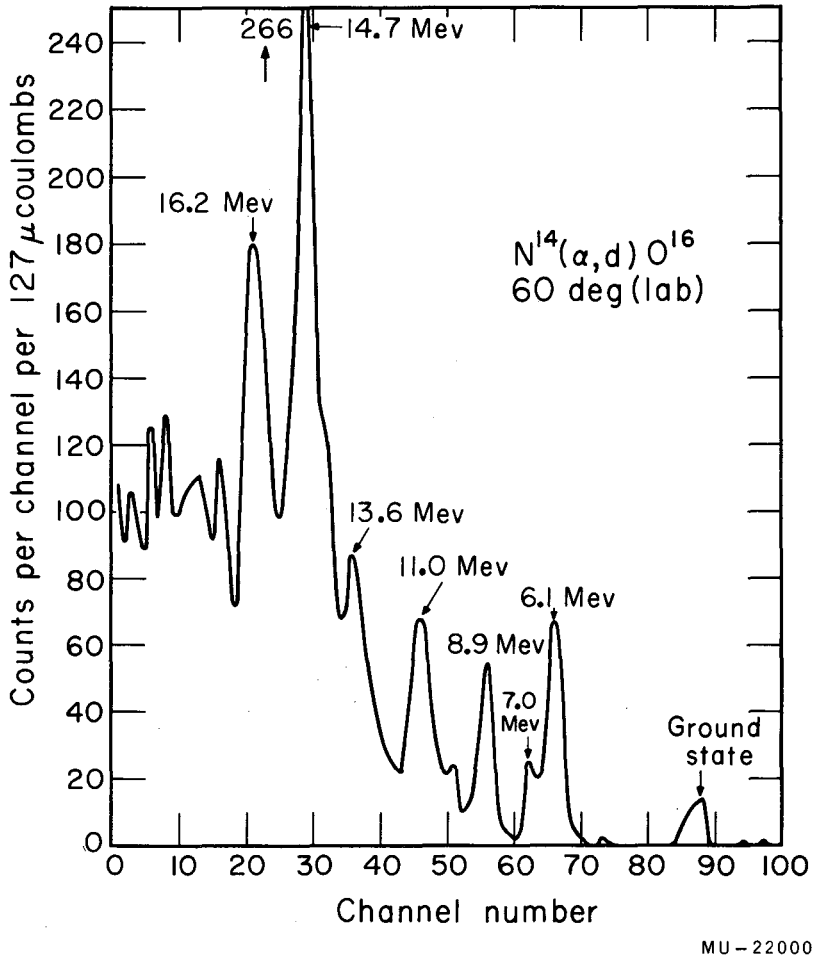

Fig. 21. Deuteron energy spectrum from the reaction $N^{14}(a,d)O^{16}$. Q values for the various peaks are shown.

Table VII. Comparison of O^{16} levels observed in this experiment with those previously reported.[a]

Levels identified (Mev)	Previously reported levels		
	Energy (Mev)	J^{π}	T
0[b]	0	0+	0
6.1[b]	6.056	0+	0
	6.135	3-	0
7.0[b]	6.923	2+	0
	7.121	1-	0
8.9[b]	8.875	2-	0
	9.58	1-	0
	9.843	2+	0
	10.363	4+	0
	(10.804)		
11.0±0.2	10.937	0-	0
	11.070	3+	(0)
	11.25	0+	0
	11.51	2+	0
	11.62	3-	0
	12.02		
	(12.29)		
12.3±0.2	12.43	1-	0
	12.52	2-	
	12.78	0-	1
	12.96	2-	1
	13.09	1-	1
	13.25	3-	1
13.6±0.2	13.65	1+	0
14.3±0.2	13.97	2-	
14.7±0.2	14.93	4+	
	15.21	2-, 3+	
	15.25	2+	
	15.41		
	15.79		
16.2±0.2	16.21	1+	
	16.3	0-	
	16.44		
	(16.82)		
	(16.93)		
	17.0		
17.0±0.2	17.12		
	17.29		

a. Reference 49.

b. See footnote b, Table I.

The energy spectra of the $C^{12}(\alpha,d)N^{14}$ reaction showed that several final states were populated whose configurations would require addition of the captured particles to different shells; therefore, the odd-parity levels of O^{16} at 6.14, 7.12, 8.88, and 10.94-Mev, which have been fairly well accounted for as admixtures of $p^{-1}d$ and $p^{-1}s$ configurations, with the predominating part of the final wave functions arising from $p_{1/2}{}^{-1}d$ and $p_{1/2}{}^{-1}s$ components,[61] should be observed. Deuteron groups corresponding to all these energies were detected, but only the transition to the 8.88-Mev level could be separately resolved. The wave function of the 8.88-Mev state is[61]

approx 75% $[(p_{1/2})^{-1}d_{5/2}]_{2-}$ + approx 7%$[(p_{1/2})^{-1}d_{3/2}]_{2-}$--the captured particles enter adjacent shells -- and the "reduced" reaction cross section, $\sigma_{8.88} \times \frac{2J_i+1}{2J_f+1} \equiv \langle\sigma_{8.88}\rangle_\omega$, is 0.46 mb. The O^{16} ground state is formed with a reduced reaction cross section, $\langle\sigma_{g.s.}\rangle_\omega$, of 1.95 mb and arises from the entry of both captured nucleons into the p shell. For this case, then, stripping into different shells is only one-fourth as probable as stripping into the same shell. A calculation of the amount of relative $^3S_1$ motion of two particles which couple with a $(p_{1/2})^2$ N^{14} (g. s.) to form the dominant configuration of each of these final states shows that the ratio of $\frac{^3S_1\text{(8.88-Mev)}}{^3S_1\text{(g. s.)}}$ is $\frac{1}{2.6}$;[63] since the captured pair in an α,d reaction is expected to be predominantly in a relative $^3S_1$ state, the origin of part of the observed hindrance in stripping across shells is indicated. The $N^{15}(\alpha,d)O^{17}$ ground-state transition (this general reaction is discussed in the next section), which involves the capture of a proton into the $p_{1/2}$ subshell and a neutron into the $d_{5/2}$ subshell, should also possess a lower cross section than the $N^{14}(\alpha,d)O^{16}$ (g. s.) transition by approximately the above factor of four. The $N^{15}(\alpha,d)O^{17}$ (g. s.) reduced cross section of 0.39 mb agrees with this prediction, being less by a factor of five than the cross section determined for stripping both particles into p shell-model states.

(All the cross sections referred to in this paragraph arise from data taken in the angular interval between 11 and 101 to 103 deg in the center-of-mass system.) These results are in qualitative agreement with the p,t data of Ball and Goodman,[64] who estimated that the pickup of two $1\,g_{9/2}$ neutrons is $\geq 8/3$ as probable as the pickup of one $2\,d_{5/2}$ and one $1\,g_{9/2}$ neutron.

The angular distributions of the deuterons from this reaction corresponding to formation of the O^{16} ground state, 6.1-Mev states, and 8.88-Mev state are shown in Figs. 22, 23, and 24, respectively. The errors shown on Fig. 22 are again due to counting statistics only; similar errors apply to the data of Figs. 23 and 24. These angular distributions were analyzed by using the Glendenning theory; in addition, fits to the ground-state angular distributions were attempted by using Butler theory and both stripping and knockout parameters, for reasons similar to those discussed earlier for the $Li^6(\alpha,d)Be^8$ reaction.

The restrictions placed on the odd-odd coupling factors by the Glendenning theory permit only a single set of reasonable individual-particle total angular momentum states for the captured particles in the ground-state transition. The angular distributions to the 6.1-Mev states were calculated on the assumption that the 6.14-Mev 3- level is involved, rather than the 6.06-Mev 0+ level, since a plausible configuration for these calculations is more readily envisioned for the former level; again only a single final-state configuration was investigated. Lastly, two configurations were tried for the $N^{14}(\alpha,d)O^{16*}$ (8.88-Mev) results. The detailed information on these fits is given in Table II.

The successful fit to the $N^{14}(\alpha,d)O^{16}$ (g.s.) results, Fig. 22, required $R_0 = 5.35$ fermi ($r_0 = 1.5_2$ f); the best stripping and knockout fits based on the Butler equation are shown in Fig. 25, and require $L = 2$, $R_0 = 7.1$ f, and $L = 0$, $R_0 = 5.6$ f, respectively. These Butler fits either fail to match the success of Glendenning's or require unrealistically large interaction radii, or both. In addition, as in the case of the $Li^6(\alpha,d)Be^8$ reaction, the best stripping fit is considerably better than the best knockout fit.

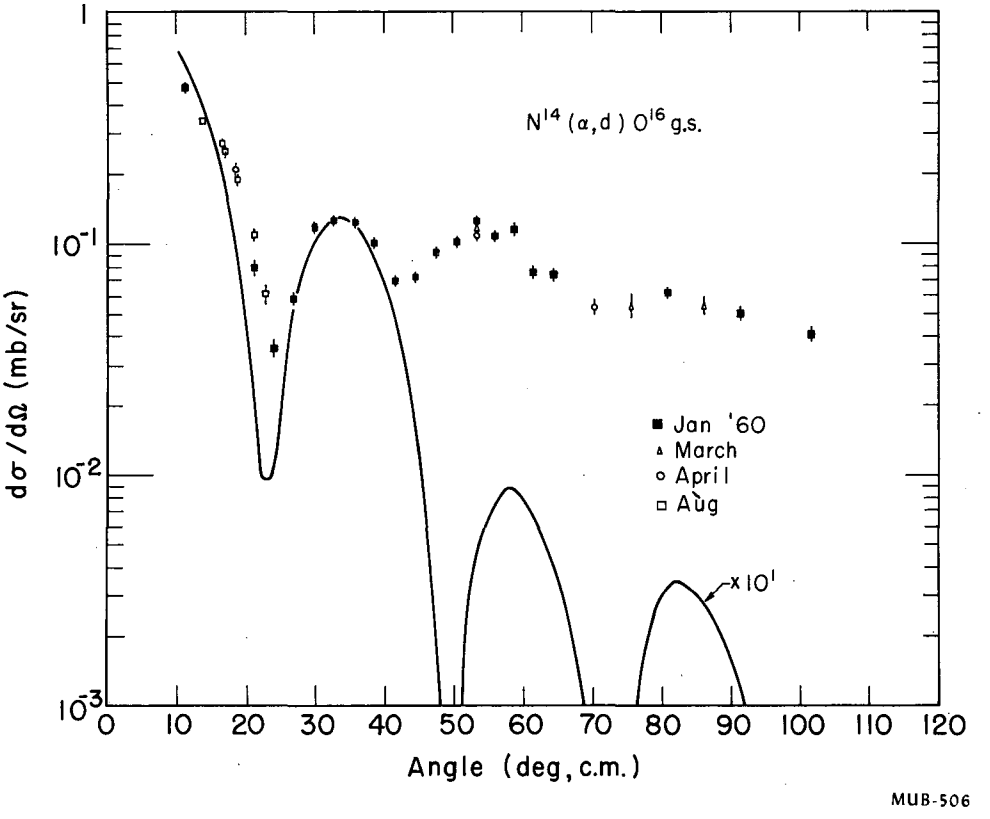

Fig. 22. Angular distribution of deuterons from formation of the ground state of O^{16}. The solid line was calculated from the Glendenning equation by using $j_n=j_p=1/2$, $R_0=5.35$ fermis.

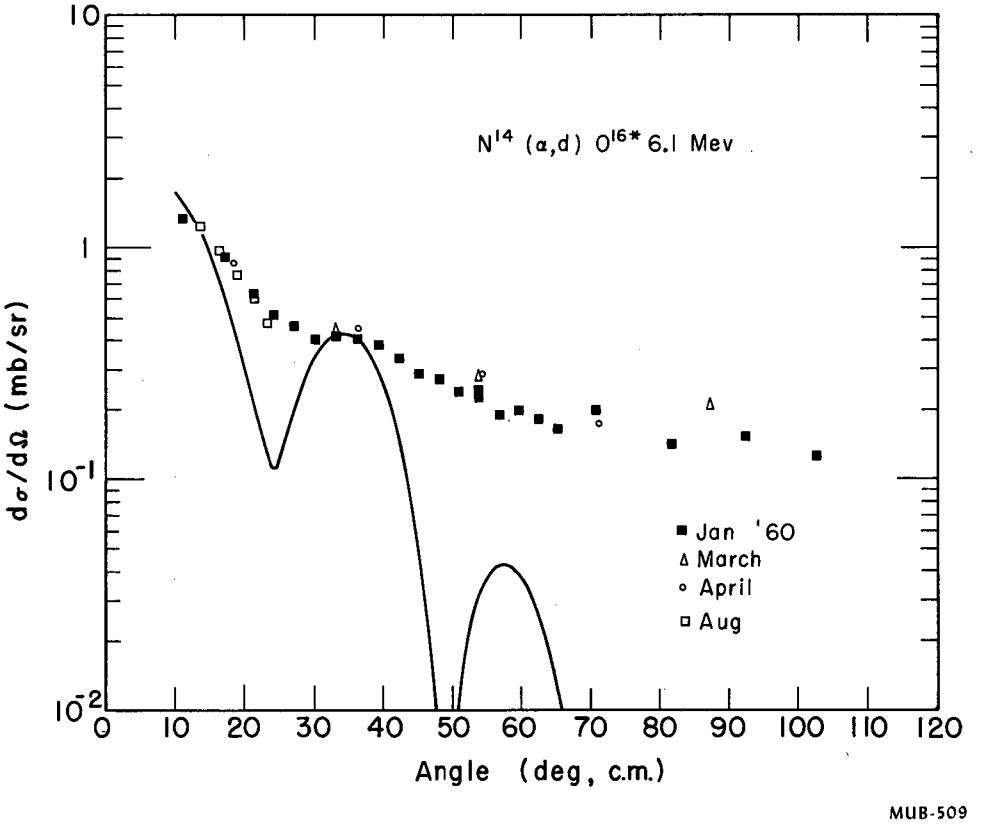

Fig. 23. Angular distribution of deuterons from formation of the 6.1-Mev level (s) of O^{16}. The solid line was calculated from the Glendenning equation by using $j_n = 1/2$, $j_p = 5/2$, $R_0 = 6.20$ fermis.

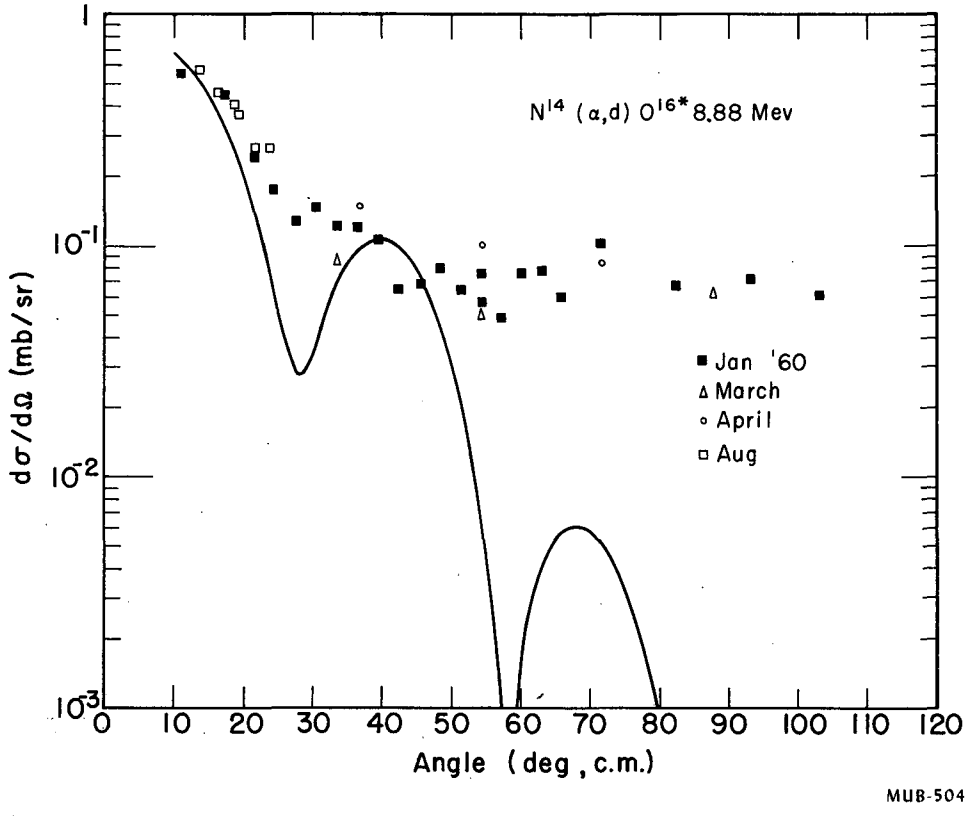

Fig. 24. Angular distribution of deuterons from formation of the 8.88-Mev level of O^{16}. The solid line was calculated from the Glendenning equation by using $j_n = 1/2$, $j_p = 5/2$, $R_0 = 5.48$ fermis.

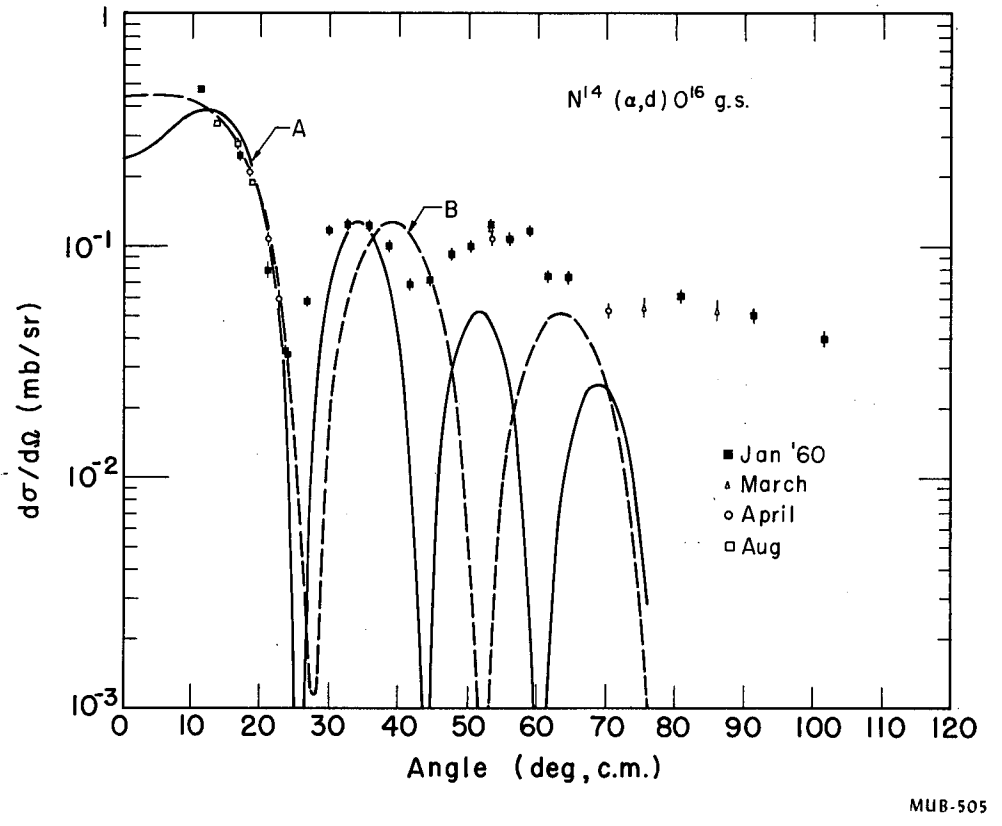

Fig. 25. Angular distribution of deuterons from formation of the ground state of O^{16}. Curve A was calculated from the Butler equation by using stripping parameters and L=2, R_0=7.1 fermis; curve B by using knockout parameters and L=0, R_0=5.6 fermis.

The fits to the fairly structureless angular distributions of the excited states do not adequately reproduce their shape. Since the ratio of the coupling factors, C_3'/C_1', for the transition to the O^{16*}(8.88-Mev) state is about the same for both final nuclear configurations tried and the $B(\ell_n \ell_p L;Q)$ are unchanged, it is not surprising that there is little difference between the resulting calculated angular distributions for the two configurations.

The C_L' max/C_L' min column of Table II again illustrates that the nature of the captured-particle shell-model states determines the preferred total orbital angular momentum transfer, and that the dominant L is not necessarily the lowest of the allowed values. For example, in the $Li^6(\alpha, d)Be^8$ (g. s.) angular distribution fit discussed earlier, B(112;Q)/B(110;Q) is typically $1 \rightarrow 4$, and in the $N^{14}(\alpha, d)O^{16}$(g. s.) fit B(112;Q)/B(110;Q) is typically $1/2 \rightarrow 3$; thus the $Li^6(\alpha, d)Be^8$ (g. s.) transition with $C_2'/C_0' = 1/25$ is determined by L = 0 transfer whereas the $N^{14}(\alpha, d)O^{16}$ (g. s.) transition with $C_2'/C_0' = 4.0$ strongly prefers L = 2 to L = 0 transfer.

F. $N^{15}(\alpha,d)O^{17}$

Figures 26 and 27 show a typical multiplier spectrum and a typical deuteron energy spectrum (15 deg lab) for $N^{15}+He^4$. Table VIII compares the energy levels observed in this experiment with those previously reported. Cross sections for transitions to weakly populated, resolvable final states could not be detected, owing to a generally higher background in this experiment, arising from α,d reactions on the N^{14} present in the target.

The $N^{15}(\alpha,d)O^{17}$ reaction is also observed to be fairly selective in the final states that are appreciably populated. Since the first T=3/2 levels of O^{17} should not appear before about 10.5 to 11.5 Mev excitation,[50] and the highest level experimentally observed was 9.15 Mev, the isotopic spin selection rules forbidding $T=1/2 \rightarrow T=3/2$ α,d transitions should not have restricted the formation of any of the excited states of O^{17} in the region observed in this experiment.

The first three positive parity states of O^{17} -- the ground 5/2+ state, the 0.87-Mev 1/2+ state, and the 5.08-Mev 3/2+ state -- are expected to be relatively pure single-particle states arising from $1d_{5/2}$, $2s_{1/2}$, and $1d_{3/2}$ neutrons, respectively, coupled to an O^{16} core.[65] Deuteron groups corresponding to the first two of these levels were separately identified; the deuterons from the 5.08-Mev state fall in the broad group corresponding to O^{17} levels from approx 4.6 to 6.0 Mev in excitation and, if present, could not be resolved. Similarly, the 3.85-Mev (7/2-) level is expected to be a fairly strong, though not pure, single-particle state[65] (a $1f_{7/2}$ neutron coupled to an O^{16} core) and a weak deuteron group from this level was observed above the background at many angles. Since the ground, 0.87-Mev, and 3.85-Mev levels all involve stripping a $p_{1/2}$ proton but require the capture of a $d_{5/2}$, $s_{1/2}$, or $f_{7/2}$ neutron, respectively, it would be interesting to compare their statistically weighted cross sections. The absolute cross section of the ground-state transition integrated from 11 to 102 deg (c.m.) is 1.1$_8$ mb, which is expected to be accurate to ± 10%. The cross

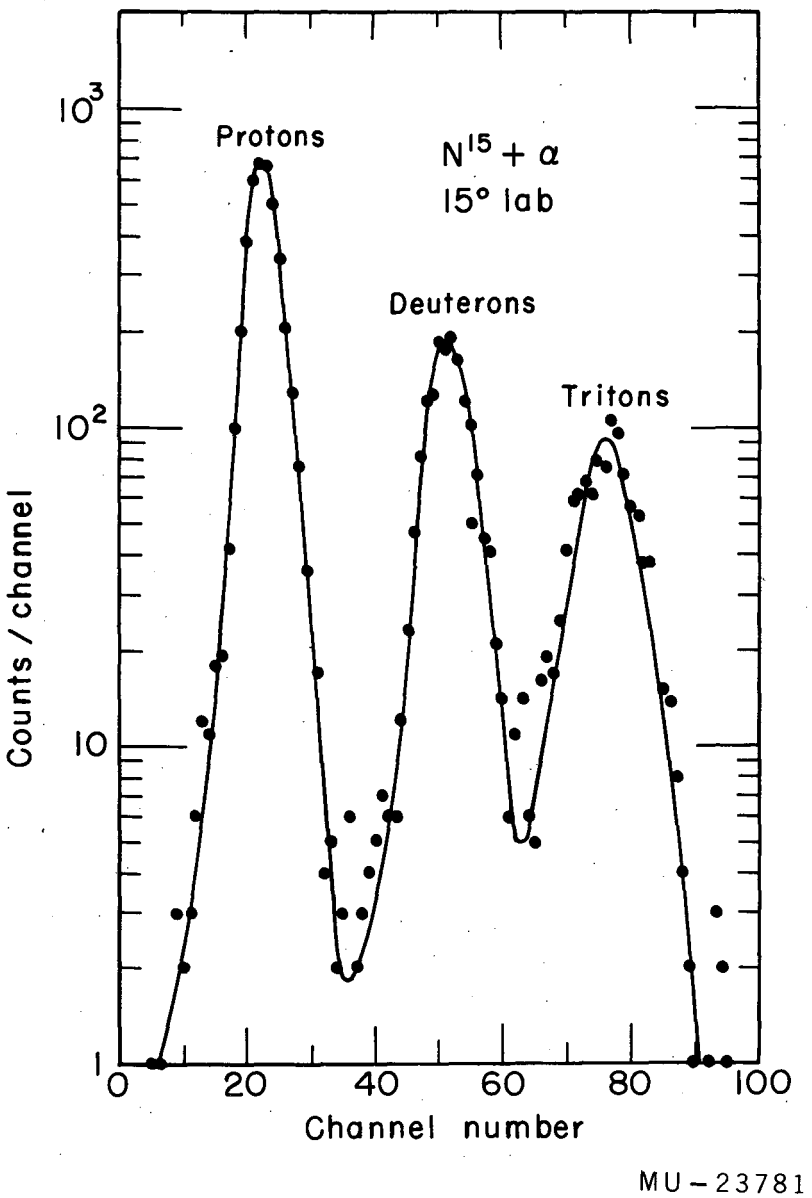

Fig. 26. Multiplier spectrum from bombardment of N^{15} with 46.5-Mev helium ions.

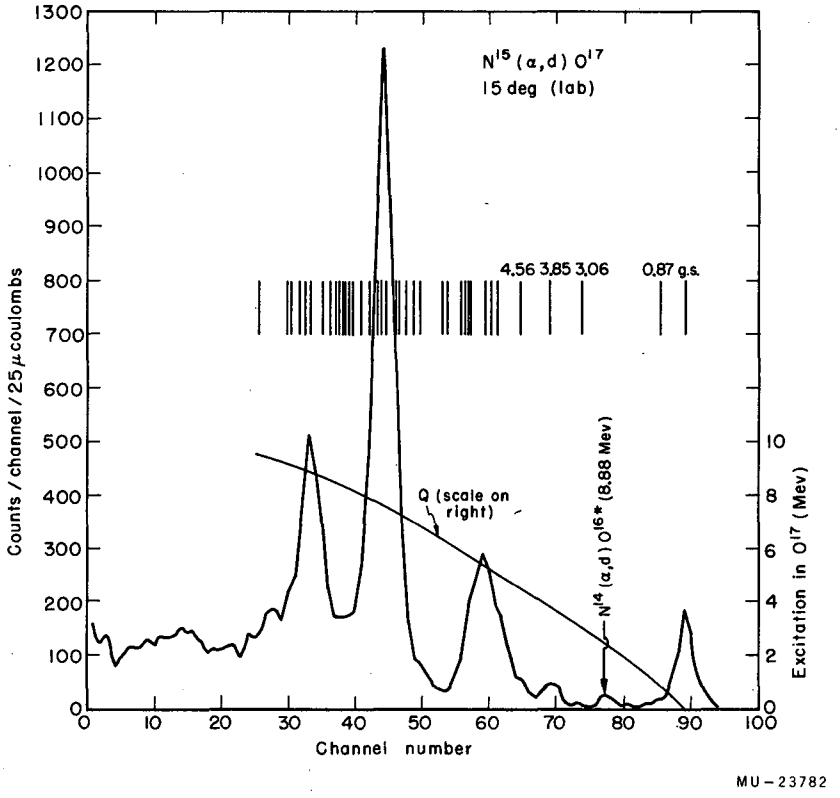

Fig. 27. Deuteron energy spectrum from the reaction $N^{15}(a,d)O^{17}$. Q values for the various peaks are shown.

Table VIII. Comparison of O^{17} levels observed in this experiment with those previously reported.[a]

Levels identified (Mev)	Previously reported levels	
	Energy (Mev)	J^{π}
0[b]	0	5/2+
0.8± 0.2	0.871	1/2+
	3.058	(1/2-)
3.7± 0.2	3.846	(7/2-)
	4.555	3/2-
	5.083	3/2+
	5.217	
	5.378	3/2-
~ 4.6± 0.2 → ~ 6.0± 0.2[c]	5.697	7/2-
	5.729	
	5.866	⩾3/2
	5.940	1/2-
	6.24	
	6.38	1/2+
	6.87	
	(6.99)	
	7.161	5/2
	7.28	3/2+
	7.373	5/2
	7.560	⩾7/2
7.6± 0.2	7.676	⩾5/2
	(7.72)	(3/2-)
	7.94	1/2
	8.07	3/2
	8.20	3/2
	8.27	
	8.340	1/2
	8.390	5/2
	8.460	7/2
	8.493	(3/2)
	(8.59)	
	8.70	3/2
	8.89	3/2
	8.96	7/2
	9.06	
9.1_5± 0.3	9.15	
	9.20	5/2
	9.50	7/2

a. Reference 49

b. See footnote b, Table I.

c. These limits define the approximate base width of a broad peak.

sections to the 0.87- and 3.85-Mev levels could not be accurately obtained because of their low population and a fairly high background; estimating them relative to the ground state, however, gives the following results. (a) The reduced cross section of the ground-state transition is ≥ 1.5 times that of the 0.87-Mev transition. (b) The ground-state transition possesses a much greater differential cross section than that of the 3.85-Mev state at all angles investigated, even though the latter state has the greater statistical weight. Also, the differential cross section of the 3.85-Mev level generally varied from only 2 to 3 times as great as to less than the differential cross section of the 0.87-Mev level, though the statistical weight of the 3.85-Mev state is four times that of the 0.87-Mev state. These rough results indicate that the reduced cross sections for stripping the captured particles across shells onto a N^{15} core vary in the manner

$$\sigma_{\omega}(p_{1/2}\, d_{5/2} \text{ capture}) > \sigma_{\omega}(p_{1/2}\, s_{1/2} \text{ capture}) > \sigma_{\omega}(p_{1/2}\, f_{7/2} \text{ capture}) --$$

apparently stripping across shells becomes less likely with increasing separation of the shells into which the particles are captured.

The previous discussion (Sec. E) on the $N^{14}(\alpha, d)O^{16}$ reaction indicated that stripping across shells was reduced in cross section by a factor of 4 to 5 relative to stripping into the same shell. Therefore, it would be valuable to compare the $N^{15}(\alpha, d)O^{17}$ cross sections obtained above with that for a transition to an O^{17} excited state which arises from capturing the two particles into the same shell. A $[(C^{12}\text{g.s.})_{J=0}\,(p_{1/2})^3\,(s_{1/2})^2]_{1/2^-}$ state, which meets the requirement, has been calculated to be at 6.69 Mev;[66] the closest known 1/2- level is at 5.94 Mev. Unfortunately, any deuterons from the 5.94-Mev level, if it does arise from two $(s_{1/2})^2$ particles coupled to a N^{15} core, would fall under the broad unresolved group previously mentioned, so that this comparison cannot be made.

The configurations of a few more low-lying negative parity levels are also known. Talmi and Unna suggest that the 3.06-Mev (1/2-) state possesses a $[(C^{12}\text{ g.s.})_{J=0}(p_{1/2})\,(s_{1/2})^4]_{1/2^-}$ configuration,[66] whereas

Armstrong and Quisenberry[67] suggest that it possesses a large admixture of a configuration consisting of the O^{18} (g.s.) with a $p_{1/2}$ hole [the O^{18} (g.s.) predominantly arises from two $d_{5/2}$ neutrons coupled to an O^{16} core]. The 3.06-Mev level was not observed above the background in the $N^{15}(\alpha,d)O^{17}$ reaction; this result would be expected if the former configuration were dominant, since the transition would require excitation of the N^{15} core and no evidence has arisen so far in this work that core excitation is likely. If the latter configuration were dominant, the transition would primarily involve adding a $(d_{5/2})^2$ pair to the N^{15} core; such a transition could very possibly possess a reduced cross section greater than that of the $N^{15}(\alpha,d)O^{17}$ (g.s.) transition. The low population of the O^{17*} (3.06-Mev) level in this (α,d) reaction can be understood, then, if this level possesses a strong $[(C^{12}\ \text{g.s.})_{J=0}\,(p_{1/2})\,(s_{1/2})^4]_{1/2^-}$ configuration. Finally, the 4.55-Mev and 5.38-Mev states, both 3/2-, are thought to contain admixtures of at least three shell-model configurations: a $[(O^{16}\ \text{g.s.})(2p_{3/2})]_{3/2^-}$ configuration (the 4.55-Mev state possesses a greater component of this than the 5.38-Mev state), a configuration arising from O^{18} with a $1\,p_{3/2}^{-1}$ hole, and a third unknown configuration.[65,67] The 4.55-Mev level is on an edge of the broad group of states mentioned before, and does not appear to be strongly populated relative to the ground state. This result, if correct, is in agreement with the general trends in these (α,d) reactions, since formation of the known components would require stripping into widely separate shells or core excitation, respectively. The 5.38-Mev deuteron group, if present, can not be resolved.

Figure 28 shows the angular distribution of the deuterons from the $N^{15}(\alpha,d)O^{17}$ (g.s.) transition. Two different final states were assumed in analyzing this angular distribution by the Glendenning theory to determine whether a unique fit was possible. The expected shell-model transition[58]

$[(\text{core})_0+p_{1/2}]_{1/2^-} \rightarrow [(\text{core})_0+(p_{1/2})^2_{J=0}(d_{5/2})]_{5/2^+}$ was one of these;

the other transition was $[(\text{core})_0+p_{1/2}]_{1/2^-} \rightarrow [(\text{core})_0+(p_{1/2})^2_{J=0}(s_{1/2})]_{1/2^+}$

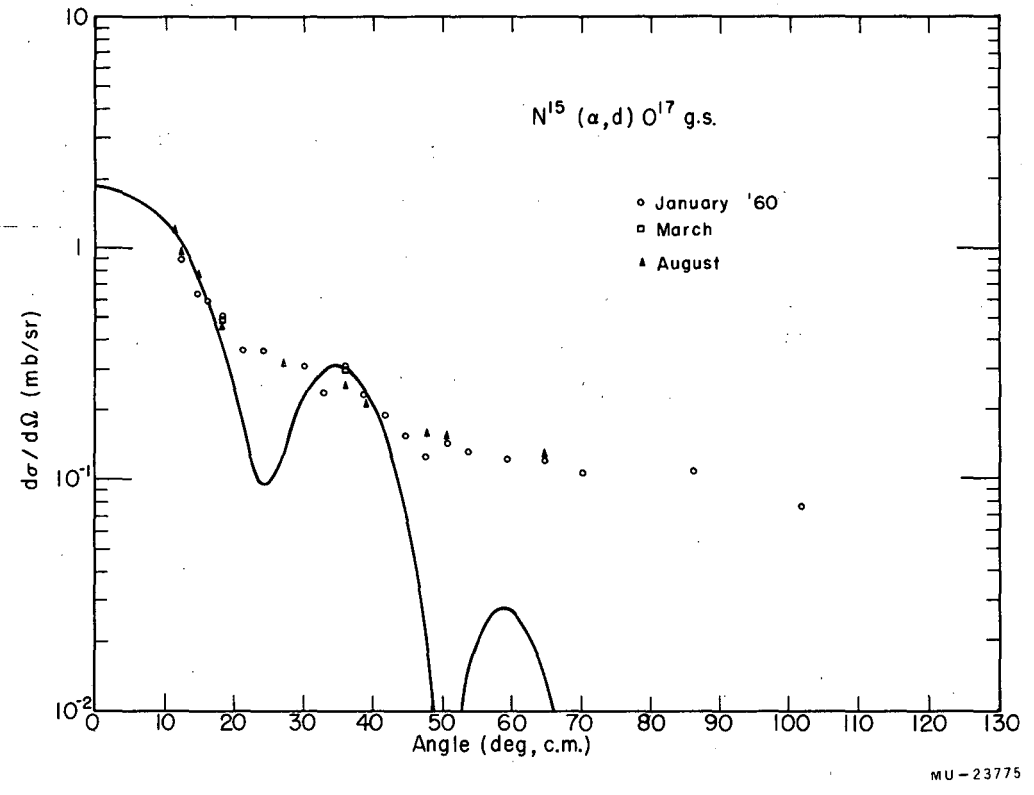

Fig. 28. Angular distribution of deuterons from formation of the ground state of O^{17}. The solid line was calculated from the Glendenning equation by using $j_n = 5/2$, $j_p = 1/2$, $R_0 = 6.00$ fermis.

which assumes, solely for purposes of comparison, that the $s_{1/2}$ level lies lower than the $d_{5/2}$ level for O^{17}. Detailed information on the results is given in Table IV.

Reasonably good fits were obtained for both the above configurations, although the fit using the expected shell-model transition is slightly better. Butler fits were again tried, and the fit for L=3, $R_0 = 7.4$ f, which is reproduced in Fig. 29, is considerably better at small angles than the best L = 1 fit ($R_0 = 7.7$ f). The Glendenning fit, however, appears to reproduce the small-angle rise the best.

The interaction radii required by the Glendenning fits are again seen to be more reasonable than those required by the Butler fits, although the Glendenning theory fits to both the $Li^7(\alpha, d)Be^9$ (g. s.)($r_0 = 1.9_7$ f) and the $N^{15}(\alpha, d)O^{17}$ (g. s.) ($r_0 = 1.7_5$ f.) angular distributions necessitate r_0 values considerably greater than 1.5 f.

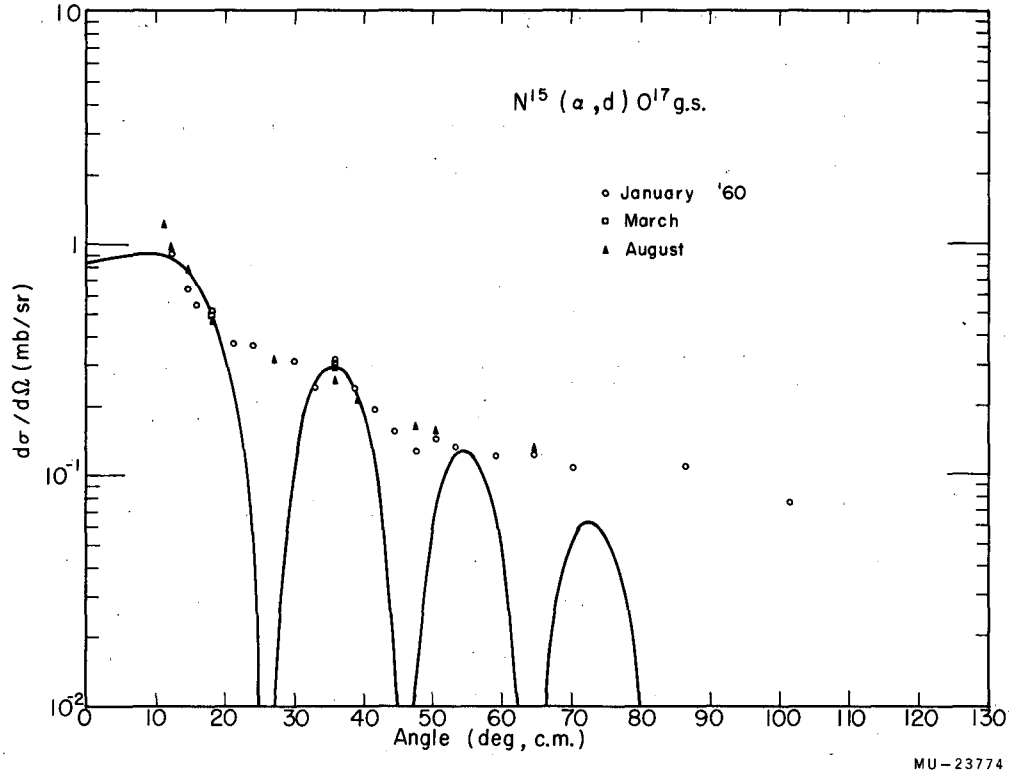

Fig. 29. Angular distribution of deuterons from formation of the ground state of O^{17}. The solid line was calculated from the Butler equation by using L=3, R_0=7.4 fermis.

G. Approximations to the Glendenning Theory

1. Approximation for $B(\ell_n \ell_p L;Q)$ ($\equiv B_L$)

Angular distribution calculations using the Glendenning theory with the approximate form of $B(\ell_n \ell_p L;Q)$, Eq. (IV-5), were compared with the angular distributions arising from the detailed theory for several different reaction conditions, inasmuch as the approximate $B(\ell_n \ell_p L;Q)$ is very easy to evaluate whereas the complete expression for B_L is not.

After the experimental data had been analyzed with the detailed theory, the equation incorporating the approximate B_L was then evaluated at the best-fit interaction radius. For all but the $Li^6(\alpha, d)Be^{8*}$ (2.90-Mev) results, very similar angular distributions are obtained from both equations -- in the latter evaluation the first maximum > 20 deg is shifted toward smaller angles by only approx 3 deg or less relative to the original fit. In many cases the interaction radius was then varied to optimize the fit with the approximate expression; these new fits always required slightly smaller interaction radii than the original ones, a change of about 0.2 fermi, or less. The $Li^6(\alpha, d)Be^{8*}$ (2.90-Mev) results, however, are not reproduced quite as well by using the approximate expression even when the radius is varied, and the best agreement is obtained with an interaction radius 0.7 fermi larger than that required by the complete expression. (It should be noted that the fit to the $Li^6(\alpha, d)Be^{8*}$ (2.90-Mev) data using the detailed theory appears to be rather fortuitous.)

Other comparisons of both expressions were calculated for lowered incident-particle energies and various interaction radii. The approximate expression reproduces the detailed expression using the original fit radii almost as well at low helium ion energies as it does with the above 47.5-Mev energy; in addition, for a constant energy of 47.5 Mev, slightly better agreement between the two calculations at the same interaction radius arises as this radius is increased.

2. The Point Alpha-Particle Approximation

The comparison of the calculated angular distributions from the Glendenning equation with the experimental results has shown that in all cases, except the $Li^6(\alpha,d)Be^{8*}$ (2.90-Mev) transition, the theoretical differential cross sections decrease much too rapidly with angle. Decreasing the size of the helium ion would permit more high-momentum transfers and therefore increase the theoretical large-angle cross section through the damping factor $e^{-k^2/8\gamma^2}$ of Eq. (IV-1). The point alpha-particle approximation of the Glendenning theory completely eliminates the damping factor, thereby producing the highest large-angle cross sections allowed by the theory. Therefore, this approximation was evaluated to determine the nature of the over-all angular distributions that arise from it.

Calculations with this approximation were performed for all the experimental angular distributions, using the best-fit parameters previously obtained from the complete theory. These calculations showed greatly improved large-angle fits in some cases and not enough damping in others; for the $N^{14}(\alpha,d)O^{16}$ (g.s.) transition, however, there was still too much large-angle damping. In addition, this approximation consistently produced much poorer agreement at small angles.

A similar calculation has been reported by Bromley et al.[68] in which excellent fits to some $Si^{28}(d,p)Si^{29}$ angular distributions were obtained by using Butler theory and setting the "deuteron factor" -- analogous to the damping factor discussed above -- independent of angle. They decided, however, that the fits so obtained were fortuitous and that the discrepancy at large angles very probably arose from neglecting distorted wave effects. Since distortion effects are expected to be even more serious in α,d reactions than in d,p reactions, better fits to the α,d experimental data should be obtained by using a distorted-wave, two-nucleon transfer theory.

H. Conclusions

The α,d direct reaction in the light elements has been shown to possess considerable potential as a spectroscopic tool. First, the direct reaction can be used in many cases to establish the isotopic spin quantum numbers of resolvable final states with the restriction that $0+ \rightarrow 0+$ α,d transitions should be avoided. Second, the observed selectivity in the population of final states, even when no transitions requiring nonconservation of isotopic spin are involved, has indicated that the stripped pair may be preferentially captured into certain nuclear configurations. Some evidence was obtained that the two nucleons prefer to be captured into equivalent shell-model states, and, when that is not possible, prefer to enter adjacent states. In addition, final states whose configurations involve three or more excited nucleons, so that their formation would require core excitation in addition to two-nucleon transfer, do not appear to be appreciably populated.

Little variation in the fits to the experimental angular distributions using the Glendenning two-nucleon stripping theory was observed for different assumed final nuclear configurations, thereby indicating that no spectroscopic identification of unknown final states through analysis of their angular distributions would have been possible. Whether this multiple fitting is due to the high linear momentum transfer prevailing under the experimental conditions is not known. However, the Glendenning theory produced excellent fits to several α,d transitions, and in almost all cases the interaction radii required were much more reasonable than those arising from the "best" Butler stripping theory fits to the data.

VI. ACKNOWLEDGMENTS

I wish to express my gratitude to Professor Isadore Perlman for his support and interest in the performance of this research.

It is a distinct pleasure to thank Dr. Bernard G. Harvey for his assistance, advice, and encouragement during the course of this work.

For help with scattering-chamber techniques and for many useful discussions, I wish to thank Dr. Jose Gonzalez-Vidal, Dr. Homer E. Conzett, Richard H. Pehl, and Dr. Robert J. Silva.

I wish to extend my appreciation to Dr. Norman K. Glendenning for many valuable discussions.

I would like to thank Jack H. Elliott for developing the solid-state detectors, Daniel O'Connell for preparing the carbon targets, Fred Goulding for the low-noise amplification equipment, and Fred Vogelsberg and Duane Mosier for their invaluable advice and assistance in the maintenance and operation of the electronic equipment.

The co-operation of W. Barclay Jones, Peter McWalters, John Wood, Robert Cox, and other members of the 60-inch cyclotron crew is greatly appreciated.

In addition, I wish to thank my wife, Barbara, for her valuable listening and for her encouragement throughout this work.

This work was performed under the auspices of the United States Atomic Energy Commission.

APPENDIX

The input and output parameters in the FORTRAN program which calculates the Glendenning theory angular distributions follow. The theory has been discussed in Section IV; α,d or d,α reactions may be calculated. (The FORTRAN listing is on pages 96 through 101, following this section).

Input

Four data cards are necessary.

The first card contains ETA, JI2, JF2, NODE, KKODE, MMODE. (E 10.4, 5I10),

where

ETA is the accuracy desired in the sum producing $B(\ell_n \ell_p L;Q)$.

JI2, JF2, are twice the initial and final spins, respectively.

NODE, KKODE, MMODE are control modes defined as follows:

NODE	Value	Computes using
	0	detailed $B(\ell_n \ell_p L;Q)$
	1	approximate $B(\ell_n \ell_p L;Q)$, Eq. (IV-5)
	2	the point α-particle approximation.

KKODE	Value	Performs (intermediate printing of)
	0	Group A (see below) every 5 angular intervals
	1	no printing

MMODE	Value	Performs
	0	no intermediate printing
	(any integer)	intermediate printing of Group B (see below) beginning with 0 deg for (any integer) number of angles. Node must be zero. If there are > 2 L values, fewer angles will print.

The second card contains $\Delta\theta$, θ_{max}, γ, E_{lab}, Q (2 F 10.0, 3 E 10.4).

where

$\Delta\theta$, θ_{max} are the angular increment and the maximum angle to be calculated--calculation begins with 0 deg, and no more than 180 angles within the angular range are allowed.

γ is any constant desired in the α-particle internale wave function.

E_{lab}, Q are the laboratory-system energy of the incident particle and the Q of the reaction, respectively.

The third data card contains m_i, m_T, m_e, m_R, KODE (4 E 10.4, I 10), where m_i, m_T, m_e, m_R are the masses of the incident, target, emitted, and residual nuclei, respectively; KODE is 0, 1, or 2 for even-even, odd-odd, or odd-even target nuclei, respectively.

The fourth data card contains ℓ_n, ℓ_p, j_n2, j_p2, $j_{np}2$, R, MODE (5 I 10, E 10.4, I 10)

where

ℓ_n, ℓ_p are the orbital angular momenta of the captured neutron and proton, respectively

j_n2, j_p2, $j_{np}2$ vary with the target nucleus and are defined below

R is the desired interaction radius

MODE is a control mode, defined

Value	Read in
0	new R, MODE only (E 10.4, I 10)
1	new "fourth" card
2	new set of 4 cards
3	nothing ; stop.

Definitions of j_n2, j_p2, $j_{np}2$

	e-e target	o-o target	o-e target
j_n2	j_n×2 (added n)	j_n×2 (added n; must have the same j as the one already present)	j_n×2 (added n)
j_p2	j_p×2 (added p)	j_p×2 (added p into any state)	j_p×2 (added p)
$j_{np}2$	0	j_p×2 (the j_p×2 of the original proton which couples with j_p' to form J_f)	"J"×2 (the intermediate $\vec{J}=\vec{j}_p+\vec{j}_p'$ [$\vec{j}_p' \equiv \vec{J}_i$]; restricted if $\vec{j}_p=\vec{j}_p'$)

Intermediate Printing

All intermediate and final output is on tape.

Group A intermediate output

K - an angle index beginning with 1 and increasing by 1 with each angular interval; the first K printed is 6.

L → the L value of the calculation

SUMR → $B(\ell_n \ell_p L;Q)$ for L even

SUMI → $B(\ell_n \ell_p L;Q)$ for L odd

FACT → $\exp(-\kappa^2/8\gamma^2)$ for the angle

SECFAC → $C_L/2L+1$

SIGB → $\exp(-\kappa^2/8\gamma^2)\left(\frac{C_L}{2L+1}\right)(B(\ell_n \ell_p L;Q))^2$

AAA → $\sum_L$ (SIGB) for as many L's as have been calculated at the time.

Group B intermediate output; this is calculated separately for each value of L.

N, LN, LP → n, λ_n, λ_p in the series calculating $B(\ell_n \ell_p L;Q)$, respectively

SP1, SP2 → $j_{\lambda_n}(QR_0/2)$, and $j_{\lambda_p}(QR_0/2)$, respectively

$B[=B(n,\lambda_n,\lambda_p)] \rightarrow \sqrt{(2\lambda_n+1)(2\lambda_p+1)}\ W(\ell_n \ell_p \lambda_n \lambda_p;Ln)$

$C^{\lambda_n \lambda_p L}_{0\ 0\ 0}\ C^{\ell_n\ n\lambda_n}_{0\ 0\ 0\ 0}\ C^{\ell_p\ n\lambda_p}_{0\ 0\ 0}$

$BES[=BES(n)] \rightarrow (-)^n(2n+1)\ I_{n+1/2}(4\gamma^2 R_0^2)$

$TERMR = BES \times i^{\lambda_n+\lambda_p} \times B \times SP1 \times SP2$

SUM R = (previous) SUMR + TERM R

Output

The output consists of:

type of calculation - complete (node 0) or simplified (node 1 or 2)

nature of target

statements involving m_i, m_T, m_e, E_{lab}

wave numbers of incident and emitted particles

accuracy of the sum calculating $B(\ell_n \ell_p L;Q)$

Q value of the reaction and γ assumed

ℓ_n, ℓ_p used

j_n, j_p, j_{np} used (all times two)

interaction radius used

J_i, J_f used (times two)

the angle, differential cross section, and relative cross section

$$\frac{d\sigma(\theta)/d\Omega}{d\sigma(0^\circ)/d\Omega}$$

the maximum value of n used in the sum calculating $B(\ell_n \ell_p L;Q)$ — the maximum allowed by the program is $n=15-\ell_n$ where $\ell_n \geq \ell_p$.

Subroutines

The ARRAY and BL subroutines (pages 102 through 104) are integral parts of this program; hence, they are also given in the Appendix. A subroutine of the form Transc (ℓ_n, ℓ_p, $j_n \times 2$, $j_p \times 2$, J, L, S) will be required which calculates the appropriate LS-jj coupling transformation coefficients.

In addition, subroutines which calculate vector coupling coefficients, Racah coefficients, spherical Bessel functions, and $I_{n+1/2}(\rho)$ will be required.

```
   1 DIMENSION B(16,16,16),BES(16),C(16,16,16),S(6),WXX(6),
    XSIGMA(181),REL(181),NTH(181)
    X,NTH2(61),NTH3(61),SIGMA2(61),SIGMA3(61),REL2(61),REL3(61)
2000 CALL EFM (0,0)
2004 READ 806,ETA,JI2,JF2,NODE,KKODE,MMODE
  10 READ 703,DTH,THMAX,GAM,ELAB,Q
  11 READ 718,EMI,EMT,EME,EMR,KODE
  19 EZ = EMT*ELAB/(EMI + EMT)
  20 EMIK = 0.2187 SQRTF(EMI*EMT*EZ/(EMI + EMT))
  21 EMEK = .0.2187 SQRTF(EME*EMR*(Q+EZ)/(EME+EMR))
2012 READ 801,LLN,LLP,JN2,JP2,JNP2,R,MODE
  59 KAR = 0
  61 DO 602 M = 1,181
 602 SIGMA (M) = 0.0
  60 ARG = 4.*((GAM*R)**2)
     DO 64 N = 1,16
     NN = N - 1
     ENN = N - 1
  64 BES(N) = ((-1.)**NN)*(2.*ENN + 1.)*BESSP(ARG,ENN)
     K = 0
     JJJ = 5
     KEE = 0
     KOO = 0
     LL = 0
     KNMAX = 0
     LBB = 0
 127 THET = 0.
 128 THETA = THET * 0.0174533
 130 K = K + 1
1900 IF (EMI - EME) 901, 2075, 133
 901 GGT= (EMEK/2.)**2 + EMIK**2 - EMEK*EMIK*COSF(THETA)
     GT = (EMR*EMIK/EMT)**2 + EMEK**2 - 2.*(EMR*EMIK*EMEK*COSF(THETA))
    X/EMT
     GO TO 136
 133 GGT =(EMEK-EMIK/2.)**2 +(2.*EMEK*EMIK)*(SINF(THETA/2.))**2
 134 GT=(EMIK-EMT*EMEK/EMR)**2+4.*(EMT/EMR)*EMEK*EMIK*(SINF(THETA/2.))
    X**2
 136 G = SQRTF(GT)
 142 A = G*R/2.
 144 EXPARG = -(GGT/(8. * GAM ** 2))
 150 FACT = EXPF(EXPARG)
     IF (KAR) 740,740,615
 740 IF (KODE - 1) 741,770,770
 741 KEE = KEE + 1
     IF (KEE - 1)742,742,615
 742 J = JF2/2
     JTEST = (-1)**J
     LTEST =(-1)**(LLN + LLP)
     IF(LTEST)14,14,13
  13 IF(JTEST) 16,16,15
  14 IF(JTEST) 15,15,16
  15 L = J
     LG = 0
     GO TO 25
  16 L = J - 1
     LG = J + 1
     IF(L) 17,25,25
  17 L = LG
     LG = 0
  25 IF (NODE) 671,671,672
 671 CALL ARRAY (LLN,LLP,L,B)
 672 ELL = L
     ALEPH = TRANSC(LLN,LLP,JN2,JP2,J,L,1)
```

```
      SECFAC = (ALEPH**2)/(2.*ELL + 1.)
      IF (LG) 744,744,743
  743 IF (NODE) 673,673,674
  673 CALL ARRAY (LLN,LLP,LG,C)
  674 ELG = LG
      ALEPH2 = TRANSC (LLN,LLP,JN2,JP2,J,LG,1)
      SECFA2 = (ALEPH2**2)/(2.*ELG+1.)
  744 LLLL = 0
      GO TO 615
  770 IF (LL) 771,771,790
  771 KOO = KOO + 1
      IF (KOO - 1) 2013,2013,615
 2013 LAND = LLN +LLP
 2016 LIND = XABSF (LLN - LLP)
 2017 L = LIND
      LIND = LIND + 2
      IF(LAND - LIND) 2025,2019,2019
 2019 LG = LIND
      LIND = LIND + 2
      IF(LAND - LIND) 2026,2021,2021
 2021 LGL = LIND
      LIND = LIND + 2
      IF(LAND - LIND) 2027,2023,2023
 2023 LGLG = LIND
      GO TO 2029
 2025 LG = 0
 2026 LGL = 0
 2027 LGLG = 0
  202 IF (KODE - 1) 2030,2030,600
 2030 WXX(1) = JI2/2
      WXX(2) = JF2/2
      EJN2 = JN2
      WXX(3)=EJN2/2.
      EJP2 = JP2
      WXX(4) = EJP2/2.
      EJNP2 = JNP2
      WXX(6) = EJNP2/2.
  772 IF (LGL) 773,773,774
  773 LLLL = 0
      GO TO 775
  774 LLLL = 1
  775 IF (NODE) 675,675,676
  675 CALL ARRAY (LLN,LLP,L,B)
  676 ASSIGN 780 TO NKM
      LAB = L
      SLAB = L
 2038 ML = XABSF (LAB - 1)
 2039 MH = LAB + 1
      RASUM = 0.
      MLL = ML + 1
      MHL = MH + 1
      DO 2045 MM = MLL,MHL
      M = MM - 1
      WXX(5) = M
      RAC2 = RACAH(WXX)
      ALEPH = TRANSC(LLN,LLP,JN2,JP2,M,LAB,1)
      RA = (RAC2*ALEPH)**2
 2041 EYX = 2*M + 1
 2045 RASUM = RASUM + RA*EYX
```

```
    GO TO NKM,(780,783,786,789)
780 SECFAC = RASUM/ (2.*SLAB + 1.)
    IF (LG) 615,615,781
781 IF (NODE) 677,677,678
677 CALL ARRAY (LLN,LLP,LG,C)
678 ASSIGN 783 TO NKM
    LAB = LG
    SLAB = LG
    IF (KODE - 1)2038,2038,607
783 SECFA2 = RASUM/ (2.*SLAB + 1.)
    IF (LGL) 615,615,784
784 ASSIGN 786 TO NKM
    LAB = LGL
    SLAB = LGL
    IF (KODE - 1) 2038,2038,607
786 SECFA3 = RASUM/ (2.*SLAB + 1.)
    IF(LGLG) 615,615,787
787 ASSIGN 789 TO NKM
    LAB = LGLG
    SLAB = LGLG
    IF (KODE - 1) 2038,2038,607
789 SECFA4 = RASUM/ (2.*SLAB + 1.)
    GO TO 615
790 LL = LL + 1
    IF (LL - 2) 791,791,615
791 SECFAC = SECFA3
    SECFA2 = SECFA4
    IF (NODE) 679,679,680
679 CALL ARRAY (LLN,LLP,LGL,B)
680 L = LGL
    LG = LGLG
    IF (LGLG) 615,615,792
792 IF (NODE) 681,681,615
681 CALL ARRAY (LLN,LLP,LGLG,C)
    GO TO 615
600 EEJI = JI2
    WXX(2) = EEJI/2.
    EEJN = JN2
    WXX(3) = EEJN/2.
    EEJNP = JNP2
    WXX(4) = EEJNP/2.
    EEJF = JF2
    WXX(5) = EEJF/2.
    EEJP = JP2
    WXX(6) = EEJP/2.
    IF(LGL) 603,603,604
603 LLLL = 0
    GO TO 605
604 LLLL = 1
605 IF (NODE) 682,682,683
682 CALL ARRAY (LLN,LLP,L,B)
683 ASSIGN 780 TO NKM
    LAB = L
    SLAB = L
607 ML = XABSF (LAB - 1)
    MH = LAB + 1
    RASUM = 0.0
    MLL = ML + 1
    MHL = MH + 1
```

```
      DO 609 MM = MLL,MHL
      M = MM - 1
      WXX(1) = M
      RAC2 = RACAH (WXX)
      ALEPH = TRANSC(LLN,LLP,JN2,JP2,M,LAB,1)
      RA = (RAC2 * ALEPH)**2
      EYX = 2*M + 1
  609 RASUM = RASUM + RA*EYX
      GO TO NKM, (780,783,786,789)
  615 KJ = 0
      IF (NODE - 1) 625,617,616
  616 FACT = 1.0000
  617 S(1) = LLN
      S(2) = LLP
      S(3) = L
      S(4) = 0.0
      S(5) = 0.0
      S(6) = 0.0
  634 CBR = CLEB(S)
      AAQ = 2. * A
      SPQ = SPHBESF(AAQ,L)
      LABT = (-1) ** L
      IF (LABT) 618,618,619
  618 SUMI = CBR * SPQ
      SUMR = 0.0
      GO TO 627
  619 SUMR = CBR * SPQ
      SUMI = 0.0
      GO TO 627
  625 CALL BL(LLN,LLP,L,B,BES,A,THET,ETA,MMODE,SUMR,SUMI,N)
  632 IF (KNMAX - N) 626,627,627
  626 KNMAX = N
  627 SIGB = (SUMR ** 2 + SUMI ** 2) * FACT * SECFAC
      SIGMA(K) = SIGMA(K) + SIGB
      IF(KKODE) 628,628,633
  628 KKK = ((K - 1)/JJJ) - 1
      IF (KKK)633,629,633
  629 AAA = SIGMA(K)
      WRITE OUTPUT TAPE 5,822,K,L,SUMR,SUMI,FACT,SECFAC,SIGB,AAA
      IF (LG) 631,631,636
  631 JJJ = JJJ + 5
      GO TO 650
  636 IF (KJ) 642,642,631
  633 IF(KJ) 640,640,650
  640 IF (LG)650,650,642
  642 NLN = L
      SEC = SECFAC
      L = LG
      SECFAC = SECFA2
      KJ = 1
      IF (NODE - 1) 643,644,644
  644 S(3) = LG
      GO TO 634
  643 CALL BL(LLN,LLP,LG,C,BES,A,THET,ETA,MMODE,SUMR,SUMI,N)
      GO TO 632
  650 NTH(K) = THET + 0.00001
  651 THET = THET + DTH
      MMODE = MMODE - 1
      IF (LG) 652,652,670
```

```
 670 L = NLN
     SECFAC = SEC
 652 IF (THET - THMAX) 128,128,653
 653 IF (LLLL)2059,2059,654
 654 LBB = LBB + 1
     IF (LBB - 1) 655,655,2059
 655 LL = LL + 1
     K = 0
     GO TO 127
2059 DO 2060 M = 1,K
2060 REL(M) = SIGMA(M)/SIGMA(1)
 227 CK = K
 229 NN1 = CK/3. + 1.0001
 230 NN2 = 2 * NN1
     DO 1231 I = 1,NN1
     K2=I+NN1
     K3=I+NN2
     NTH2(I) = NTH(K2    )
     NTH3(I) = NTH(K3      )
     SIGMA2(I) = SIGMA(K2)
     SIGMA3(I) = SIGMA(K3)
     REL2(I) = REL(K2)
1231 REL3(I) = REL(K3)
     IF (NODE) 2,2,3
   2 WRITE OUTPUT TAPE 5,827
     GO TO 4
   3 WRITE OUTPUT TAPE 5,828
   4 IF (KODE - 1) 5,6,7
   5 WRITE OUTPUT TAPE 5,829
     GO TO 1232
   6 WRITE OUTPUT TAPE 5,830
     GO TO 1232
   7 WRITE OUTPUT TAPE 5,831
1232 WRITE OUTPUT TAPE 5,704,EMT,EMI,ELAB,EME
     WRITE OUTPUT TAPE 5,706,EMIK,EMEK,ETA
     WRITE OUTPUT TAPE 5,825,Q,GAM,LLN,LLP,JN2,JP2,JNP2,R,JI2,JF2
 231 WRITE OUTPUT TAPE 5,716
 232 WRITE OUTPUT TAPE 5,717,(NTH(I),SIGMA(I),REL(I),NTH2(I),SIGMA2(I),
    XREL2(I),NTH3(I),SIGMA3(I),REL3(I), I = 1, NN1)
 233 WRITE OUTPUT TAPE 5,719,KNMAX
2065 IF(MODE - 1)2070,2012,2075
2070 READ 810,R,MODE
     IF (LLLL)2072,2072,59
2072 KAR = 1
     GO TO 61
2075 IF (MODE - 2) 2012,2004,2080
2080 END FILE 5
2082 REWIND 5
     STOP
 703 FORMAT(2F10.0,3E10.4)
 704 FORMAT (45H THIS REACTION IS THE BOMBARDMENT OF A MASS =E10.4,18H
    XTARGET BY A MASS=E10.4, 22H PARTICLE WHOSE ELAB =E10.4
    X//36H    THE EMERGENT PARTICLE HAS MASS =E10.4//)
 706 FORMAT (25H K OF INCIDENT PARTICLE =E10.4,24H K OF EXITING PARTICL
    XE =E10.4, 19H ACCURACY OF SUM = E10.4  )
 716 FORMAT(3(37H      THETA         SIGMA     RELATIVE)//)
 717 FORMAT(3(I11,2E13.4))
 718 FORMAT(4E10.4,I10)
 719 FORMAT(30H THE MAXIMUM VALUE OF N USED =I5,/ 1H1 )
```

```
801 FORMAT (5I10,E10.4,I10)
806 FORMAT(E10.4,5I10)
810 FORMAT(E10.4,I10)
822 FORMAT(4H K= I2,4H L= I2,7H SUMR= E10.4,7H SUMI= E10.4,7H FACT= E1
   X0.4,9H SECFAC= E10.4,7H SIGB= E10.4,6H AAA= E10.4   )
825 FORMAT(18H THE REACTION Q = E12.4, 9H GAMMA = E12.4 //
   X 6H LN = I3, 6H LP = I3, 6H JN = I3, 6H JP = I3,7H JNP = I3,
   X20H RADIUS IN FERMIS = E12.4,12H JINITIAL = I2,10H JFINAL = I2 //)
827 FORMAT(44H TWO-NUCLEON TRANSFER CALCULATION, COMPLETE.   )
828 FORMAT(46H TWO-NUCLEON TRANSFER CALCULATION, SIMPLIFIED.   )
829 FORMAT(17H EVEN-EVEN TARGET //)
830 FORMAT(15H ODD-ODD TARGET //)
831 FORMAT(16H EVEN-ODD TARGET //)
850 END(0,1,0,0,1)
```

```
      SUBROUTINE ARRAY (LLN,LLP,L,B)
      DIMENSION B(16,16,16),X(6),Y(6),Z(6),W(6)
      X(4) = 0.
      X(5) = 0.
      X(6) = 0.
      Y(1) = LLN
      Y(4) = 0.
      Y(5) = 0.
      Y(6) = 0.
      Z(1) = LLP
      Z(4) = 0.
      Z(5) = 0.
      Z(6) = 0.
      W(1) = LLN
      W(2) = LLP
      W(5) = L
      X(3) = L
   26 DO 41 N = 1,16
      NN = N - 1
      W(6) = NN
      Y(2) = NN
      Z(2) = NN
      LMIN = XABSF(LLN - NN)
      LMAX = LLN + NN
      LN = LMIN
      LPL = XABSF(LLP-NN)
      LPH = LLP + NN
   27 LLNE = XABSF (L - LN)
      LTWO = L + LN
   28 LPMIN = XMAXOF ( LPL,LLNE)
      LPMAX = XMINOF ( LPH, LTWO)
      IF(LMAX - 15) 29,29,43
   29 IF (LPMAX - 15) 30,30,43
   30 LP = LPMIN
   32 W(3) = LN
      W(4) = LP
      X(1) = LN
      X(2) = LP
      Y(3) = LN
      Z(3) = LP
      LNADJ = LN + 1
      LPADJ = LP + 1
      ELN = LN
      ELP = LP
      CBX = CLEB(X)
      CBY = CLEB(Y)
      CBZ = CLEB(Z)
      RAC = RACAH(W)
   33 B(N,LNADJ,LPADJ) = RAC*CBX*CBY*CBZ*SQRTF((2.*ELN+1.)*(2.*ELP+1.))
   37 LP = LP + 2
      IF(LP - LPMAX)32,32,39
   39 LN = LN + 2
      IF (LN - LMAX) 27,27,41
   41 CONTINUE
   43 RETURN
      END(0,1,0,0,1)
```

```
      SUBROUTINE BL(LLN,LLP,L,B,BES,A,THET,ETA,MMODE,SUMR,SUMI,N)
      DIMENSION B(16,16,16), BES(16)
      IF (MMODE - 1) 152,115,115
  115 WRITE OUTPUT TAPE 5,826,THET
  152 SUMR = 0.
  153 SUMI = 0.
      N = 0
  157 NN = N
      LMIN = XABSF(LLN-NN)
      LMAX = LLN + NN
      LN = LMIN
      LPL = XABSF(LLP-NN)
      LPH = LLP + NN
  527 LLNE = XABSF (L - LN)
      LTWO = L + LN
  528 LPMIN = XMAXOF ( LPL , LLNE)
      LPMAX = XMINOF ( LPH,LTWO)
      LP = LPMIN
  172 NTEST = (-1.)**(LN+LP)
      IF(NTEST) 174,174,190
  174 NP = (LN+LP-1)/2
      SP1 = SPHBESF(A,LN)
  178 SP2 = SPHBESF(A,LP)
      NX = N + 1
      LX = LN + 1
      LPX = LP + 1
  180 TERMI = (-1.)**NP * SP1 * SP2 * B(NX,LX,LPX)*BES(NX)
  181 SUMI = SUMI + TERMI
      IF(MMODE - 1) 205,184,184
  184 WRITE OUTPUT TAPE 5,713,N,LN,LP,SP1,SP2,B(NX,LX,LPX),BES(NX)
  185 WRITE OUTPUT TAPE 5,714,TERMI,SUMI
      GO TO 205
  190 NP = (LN + LP)/2
  192 SP3 = SPHBESF(A,LN)
  193 SP4 = SPHBESF(A,LP)
      NX = N + 1
      LX = LN + 1
      LPX = LP + 1
  195 TERMR = (-1.)**NP*SP3*SP4*B(NX,LX,LPX)*BES(NX)
  196 SUMR = SUMR + TERMR
      IF (MMODE - 1) 205,200,200
  200 WRITE OUTPUT TAPE 5,713,N,LN,LP,SP3,SP4,B(NX,LX,LPX),BES(NX)
  201 WRITE OUTPUT TAPE 5,715,TERMR,SUMR
  205 LP = LP + 2
      IF(LP-LPMAX) 172,172,208
  208 LN = LN + 2
      IF(LN - LMAX) 527,527,213
  213 IF (SUMI) 214,179,214
  214 AI = ABSF(TERMI/SUMI)
      GO TO 183
   17 AI = 0.0
  183 IF (SUMR) 215,186,215
  215 AR = ABSF(TERMR/SUMR)
      GO TO 216
  186 AR = 0.0
  216 IF(AI - ETA) 217,217,221
  217 IF (AR - ETA) 199,199,221
  221 IF(LLN + N - 15)222,900,900
  222 N = N + 1
      GO TO 157
  900 WRITE OUTPUT TAPE 5,805,N,THET,TERMI,SUMI,TERMR,SUMR
  199 RETURN
  713 FORMAT(3H N=I3,3H L=I3,4H LP=I3,5H SP1=E11.4,5H SP2=E11.4,4H B=
```

```
   XE11.4,5H BES=E11.4)
714 FORMAT(9H TERM I =E12.4,8H SUM I = E12.4//)
715 FORMAT (9H TERM R =E12.4,8H SUM R = E12.4//)
805 FORMAT(36H CALCULATION REQUIRES N HIGHER THAN I3, 7H ANGLE=  F4.0,
   X7H TERMI=E11.4,6H SUMI=E11.4,7H TERMR=E11.4,6H SUMR=E11.4 //)
826 FORMAT (14H FOR ANGLE OF F4.0)
    END (0,1,0,0,1)
```

FOOTNOTES AND REFERENCES

1. D.A. Bromley and E. Almqvist, Repts. Progr. in Phys. 23, 544 (1960). See also Chalk River Report CRP-881 (1960).
2. D.A. Bromley, in Proceedings of the International Conference on Nuclear Structure, (University of Toronto Press, 1960).
3. D.H. Wilkinson, "Open Questions in Nuclear Structure, Some Experimental Approaches," Brookhaven National Laboratory Report BNL-5013, 1960.
4. B. Zeidman and J.L. Yntema, Nuclear Phys. 12, 298 (1959).
5. S.V. Starodubtsev and K.V. Makaryunas, Doklady Akad. Nauk. SSSR 129, 547 (1959); translated Doklady 4, 1292 (1959).
6. R.J. Silva, "Mechanism of the (α,pn) Reaction," Lawrence Radiation Laboratory Report UCRL-8678, March, 1959 (unpublished).
7. W.E. Burcham, Progr. in Nuclear Phys. 4, 171 (1955).
8. G.E. Fischer and V.K. Fischer, Phys. Rev. 114, 533 (1959).
9. B.L. Cohen and T.H. Handley, Phys. Rev. 93, 514 (1954).
10. I. Nonaka, H. Yamaguchi, T. Mikuna, I. Umeda, T. Tabata, and S. Hitaka, J. Phys. Soc. (Japan) 14, 1260 (1959).
11. S.T. Butler, Phys. Rev. 106, 272 (1957).
12. H.E. Conzett and J. Gonzalez-Vidal, (Lawrence Radiation Laboratory), private communication.
13. N.K. Glendenning, "The Two-Nucleon Stripping Reaction," to be published in Nuclear Physics; (UCRL-9505, Nov. 1960).
14. S.T. Butler, Nuclear Stripping Reactions (John Wiley and Sons, Inc., New York, 1957).
15. A.M. Lane and R.G. Thomas, Revs. Modern Phys. 30, 257 (1958).
16. Y. Hashimoto and W. Parker Alford, Phys. Rev. 116, 981 (1959).
17. H.C. Newns, Proc. Phys. Soc. (London) 76, 489 (1960).
18. This point has also been noted by D.H. Wilkinson, Ref. 3.
19. E.P. Wigner, Phys. Rev. 51, 106 (1937).
20. W. Heisenberg, Z. Physik 77, 1 (1932).
21. W.M. Macdonald, Nuclear Spectroscopy, Part B, ed. F. Ajzenberg-Selove (Academic Press, New York and London, 1960), p. 932.

22. J.P. Davidson, Am. J. Phys. 27, 457 (1959).
23. This was first discussed by R.K. Adair, Phys. Rev. 87, 1041 (1952).
24. W.M. Macdonald, Phys. Rev. 100, 51 (1955).
25. W.M. Macdonald, Phys. Rev. 101, 271 (1956).
26. D.H. Wilkinson, Phil. Mag. [8] 1, 379 (1956).
27. H. Morinaga, Phys. Rev. 97, 444 (1955).
28. A similar point is mentioned by Lane and Thomas, Reference 15, page 347.
29. W.L. Briscoe, Rev. Sci. Instr. 29, 401 (1958).
30. R.H. Stokes, J.A. Northrup, and K. Boyer, Rev. Sci. Instr. 29, 61 (1958).
31. R.E. Ellis and L. Schecter, Phys. Rev. 101, 636 (1956).
32. G.E. Fischer, Phys. Rev. 96, 704 (1954).
33. R.G. Summers-Gill, Phys. Rev. 109, 1591 (1958).
34. R.E. Ellis, R.G. Summers-Gill, and F.J. Vaughn (private communication to Homer E. Conzett).
35. H. Bichsel, R.F. Mozley, and W.A. Aron, Phys. Rev. 105, 1788 (1957).
36. The detector was made by J.H. Elliott.
37. F.S. Goulding and W.L. Hansen, "Leakage Current in Semiconductor Junction Radiation Detectors and Its Influence on Energy-Resolution Characteristics," Lawrence Radiation Laboratory Report UCRL-9436, to be submitted to Nuclear Instr. & Methods.
38. M.S. Livingston and H.A. Bethe, Revs. Modern Phys. 9, 263 (1937).
39. W.A. Aron, B.G. Hoffman, and F.C. Williams, "Range-Energy Curves," Atomic Energy Commission Report AECU-663, May, 1951 (unpublished).
40. K.B. Mather and P. Swan, Nuclear Scattering (Cambridge University Press, 1958), Chapter 2.
41. M.K. Banerjee, Nuclear Spectroscopy, Part B, ed. F. Ajzenberg-Selove (Academic Press, New York and London, 1960), p. 695.
42. M. el Nadi, Proc. Phys. Soc. (London) A70, 62 (1957).
43. M. el Nadi and M. el Khishin, Proc. Phys. Soc. (London) 73, 705 (1959).

44. J.S. King and W.C. Parkinson, Phys. Rev. 88, 141 (1952).
45. R. Herman and R. Hofstadter, High-Energy Electron Scattering Tables (Stanford University Press, 1960).
46. D.R. Inglis, Phys. Rev. 87, 915 (1952).
47. D.R. Inglis, Revs. Modern Phys. 25, 390 (1953).
48. D. Kurath, Phys. Rev. 101, 216 (1956).
49. F. Ajzenberg-Selove and T. Lauritsen, Nuclear Phys. 11, 1 (1959).
50. F. Ajzenberg-Selove and T. Lauritsen, Ann. Rev. Nuclear Sci. 10, 409 (1960).
51. G.C. Phillips and T.A. Tombrello (The Rice Institute, Houston, Texas), "Two-Body Cluster States in Nuclei" (preprint).
52. V.J. Ashby and H.C. Catron, " Tables of Nuclear Reaction Q Values," UCRL-5419 Feb. 1959.
53. A. Galonsky and M.T. McEllistrem, Phys. Rev. 98, 590 (1955).
54. R.R. Spencer, G.C. Phillips, and T.E. Young, Nuclear Phys. 21, 310 (1961).
55. H.H. Thies and B.M. Spicer, Australian J. Phys. 12, 293 (1959).
56. W.T. Pinkston, Phys. Rev. 115, 963 (1959).
57. E.K. Warburton and W.T. Pinkston, Phys. Rev. 118, 733 (1960).
58. I. Talmi and I. Unna, Ann. Rev. Nuclear Sci. 10, 353 (1960).
59. G. Racah, Physica 16, 655 (1960).
60. W.M. Visscher and R.A. Ferrell, Phys. Rev. 107, 781 (1957).
61. J.P. Elliott and B.H. Flowers, Proc. Roy. Soc. A242, 57 (1957).
62. W.W. True and E.K. Warburton, "On the 5.16 Mev and 7.56 Mev States of B^{10}" (to be submitted to Nuclear Phys.)
63. N.K. Glendenning (Lawrence Radiation Laboratory), private communication.
64. J.B. Ball and C.D. Goodman, Phys. Rev. 120, 488 (1960).
65. E.L. Keller, Phys. Rev. 121, 820 (1961).
66. I. Talmi and I. Unna, Phys. Rev. 112, 452 (1958).
67. J.C. Armstrong and K.S. Quisenberry, Phys. Rev. 122, 150 (1961).
68. D.A. Bromley, J.A. Kuehner and E. Almqvist, in Proceedings of the International Conference on Nuclear Structure (University of Toronto Press, 1960) p. 349.